ASSESSING THE IMPACTS OF COMPOUNDING HAZARDS LIKE HEAT WAVES AND FLOODS IN KERALA, INDIA

FAHEED JASIN KOLAPARAMBIL

June, 2024

SUPERVISORS:

Prof. Dr. C.J. Van Westen
Dr. B. van den Bout

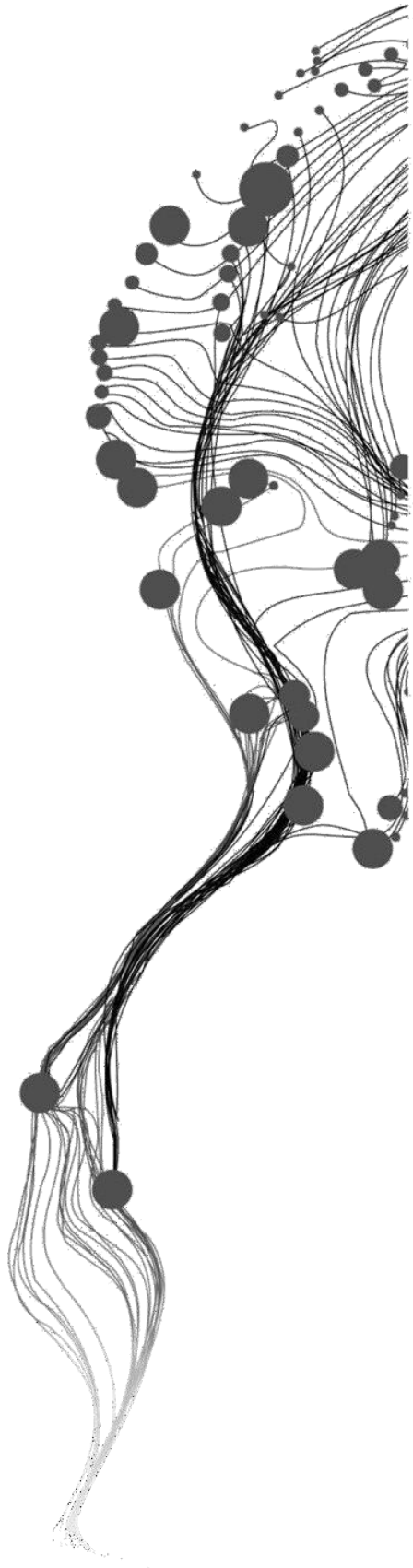

ASSESSING THE IMPACTS OF COMPOUNDING HAZARDS LIKE HEAT WAVES AND FLOODS IN KERALA, INDIA

FAHEED JASIN KOLAPARAMBIL

Enschede, The Netherlands, June, 2024

Thesis submitted to the Faculty of Geo-Information Science and Earth Observation of the University of Twente in partial fulfilment of the requirements for the degree of Master of Science in Geo-information Science and Earth Observation.
Specialization: Natural hazards and disaster risk reduction

SUPERVISORS:
Prof. Dr. C.J. van Westen
Dr. B. van den Bout

THESIS ASSESSMENT BOARD:
Prof. Dr. V.G. Jetten (Chair)
Dr.ir. Anne van Loon (External Examiner, VU Amsterdam)
B. Virgilio Portela (Procedural advisor)

DISCLAIMER

This document describes work undertaken as part of a programme of study at the Faculty of Geo-Information Science and Earth Observation of the University of Twente. All views and opinions expressed therein remain the sole responsibility of the author, and do not necessarily represent those of the Faculty.

ABSTRACT

In several regions across the world there is an increasing trend in compounding heat wave and flooding events. Heat waves and floods can, when occurring close to each other in time, significantly alter the water processes and dynamics during a multi-hazard event. Even though these type of multi-hazard occurrences can compound impact, they are generally studied separately, resulting in a poor understanding of their changes under climate change. In this study we consider the Periyar river basin of Kerala, India to assess the evolution of these hydrometeorological hazards with the help of Extreme temperature and precipitation indices to detect temperature and extreme precipitation events. The Floods and heatwaves were identified in historical (1986-2023) and future periods; near term (2015-2045), medium term (2046-2075) and Far term (2076-2100) under two SSP scenarios (SSP2-4.5 and SSP5-8.5). A flood model was set up and calibrated using the FastFlood.org simulation platform. The population exposure to floods and heat waves were calculated for low land, mid land and high land in the region using projected population data. The study found an increasing trend in extreme precipitation and peak discharges, with higher peaks from 2001 to 2010, while extreme temperature indices rose, peaking between 2011 and 2023. The lowland and midland regions experienced higher precipitation extremes, and midlands saw the most significant increase in temperature extremes. The flood model showed 92% accuracy for the historical 2018 floods and the population exposure analysis to floods revealed midlands had the highest exposure for both 20 and 100 year return period flood scenarios. SSP2-4.5 showed medium-term peaks in extreme precipitation, while SSP5-8.5 indicated far-term peaks. Lowlands are projected to experience the highest precipitation extremes, and midlands the highest temperature extremes. Heatwave analysis suggested minimal events under SSP2-4.5 but up to 90 days under SSP5-8.5 in the far term. Population exposure to both floods and heatwaves is predicted to be higher under SSP2-4.5, particularly in the midlands. The study concludes that compounding heatwave-flood events, though historically rare, are likely to become more frequent and intense under future climate scenarios and to accurately predict and study this there should be more investment in accurately recording observation data. Future research should incorporate higher resolution datasets, region specific indices, consider dam discharge impacts, and utilize an ensemble of climate models for more accurate projections.

Keywords: Floods, heat waves, compounding hazards, exposure analysis, flood simulation, climate change, extreme indices, Periyar river basin, Kerala

ACKNOWLEDGEMENTS

I am deeply grateful to all those who have supported and guided me throughout the process of completing this thesis. First and foremost, I would like to extend my heartfelt thanks to my supervisors, Prof. Dr. C.J. Van Westen and Dr. B. van den Bout, for guiding me through the different phases of this research. Your insightful feedback has been instrumental in shaping this work. Your combined expertise have greatly enriched my research. A special thanks to the Chair, Prof. Dr. V.G. Jetten, for providing critical feedback during the proposal and mid-term presentations, allowing me to better streamline my research. I am thankful to my procedural advisor, B. Virgilio Portela, for the encouragement and support you provided during the research period. I would also like to thank Dr.ir. Anne van Loon, for accepting me as my external supervisor and taking the time to review my work. I would also like to thank Dr. Shekhar Lukose, Dr Shinu, Dr Ravi and Rajeevan of the Kerala State Disaster Management Authority for helping me find the relevant data and for having great discussions on the study.

This Journey would have been much harder without my fellow travellers; I would like to extend my warm gratitude to my friends at ITC. Heartfelt thank you to Ms Raunak for supporting me and motivating me throughout this journey. I would also like to thank my family for believing in me and supporting me to pursue this Masters.

Thank you.

TABLE OF CONTENTS

List of Abbreviations

CDD	- Consecutive Dry Days
CDO	- Climate Data Operator
CRED	- Centre for Research on the Epidemiology of Disasters
CWD	- Consecutive Wet Days
DEM	- Digital Elevation Model
EC	- Earth Consortium
EHF	- The Excess heat factor
ETCCDI	- Expert Team on Climate Change Detection and Indices
EQM	- Empirical Quantile Mapping
FRL	- Full Reservoir Level
GCM	- Global Climate models
HWDI	- Heatwave duration index
IMD	- Indian Meteorological Department
KSDMA	- Kerala State Disaster Management Authority
MME	- Multi-Model Ensemble
NRSC	- National Remote Sensing Centre
PRB	- Periyar River Basin
RCP	- Representative Concentration Pathways
SMHI	- Swedish Meteorological and Hydrological Institute
UNISDR	- United Nations International Strategy for Disaster Reduction
UTCI	- Universal Thermal Climate Index
UTM	- Universal Transverse Mercator
WMO	- World Meteorological Organization

List of figures

List of tables

Chapter 1: Introduction

1.1. Hydro-meteorological hazards

Hydro-meteorological hazards are defined as a "process or phenomenon of atmospheric, hydrological or oceanographic nature that may cause loss of life, injury or other health impacts, property damage, loss of livelihoods and services, social and economic disruption, or environmental damage" (United Nations International Strategy for Disaster Reduction, UNISDR, 2009). This includes a wide range of hazards such as floods, droughts, heat waves, cold waves, precipitation extremes, hurricanes, and tornadoes. Global climate change is intensifying the severity and frequency of hydro-meteorological hazards in most climate zones around the world (Shah et al., 2020).

The Centre for Research on the Epidemiology of Disasters (CRED) estimated that in the period from 2000 to 2019, floods accounted for 44% of all disaster events, impacting 1.6 billion people globally, making it the most common disaster type. It also reports that extreme temperature events and floods have increased by approximately 232% and 134%, respectively, in the decade 2000 to 2019 compared to the previous decade (1980 to 1999), accounting for 13% and 9% of global deaths during this period (CRED,2020). In terms of economic damage, floods and extreme heat events alone have resulted in an average annual damage of $15.1 and $2.8 billion globally respectively, since the 1960s (Gu et al., 2022).

1.2. Compounding hazards

Heatwaves and floods can lead to devastating impacts by themselves as is evident by the economic damage and the lives lost to these disasters discussed in section 1.1.
However, natural hazards are often not discrete and independent events; they interact spatially and temporally with other hazards, creating aggravated impacts on the socioeconomic systems (de Brito, 2021).

Heatwaves are typically considered dry hazards and are often studied in conjunction with droughts and low precipitation events. However, high daily temperatures are also linked to precipitation extremes. These compounding hot-wet hazard events remain relatively understudied (Sauter, Fowler, et al., 2023). Due to global warming and an associated increase in extreme heat events, an upward trend in compound wet-warm events is expected at a global scale posing an additional threat to food security, water and ecosystem services (Meng et al., 2022). This leads to more compounding interactions of extreme heat events such as heatwaves with wet events like flooding.

During a heatwave or an extended warm period in a region, the atmosphere is warmer, which increases the moisture-holding capacity of the atmosphere, which may lead to extreme precipitations (Brutsaert, 2017). Prolonged hot periods compact the soil, forming crusts, reducing the infiltration and increasing runoff, which may result in intense flooding (Zhang et al., 2023). Also, heatwaves decrease the baseflow and water-carrying capacity of rivers making them vulnerable to flooding in case of extreme precipitation (van Vliet et al., 2023).

Also, a compounding heatwave and flood can have profound impacts on society. They disrupt economic activities like inland shipping, agriculture, tourism, and hydroelectric power generation. Heatwaves can lead to dehydration, heat exhaustion, and heatstroke, particularly affecting vulnerable populations, while floods can further exacerbate the situation by contaminating drinking water, causing outbreaks of waterborne diseases (Arsad et al., 2022; Shafii et al., 2023). Also, a region facing a heatwave is unlikely to be prepared for a wet hazard like floods, and often, the society is caught off-guard, making

them more vulnerable. Also, the vulnerability of population, livestock and crops that are already affected by a heatwave would even be higher for flooding events, increasing the risk significantly. Moreover, risk reduction measures for floods might be negatively affected by the heatwaves; for example, dikes and levees will develop cracks when exposed to longer periods of heat waves, also dams will be operated to save more water during the heat wave event and might not be in a capacity to reduce the flooding (Ward et al., 2022).

(Sauter et al. (2023) used meteorological data to identify the predominant weather patterns during the transition from a heatwave to extreme rainfall events over Europe and Australia. The study reported that after a heat wave, the atmospheric instability and moisture levels are significantly higher than the climatological norm for the same time of the year most likely leading to more extreme rainfall events. It was also noted that the non-arid, mid and high latitudes, which have ample moisture supply and high summer temperatures, have a higher likelihood of such compounding events (Sauter et al., 2023)

A lot of regions around the world have experienced such temporally compounding hot-wet extremes. For instance, in July 2018, Japan faced a devastating flood which was preceded by unprecedented heatwaves (Zhang & Villarini, 2020). Pakistan faced a similar situation in June 2022 , when there was a massive flooding event which followed a heat wave in May 2022(Iqbal et al., 2022). Similarly, in June 2024, Delhi experienced significant flooding shortly after enduring one of the worst heatwaves in the region (Economic Times, 2023). Sauter et al. (2023) examined rainfall at the end of the heat wave period and reported a compounding relationship between heatwaves and rainfall extremes in Australia. Zhang & Villarini, (2020) reported that such compounding heat wave flood events are becoming more common in the Central United States.

There are also increasing occurrences of compounding flooding and heat wave events, especially in China. Zheng et al. (2024) studied sequential flooding and heat waves in China, using a weighted average of precipitation to determine floods and minimum temperature to detect heat waves; the study found that urban areas experienced a greater increase in such events. Qian et al. (2023) studied the anthropogenic influence in spatially compounding flooding and heat waves in China and concluded that anthropogenic climate change has increased the probability of such events 10 times more and such events are predicted to likely increase 14 times by the end of the 21st century.

Also, there are studies which look at abrupt transitions from dry to wet periods based on precipitation and moisture anomalies. Such abrupt alterations are often termed dry-wet abrupt alterations (DWAA) and often focus on deviations in precipitation patterns (Ren et al., 2023). However, studies that explore the DWAA events often employ indices which are often based on precipitation and focus on drought–flood alternate events and do not include heat waves.

Although the occurrences of compounding heat wave-flood events are on the rise, studies that analyze both together are limited, and they are often analyzed individually, owing to the complexity of accurately defining the events and modelling them. As a result, studies that integrate both flood and heat waves for the same region are limited (Alves et al., 2023).

The following section gives a brief outline of the current methodologies that are used to analyze heatwaves and floods.

1.3. Heat waves

The definition of heat waves varies by region, and there is no globally accepted standard. However, most existing definitions are based on having consecutive days that exceed a specific temperature threshold, which is determined by the local climate and the physiology

of the population (Awasthi et al., 2022). Defining heat waves is challenging because similar meteorological conditions might cause a heat wave in one location but not in another. For instance, 5 consecutive days exceeding 30°C might be normal temperatures in the tropics, but in the poles, it would mean abnormally high temperatures. Owing to this lack of universal definition, various countries and organizations use different criteria for determining heat waves.

The World Meteorological Organization (WMO) defines heatwaves as a period where maximum temperatures exceed the daily normal temperature (1961-1990) by 5°C for more than 5 consecutive days (WMO,nd). When we look at country-wide definitions, they, too, vary in their approach to defining a heat wave. South Africa defines heatwaves as periods when daily maximum temperatures exceed the 90th percentile for at least three consecutive days (Lyon, 2009). Whereas for Australia, a period of three or more consecutive hot days where temperatures exceed relative thresholds (varies within the country) is termed a heat wave (Jyoteeshkumar reddy et al., 2021). In China, it is defined as three or more consecutive days of temperatures exceeding 35°C (Ji et al., 2023). The heatwave definitions across the world are based on a threshold for duration and a threshold for temperature, this could be either relative or absolute thresholds (Awasthi et al., 2022).

Several heatwave indices are commonly used in the literature to quantify and analyze heatwave events. These indices vary in complexity and the variable they use. Some of the indices which measure the intensity of heat waves include, 'The Excess heat factor' (EHF), 'Universal Thermal Climate Index (UTCI)', 'Heat Index (HI)' and 'Maximum value of daily maximum temperature (TXx)'. EHF is an index based on excess heat and heat stress and is widely used to study heatwaves around the world as it is not based on any region-specific thresholds (Trancoso et al., 2020). HI combines the relative humidity and dry bulb temperatures to estimate temperatures that would perceived by humans (Awasthi et al., 2022).UTCI is a heat stress index that includes both physiological and meteorological factors. It accurately reflects the heat stress experienced by the human body in outdoor environments, based on variables such as air temperature, solar radiation, humidity, and wind speed and is highly sensitive to changes in these environmental parameters (Pecelj et al., 2020). TXx is the maximum daily temperature in a period (year or month) and is one of the extreme indices defined by the Expert Team on Climate Change Detection and Indices (ETCCDI). TXx is widely used for climate change-related studies to assess heat waves and is recommended by WMOs for the same (Thompson et al., 2023). Some examples of indices which attributes for the frequency of heatwaves include "Tropical nights", "summer days", "Number of days with maximum temperatures greater than 90th percentile (TX90"), "Warm spell duration index (WSDI)" (Barriopedro et al., 2023).

Since there exist a plethora of definitions for heatwave depending on the region, for this study, we will use the definition used by the Indian Meteorological Department (IMD) as it is developed specifically based on the climatic characteristics of the region. More on the IMD definition will be discussed in section 4.1.4.

1.4. Flood modeling

Flood modelling is a critical tool in understanding and predicting flood behaviour, which enables effective risk reduction and mitigation strategies. Various flood modelling approaches are in use, each having its own advantages and disadvantages. (Kumar et al. (2023) conducted a comprehensive review of flood modelling approaches and stated that some of the common types of flood models are Hydrological models, Hydraulic models, Hydrodynamic models, statistical models and physically based models.

Hydrologic modelling simulates water flow in a river or stream system using mathematical and computer tools. It requires input data such as elevation, land use, precipitation, evaporation, and soil moisture and simulates the flow rate, volume, and water arrival time (Herrera et al., 2022). Moreover, the results of hydrologic modelling can be used as input for hydraulic modelling, which models water behaviour during flood events providing the depth and extent of flooding and the peak flows predicted (Munir et al., 2020). One of the main limitations of these modelling approaches is the complexity of setting up the model and interpreting the outputs, making it difficult for non-specialists (Kumar et al., 2023).

Statistical models rely on the historical data to predict future flooding events. They rely on creating a statistical relationship between meteorological, hydrological and topographical variables with historical flood occurrence. Major limiting factors for this approach are that it only gives the flood probability and does not consider the hydrological processes and is based on the assumption that future events will follow the past patterns (Hakim et al., 2024) . Currently, there have been a lot of advancements in flood modelling using Artificial Intelligence (AI) and Machine learning (ML). AI and ML algorithms require a large amount of quality training data, including meteorological, hydrological, and topographical data and historical flood data to accurately model floods of a region (Karim et al., 2023). However, a major challenge in applying these innovative methods is the lack of high-quality data available for training in many regions. Additionally, the inherent uncertainty and "black box" nature of these algorithms make their flood predictions difficult to interpret and trust.

Physical-based models are rainfall – runoff models, which are based on the understanding of physical processes involved in run-off production and consider processes such as infiltration, evapotranspiration, runoff routing etc. These models are capable of accurately reproducing catchment behaviour to various hydrological conditions and are widely used in flood modelling (Kumar et al., 2023). Physical process based models such as The Soil and Water Assessment Tool (SWAT) have been used extensively around the globe to model floods and other hydrological processes (Boithias et al., 2017; Yu et al., 2017). Another extensively used model is HEC-RAS (de Macedo et al., 2024). The main limitation of physically based models are that they require a lot of computation power and time ,along with precise input data (Kumar et al., 2023). This makes it less accessible for rapid flood assessment especially in regions with limited data availability.
This necessitates models that can achieve high accuracy with faster processing times. One such model called FastFlood, is discussed in the next section.

1.4.1.The FastFlood model

FastFlood is a browser-based flood simulation model developed by Bout et al. (2023) which combines computational efficiency with robust accuracy and can be used to perform rapid flood hazard simulations in data-scarce regions. Bout et al. (2023) reported that the model can simulate flash and fluvial floods 1500 times faster and with similar accuracy when compared with full simulation models. The model incorporates a fast, steady-state flow accumulation solver and an adaptive pressure-driven inundation solver, which allows the model to generate detailed flood hazard maps significantly faster than conventional models without sacrificing accuracy. The input requirement for the flood simulation in FastFlood include data representing the event duration, elevation of the region, rainfall intensity and terrain roughness. Additional parameters such as infiltration and soil moisture can also be added to the model for a better representation of the region and event.

The overview of methodology involved in the working of the FastFlood model as described in Bout et al. (2023) can be divided in to five steps and is presented in Figure 1.
The initial step involves creating a monotonically increasing elevation model by applying a fast sweeping algorithm on the grid cells of the input elevation model. It ensures that the grid cells are at least as high as the lowest neighbour. The second step involves the derivation of the flow network. The hydrologically corrected elevation models are then used to derive flow network based on the local derivatives. The direction of flow is determined based on the angle of the steepest descent. The third step is the creation of a steady state discharge over the derived flow networks. This routing is done using a simple flow accumulation which uses a fast sweeping numerical algorithm to speed up the process. Since it is highly improbable to steady state flow in nature mostly due to dynamic rainfall, infiltration and other additional factors, the steady state assumption of the model should be compensated. This correction for partial steady state is done in step four. This correction is based on the duration of the event and the properties of the catchment and is used to calculate the actual peak flow for every location. The final step in the process is the reconstruction of a flood map. The flow depths are reconstructed from the discharge values using stage-discharge relationships. This is achieved by using exponentially cascaded profile approximations that integrate channel information with elevation data.

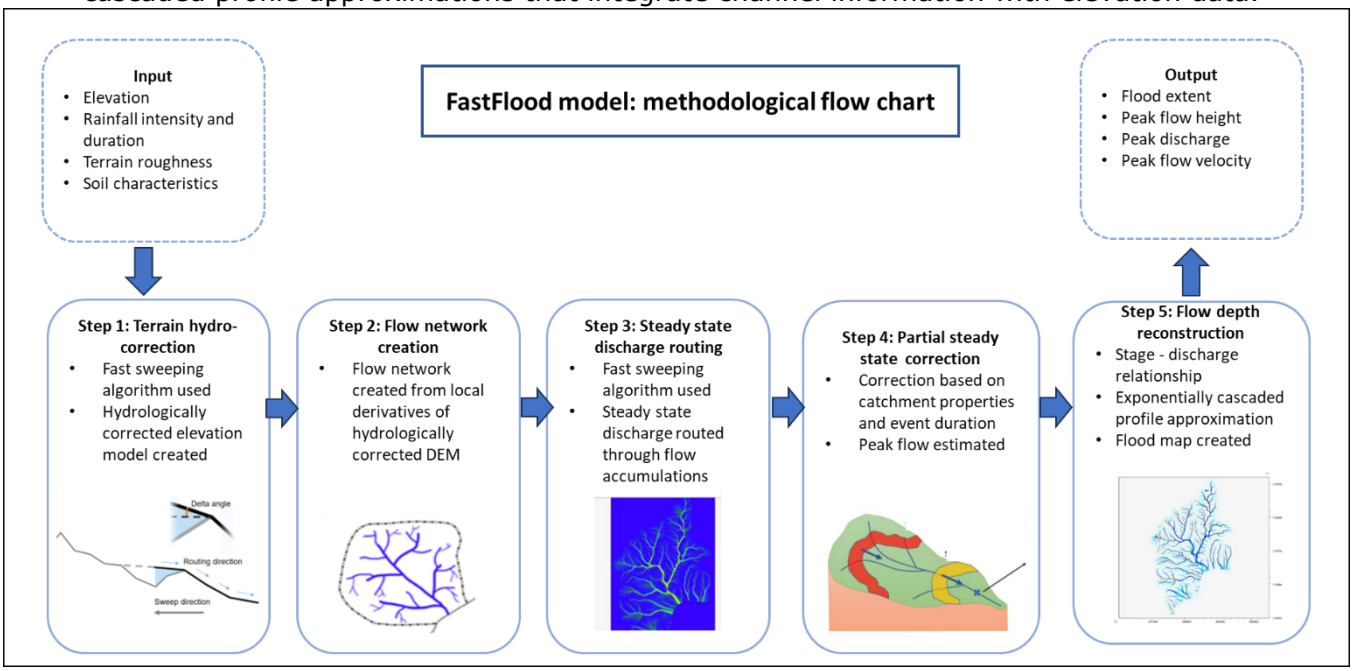

Figure 1: Methodological flow chart for FastFlood model based on Glas (2023) and Bout et al. (2023)

1.5. Climate change and evolving hazards.

As per the Sixth Assessment Report (AR6) of the Intergovernmental Panel on Climate Change (IPCC), a considerable increase was observed in global surface temperatures in recent decades. This rise in temperatures can vary the distribution of global and regional water resources spatially and temporally, which would result in altering the rainfall distribution and aggravating extreme weather events like floods and heatwaves (Zhang et al., 2023). In a warming climate, it is necessary to understand how these hazards and their interactions will evolve. Precipitation and temperature data from Global climate models can be used to investigate these changes. Several studies use historical and future projections of extreme precipitation data from the Coupled Model Intercomparison Project

Phase 6 to study the occurrence of Heat waves and floods in the future (Chen et al., 2021; Meng et al., 2022; Try et al., 2022; Wang et al., 2021; Zhao & Dai., 2021).

The CMIP6 climate models take into account both the shared socioeconomic pathways (SSPs) and the representative concentration pathways (RCP). The shared socioeconomic pathways (SSPs) are used as input for climate models to simulate how greenhouse emissions will change depending on societal choices. There are five SSP pathways which simulate different scenarios. The SSPs range from SSP1 (sustainable development) to SSP5 (fossil-fueled development)(Gidden et al., 2019). The five SSPs and their brief descriptions are shown in Table 1. The RCP values provide different scenarios of greenhouse gas emissions and the associated radiative forcing. For each SSP scenario a number of radiative forcing could be achieved based on the policies implemented and the values of the forcing outcomes ranged from 1.9 to 8.5 $W\,m^{-2}$ (Gidden et al., 2019). SSP1-2.6, SSP2-4.5, SSP4-6.0, and SSP5-8.5 are the four common scenarios used in climate change-related studies as they were designed as the continuation of CMIP5 scenarios (Tebaldi et al., 2021). Out of this scenarios which has forcing levels of 6.0 or higher are considered as high emission scenarios and those between 1.9 and 4.5 W/m^2 are considered low emission scenarios (Y. Chen et al., 2020).

Scenario	Description
SSP1	Sustainable path: low challenges to mitigation and adaptations
SSP2	Middle of the road: medium challenges to mitigation and adaptation
SSP3	Regional rivalry: High challenges to mitigation and adaptation
SSP4	High inequality: low challenges to mitigation, high challenges to adaptations
SSP5	Fossil fuelled development: High challenges to mitigation, low challenges to adaptation

Table 1: SSP scenarios and their descriptions based on (Riahi et al., 2017).

With the shifting dynamics of extreme weather events under a changing climate, it is essential to analyze the compounding heat wave–flood hazards under a changing climate.

1.6. ETCCDI indices

The Expert Team on Climate Change Detection and Indices (ETCCDI) were established in early 2000 to address the limitations of the lack of long-term global climate data and a standard definition of extreme event indicators across different countries, which hindered studies on global extreme weather and climate events (Yin & Sun, 2018). ETCCDI includes 27 representative climate indices which can be used to analyze extreme climate change on both global and regional levels. This index were used by multiple studies to analyze extreme temperature and precipitation events. Yin & Sun, (2018) used the ETCCDI indices such as annual maxima of daily maximum temperature (TXx), Extreme wet day precipitation (R99p) and Very heavy precipitation days (R20mm) to study the characteristics of extreme temperature and precipitation in China. Panda et al. (2014) used ETCCDI indices like TXx , warm day frequency (TX90p) along with other indices to study the spatial-temporal patterns in extreme temperature events in India for the period 1971 to 2005 and concluded that the intensity and frequency of warm extremes have increased, while the cold extremes in large parts of the country are declining. Yapo et al. (2023) studied the changes in the seasonal cycle of heatwaves, dry spells and wet spells using the ETCCDI indices, consecutive dry days (CDD), consecutive wet days (CWD) and Heatwave duration index (HWDI).

The ETCCDI indices were found to be useful in determining extreme temperature and precipitation events and could be seen applied in different regions of the world. The ETCCDI indices used for the study will be discussed in detail in section 4.1.

1.7. Research Gap

Several studies have shown that there is an increasing trend in heat waves and floods especially in regions with high temperatures and high moisture availability where there in an increasing likelihood of occurrence of compounding heatwaves and floods. Even though these compounding hazards create a higher risk to the region, these hazards are most often analyzed separately. This approach might misinterpret the overall risk of the region by underestimating the hazard (Kappes et al., 2012). It is essential to incorporate both these hazards and their occurrence together and analyze their evolution in a changing climate to enhance the stakeholders to mitigate the impacts of these increasing compound events.

This study aims to bridge this gap by analyzing the evolving floods and heat waves in a region, with a wet and humid climate and assess the changes in the occurrences of these hazards in the future period and evaluate corresponding changes in exposure. The Periyar River basin, which is the river basin of the longest river in the state of Kerala, India, was selected for this. The objectives of this study and the research questions that will be covered are discussed in the next chapter.

Chapter 2: Objectives and research questions

The main objective of this research is to model the evolution of hot, dry extremes, such as heatwaves, and wet extremes, including extreme precipitation and floods, and their compounding occurrences in the Periyar River Basin, Kerala, India.

The sub-objectives and research questions are discussed below.

Sub-Objective 1: Analyze the historical occurrence, severity and frequency of climate extremes such as heat waves, extreme precipitation and floods in the Periyar River basin.

1.1. How has the frequency and intensity of hydrometeorological extremes evolved in the past decades?

1.2. To what extent were these extreme events temporally compounding in the study area?

Sub-Objective 2: Calibrate FastFlood model to model the floods in the region.

2.1. How can the flood model built predominantly on global datasets be calibrated with historical data?

Sub-Objective 3: Evaluate how the hydrometeorological hazards and their occurrences change under SSP2-4.5 and SSP5-8.5 climate scenarios using best-fit GCMs from CMIP6.

3.1.How are hydrometeorological hazards and their intensity and frequency altered under SSP2-4.5 and SSP5-8.5 climate scenarios?

3.2. How does the exposure to floods and heat waves change under the SSP pathways for different future periods?

Chapter 3: Study area

3.1.Introduction to Kerala.

Kerala, often referred to as "God's own Country", is a state located on the southwestern coast of India. The geographical location of the state is approximately between 8° 18' to 12° 48' N latitudes and 74° 02' to 77° 22' E longitudes, covering an area of approximately 38,863 Km^2. The state has a population of about 33.4 million as per the 2011 census (Last available official record. The state has a high population density of about 860 per Km^2, which is higher than the national average of 382 per Km^2 (Lal et al., 2020) . It is bordered by the state of Karnataka to the north and northeast, the state of Tamil Nadu to the east and south, and the Arabian Sea to the west. The diverse topography of the state ranges from the high Western Ghats mountain range in the east to the coastal plains in the west. The altitudinal variation of the state varies from 5m above sea level in the west to about 2695m above sea level in the East. The coastline spans 560 Km, and the width from west to east spans from 11 Km to 124 Km. In terms of physiography, the state is divided into three regions: lowlands (0 to 7.5 m), midlands (7.5 to 75 m) and highlands (>75 m) (Tripathi & Davis, 2020).

The state of Kerala experiences a tropical monsoon climate characterized by seasonally excessive rainfall, high humidity, and hot summers. There are four main seasons: summer (March to May), the southwest monsoon (June to September), the northeast monsoon (October to December), and winter (January and February) (ENVIS, n.d.). Kerala receives an average annual rainfall of approximately 3000mm, peak rainfall in June and July. The southwest monsoon, which lasts from June to October, is the primary rainy season, accounting for about 70% of the state's annual rainfall.

Kerala is categorized as a multi-hazard zone with 39 hazards that are specific to the state according to the Kerala State Disaster Management Plan 2016. The state is most vulnerable to multiple hazards, including floods, landslides (especially in the highlands), heat waves, droughts, forest fires, lightning and strong winds (KSDMA, 2019). The following subsections explore the historic floods and heatwaves that were recorded in the state.

3.1.1.Historic floods in Kerala.

Kerala is among the most flood-prone states in India due to its geographical location and topography and has witnessed multiple flood events in the past Mishra, (2021). One of the oldest recorded floods in the state was that of 1924 and is referred to locally as the "great floods of '99" (as per the Malayalam calendar, the year was 1099). The 1924 flood was caused by the southwest monsoon and recorded maximum one-day, two-day and three-day rainfalls of 484mm,751mm and 897mm, respectively (CWC,2018). The peak rainfall was recorded in mid-July, and the floods led to a heavy loss of life, property and crops in the state. The year 1961 also recorded a severe flood event as the southwest monsoon brought intense rainfalls, which were 57% above the normal rainfall, with maximum daily rainfalls of 234mm recorded in the district of Kozhikode (CWC,2018).

The most recent floods recorded in the state were in the years 2018 and 2019. In the southwest monsoon period of 2018, Kerala received rainfall exceeding 164% from the normal rainfall of the period. The one-day and two-day maximum rainfall values were reported to have a return period of about 75 and 200 years, respectively (Hunt & Menon, 2020). The 2018 floods and associated landslides killed more than 400 people and left millions of people displaced. The economic loss of the event was estimated to be more than 3.8 million dollars (Lal et al., 2020). Mishra et al. (2018) reported that six out of the

seven major reservoirs in the state were at 90% of their full capacity before the onset of the extreme event precipitation, which increased the severity of the floods. However, a study by Sudheer et al. (2019) used a hydrological model to investigate the role of dams in the Periyar river basin during the 2018 floods and reported that even if the reservoirs were empty before the start of the extreme precipitation event it would not have reduced the floods significantly as most of the runoff was caused by sub-catchment which were not controlled by any dams. The study also found that with better reservoir management, the floods would have only reduced by about 16 to 20 per cent.

In 2019, the southwest monsoon season, the state received 32% deficient rainfall during the period from June and July and 123% excess rainfall during the month of August (KSDMA,2019).Mishra, (2021) reported that the 2019 flooding event was caused by a low-pressure system that developed over the Bay of Bengal and moved toward the west coast, causing increased convection over Kerala leading to extreme rainfall events in several districts during July and August, resulting in heavy cumulative rainfall and catastrophic flash flooding.(Vijaykumar et al. (2021) attributed the 2019 floods to a mesoscale mini cloud burst event that happened over Kerala. KSDMA reported that the peak of the 2019 period was from August 6 to August 14, during which the state received a rainfall of 602mm as opposed to the normal rainfall expected in the period (122mm). It also states that some IMD stations recorded extreme rainfalls exceeding 200mm in a day (KSDMA,2019).125 people were killed due to floods and landslide during the 2019 Floods.

Sreelash et al. (2018) studied the rainfall variability in Kerala and found a declining trend in moderate rain days and an increase in high-intensity rainfall events. The study also underlined the reduction in groundwater recharge as a consequence of this variability in rainfall. This implies that Kerala is likely to experience alternating hazards like floods due to the high-intensity short, duration rainfall and exacerbated heatwave effect due to the overall decline in rainfall days and reduced groundwater levels.

3.1.2. Heat wave occurrences in Kerala.

Heat waves in Kerala are not as frequent as floods, 2016 there were no reported cases of heatwave incidents; as per the Kerala state disaster management plan, the first reported heat wave warning was issued on April 2016 when the district of Palakkad recorded temperatures exceeding 6°C from normal. Districts such as Alappuzha and Kozhikode also showed temperature increase of more than 4°C. Even though the media reported 324 sunburn cases and 10 deaths, the Directorate of Health Services did not confirm these deaths as a result of sunstroke (KSDMP,2016).

In 2019, the state reported 109 cases of sunstroke, even though heat warnings were communicated, these years were not officially considered as heatwaves (Onmanorama, 2019). 2023 also recorded nine districts exceeding the normal temperatures by 5°C but was not considered as a heat wave. In April 2024 Kerala declared heat wave when temperatures crossed 41°C in Palakkad district exceeding 5.5°C from the normal. More than 400 people suffered from heat-related ailments, and 2 people were reported dead because of heatstroke (Kallungal,2024).

According to some sources 2016 is regarded as the first heatwave event in Kerala but some sources report 2024 as the first official heatwave event. Also, there is mismatch between the death tolls recorded due to heat-related events; the central government claimed there were 120 reported deaths in 2023 where, as KSDMA rejected the numbers and stated that there were no deaths reported due to heatwaves in 2023 and it was a human error in data entry (Kumar, 2023). This underlines the need for better documenting of heatwave events and casualties.

The increasing heat wave events in Kerala may be attributed to global warming, land use changes (increased urbanization and reduced green cover), and the presence of anti-cyclones, which prevent the hot air from the ground from rising higher. also, El Nino events tend to favour these events (Benjamin, 2024). Ravindra et al. (2024) studied the heat wave attribution over India and reported that states like Kerala which have not experienced heatwaves in the past are showing higher frequency of extreme temperatures.

3.2.Introduction to the Periyar river basin.

Periyar River Basin (PRB) is located in the Western Ghats, spreading over 3 districts: Idukki, Thrissur and Ernakulam. The population living in the region is highly dependent on the Periyar River for drinking, agriculture, and navigation needs. The Periyar River is regarded as the lifeline of Kerala due to its significance to Kerala's economy, generating a substantial proportion of the state's electrical power through the Idukki Dam while flowing through a region rich in industrial and commercial activities (Irrigation Department, 2020). The Periyar River is the longest river in Kerala and has the highest water discharge. It originates in the western ghats at an elevation of 1830 m, with a total length of 244 Km and draining an area of 5398 Km^2. The river divides into two branches at Alwaye, one flowing north to combine with the Chalakudy River, and the other divides into smaller streams, eventually flowing into the Vembanad-Kol wetlands and eventually joining the Arabian Sea. Figure 2 shows the location map of the Periyar river basin.

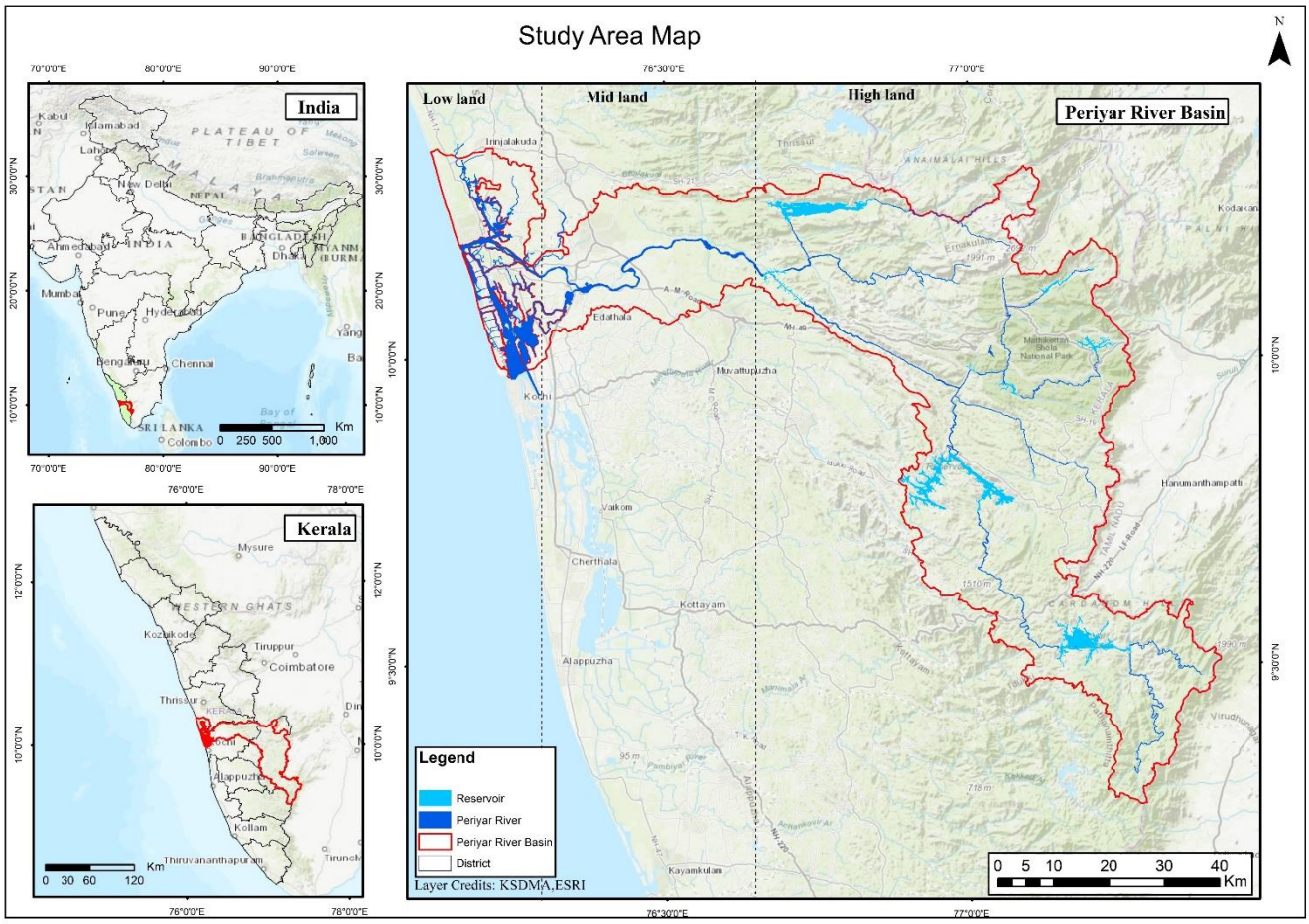

Figure 2:Study area map of Periyar River Basin.

The basin receives an average rainfall of 3200 mm annually. The temperatures in the region range from 14 to 32°C (Sadhwani et al., 2023). The major land cover of the area is plantations (52.02%) and forests (33.2%). The built-up constitutes only 5.31% of the area. PRB displays three primary geological formations: Precambrian crystalline rocks, Tertiary formations, and Quaternary deposits. The crystalline rocks include charnockites, migmatites, gneisses, and intrusive rocks from the Proterozoic to the Tertiary era. Above this, there are sedimentary layers from the Eocene to Miocene periods, as well as more recent deposits near the coast, including Sub-Recent laterite and Recent alluvium (Sudheer et al., 2019).

The PRB has a total of 17 dams, reservoirs and two barrages, which are mainly for hydroelectric power generation and irrigation. These infrastructure projects regulate the stream flow of the river (Sudheer et al., 2019). The three major reservoirs include Idukki, Mullaperiyar and Idamalayar. The largest reservoir is the Idukki Reservoir which includes Idukki, Cheruthoni, and Kulamavu dams. The basin is also part of inter-basin transfer projects such as Mullaperiyar Dam which links the basin to the Vaigai River in Tamilnadu and the Idukki hydroelectric project which is connected to the Muvattupuzha River. The region, with multiple dams and power stations, is crucial for the state's economy (Singh et al., 2022).

For the purpose of this study, we have divided the Periyar River Basin into three regions, following the same physiographical classification for Kerala that is into lowlands (0 to 7.5 m), midlands (7.5 to 75 m) and highlands (>75 m).

A study by Kumar & Mishra (2020) found that dry extremes during the monsoon season in India have increased by 1% each decade from 1951 to 2015 and the frequency of both dry and wet events is expected to rise if there is a global temperature rise of 1.5°C or more. Kerala was subjected to severe floods in 2018 and 2019, disrupting the whole state affecting thousands and causing widespread damage to agriculture and infrastructure (Vijaykumar et al., 2021). Periyar river basin (PRB) which is the second largest river basin of Kerala, was one of the worst affected regions during these floods (Krishnakumar et al., 2022). PRB was also severely affected by the historic floods of 1924 and 1961 (Central Water Commission, 2018).

Floods and heat waves pose a grave threat to the lifeline of thousands of people and their livelihoods in the region. Numerous studies have been done on flood hazards in the Periyar River basin. Singh et al. (2022) investigated the effectiveness of advanced hydrological and hydrodynamic tools like HEC-HMS, HEC-RESSIM and HEC-RAS combined with remote sensing data and observation data to increase the accuracy of flood forecasting in the region. This was achieved by reconstructing the historic flood events and calibrating them with observations. Sudheer et al. (2019) investigated the role of dams in the floods of 2018 in the PRB. All the studies conducted were focused mainly on individual flood hazards and often limited the study to reconstructing the 2018 floods.

The studies dealing with 'dry' hazards in the region are comparatively less than those of floods. Abhilash et al.(2019) studied the changing characteristics of droughts in Kerala using gridded rainfall data from IMD and using it to calculate the SPI values. The study shows that long-term droughts are becoming more frequent in recent decades. Gopinath et al. (2020) developed a browser-based environmental model named Northern Kerala Drought Information System (NKDIS) which calculates the drought risk index based on the Normalized difference vegetation index (NDVI) anomaly calculated from MODIS Terra satellite. In terms of regional heatwave hazards, no studies were found.

A study by Sadhwani & Eldho (2023) assessed the vulnerability of water balance to climate change in the Periyar river basin by using the SWAT hydrological model. The study

analyzed different water balance variables such as precipitation, surface runoff, groundwater flow and percolation with 3 GCMs from the CMIP 6 scenarios. In the analyses, it was found that there would be a considerable increase in runoff (>40%) and stream flow (>65%) in the mid and far future, implying an increased potential for flooding. However, in the near term, runoff and streamflow were found to be reduced by 15% and 5% respectively. The temperature values were also exhibiting increasing trends, which can be seen in Figure 3.

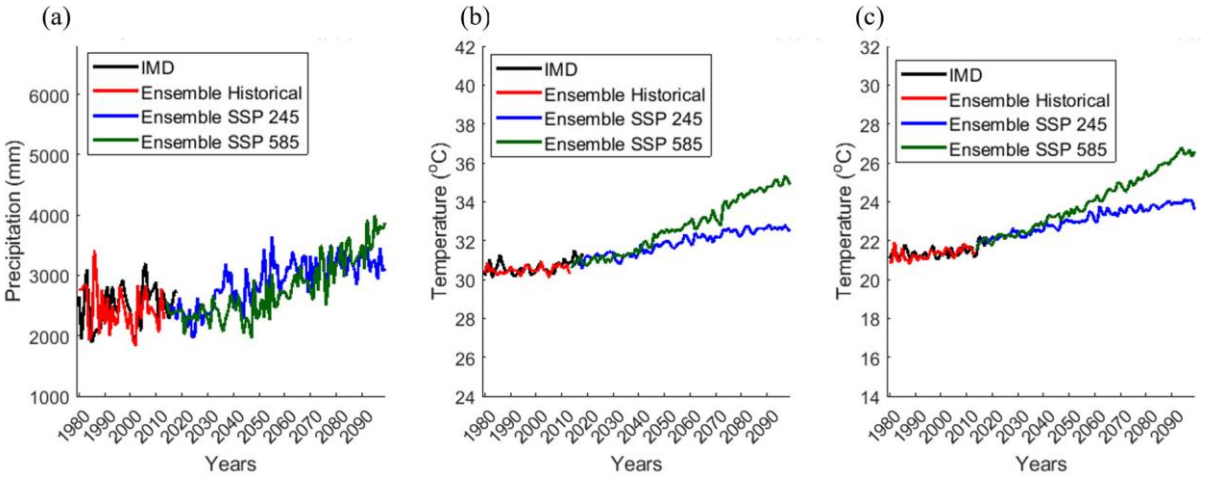

Figure 3: Comparison of temperature IMD and GCM ensembles Source: Sadhwani &Eldho (2023)

3.3.Role of hydropower plants in hazard reduction

Given the numerous dams in the PRB, it is also significant to consider the roles of hydropower plants in the region. During a flood event, these dams could store the flood waters and release it in a controlled manner to reduce flood intensity and similarly, the water stored in the reservoirs could be utilized during a heat wave event to reduce its impacts. Studies like Sun et al. (2023) and Lazin et al. (2023) have demonstrated the effectiveness of dams and hydropower plants to mitigate floods by controlling the outflow. However, during the 2018 floods, all the reservoirs in the region were near full reservoir level (FRL) and had to be opened which aggravated the floods in the region (Sudheer et al., 2019). This implies that the dams in the region can have an effect in both reducing and increasing the hazard intensities. A long period of heat wave would mean that the dams would be storing as much water as they could and a sudden onset of flood event would render them ineffective in regulating the flood hazard. Even though Dams can play a significant role in flooding, these effects could not be incorporated in the study as the dam discharge data were not available to public.

Chapter 4: Methodology

This chapter will provide an overview of the research methods that were used to answer the research questions and achieve the objectives. The conceptual framework for this study is given in Figure 4.

The methodology used for this research can be broken down to three general sections

1. Analyzing Past hydrometeorological extreme events
2. Calibrating the Flood model
3. Analyzing future hydrometeorological extreme events.

These general sections are further explained in detail in the following subsections.

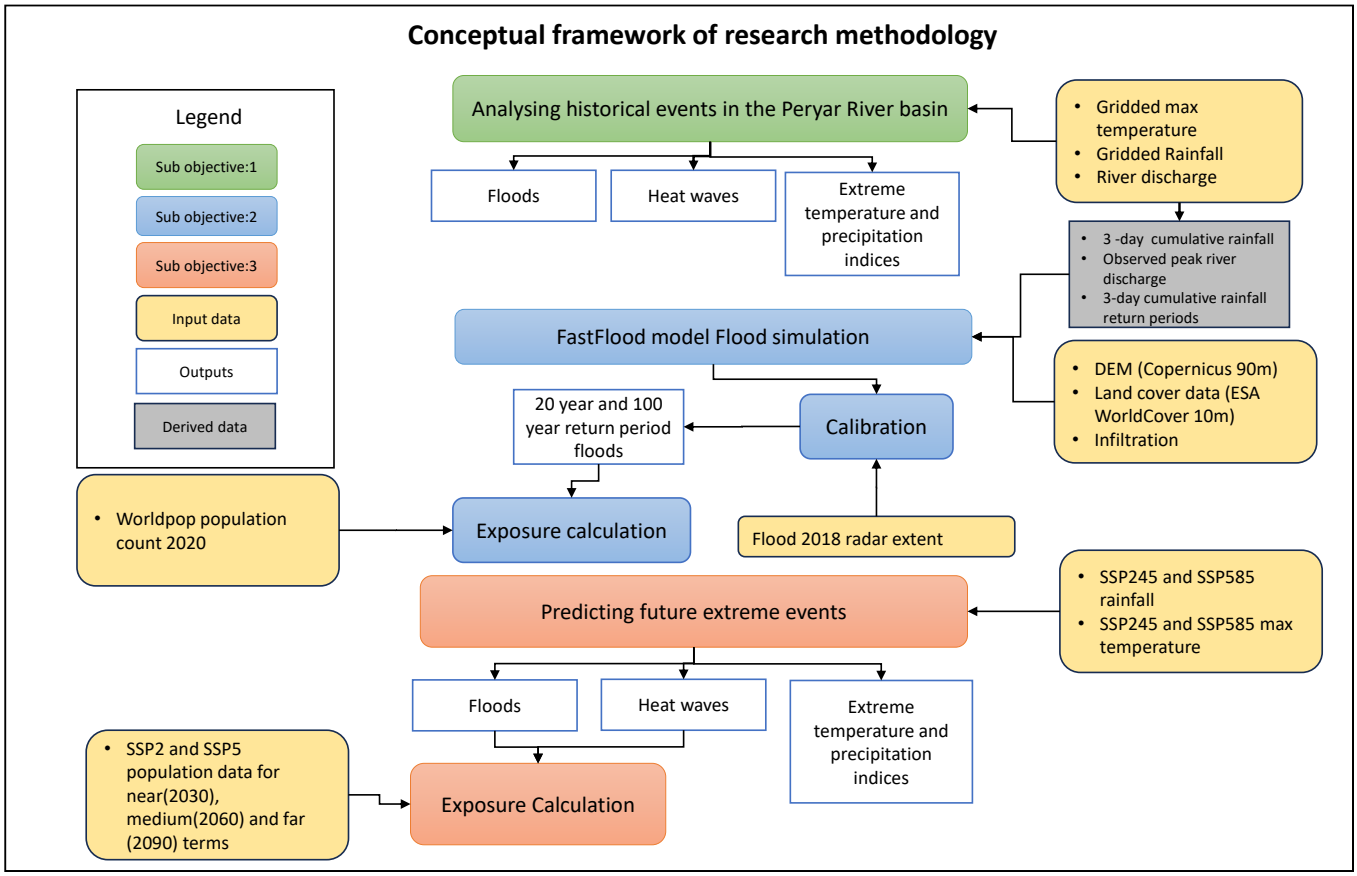

Figure 4: Conceptual framework for the study linking the subobjectives.

4.1.Analyzing historical events

The initial step was to explore how had the hydro meteorological hazards like Flooding extreme precipitation events, extreme temperature events and heat waves evolved in the study area during the historical period. To achieve this the river discharge data, precipitation data and the maximum temperature data available in the region were used. The river discharge data was available only for the period from 1980 to 2020, while the precipitation and temperature data were available for the period from 1986 to 2023. The following sub section delve into each type of data and the analysis done.

4.1.1.River Discharge

The river discharge data (1980-2022) for three discharge gauges (Kalady, Mangalapuzha and Marthandavarma) in the Periyar river basin were collected from the Kerala State Disaster Management Authority (KSDMA). Out of the three gauges , Kalady had a missing data for 8.2% of the total record, Mangalapuzha had 68.7% missing values and Marthandavarma had 53.7% missing values. The locations of the river gauges are shown in Figure 5.

The river discharge data from the three stations were used to calculate the return periods of discharge using Gumbel analysis. Gumbel analysis is a statistical method used to identify the probability of extreme events by fitting a Gumbel distribution to the maximum or minimum observation. To calculate the return periods, first the maximum annual discharges were identified and ranked in descending order and each value was assigned a rank, with one representing the highest value.

Cumulative probability for each discharge is given by

$$P_{Theoretical}(x) = \exp\left(-\exp\left(-\frac{x-u}{\alpha}\right)\right) \quad (1)$$

Where,

$$u = \bar{x} - 0.5772\alpha$$

$$\alpha = \frac{\sqrt{6}s_x}{\pi}$$

$$s_x^2 = \frac{1}{n-1}\sum_{i=1}^{n}(x_i - \bar{x})^2$$

x= observed annual maximum discharge point

$\bar{x}$ = average of annual maximum discharge

n= number of observations

i= rank of the observation

The return period for each discharge value is given by

$$T_P(x) = \frac{1}{1-P_{Theorotical}(x)} \quad (2)$$

Equations 1 and 2 are used to calculate the return periods corresponding to each discharge. Further the return periods were plotted against the discharge value and a line is fitted through this distribution to derive the corresponding discharge for different return periods.

The Kalady river gauge was missing the discharge data on the peak of the 2018 flood (August 13 to 30) probably due to damage to the discharge gauge during the peak event. The threshold of 5 year return period was set as the flood threshold. This threshold was decided based on the historical flood occurrences, where 5 year return period was resulting in floods. The years where the discharges exceeded this threshold were considered as flood years.

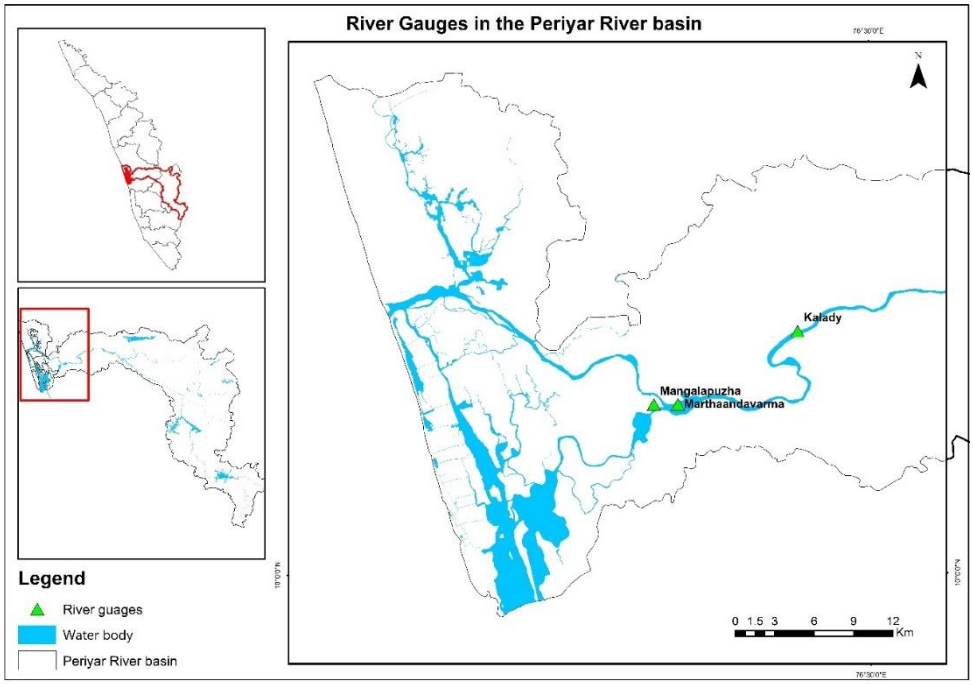

Figure 5: River Gauges in Periyar River basin.

4.1.2.Rainfall data

Initially rainfall data from six stations were collected from KSDMA for the period from 1986 to 2022. Out of the six station two were in the lowlands (Irinjalakuda and Kodungallur), two in the midlands (Aluva and Perumbavur) and two in the highlands (Idukki and Munnar). The locations of all the rainfall gauges are shown in Figure 6. Upon closer inspection of these gauge data, they showed extremely high rainfall values for multiple years, which exceeded 10000mm annually (shown in Figure 7).The highest recorded annual rainfall in Kerala is about 4258mm in 1961 (Nambudiri,2021). Since the values shown by the rainfall gauge data were not considered realistic and the authorities could not confirm or reject the values, we decided not to use these data in further analysis. We used daily gridded rainfall data (0.25° × 0.25°) provided by the Indian Meteorological Department (IMD) instead for further analysis. IMD daily gridded rainfall data (IMD4) is a gridded precipitation dataset created by interpolating data from 6695 rain gauges across India using the Shepard (Inverse Distance Weighted) interpolation method (Pai et al., 2014)(Pai et al., 2014). This IMD4 dataset has been extensively used in different studies in India as reference precipitation data (Reddy & Saravanan, 2023)(Reddy & Saravanan, 2023). The rainfall values for each station were extracted from the IMD4 dataset using the climate data operator (CDO).The daily rainfall data from 1986 to 2023 for each station were stored in different NetCDF files. Only five stations out of six were used, as the stations Aluva and Perumbavur stations in the midland region were lying on the same pixels.

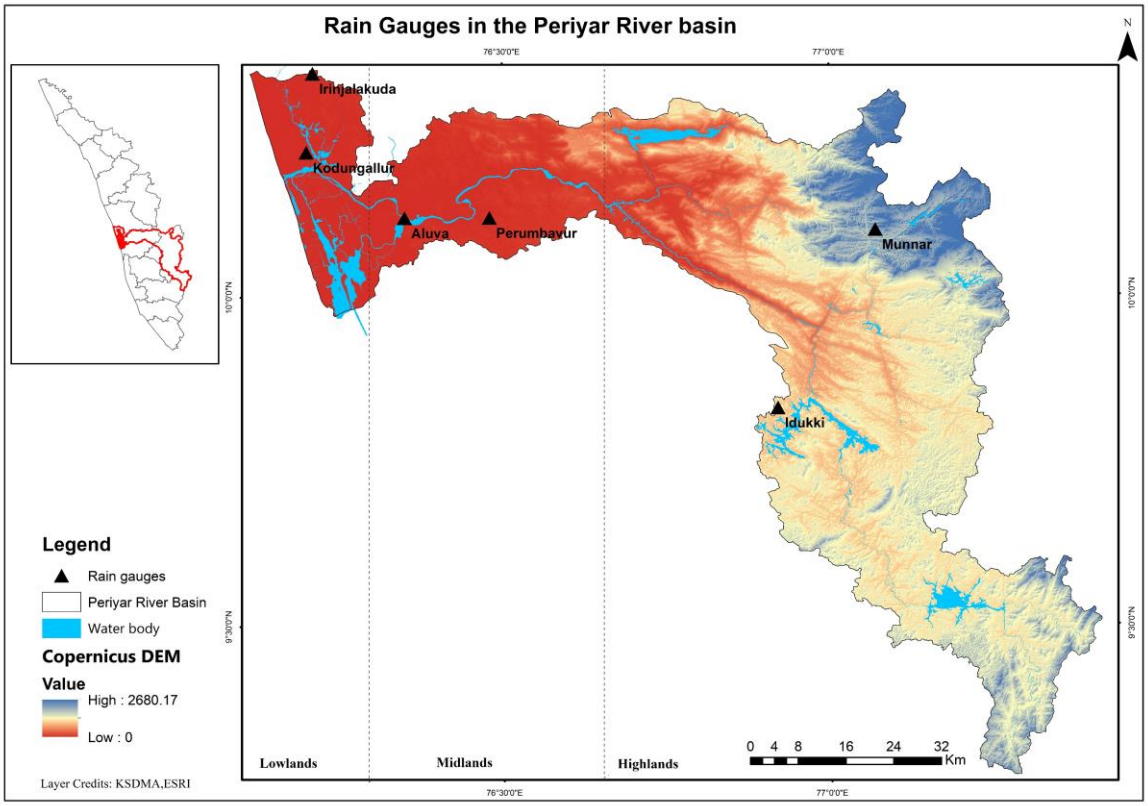

Figure 6: Rain gauges in the study area.

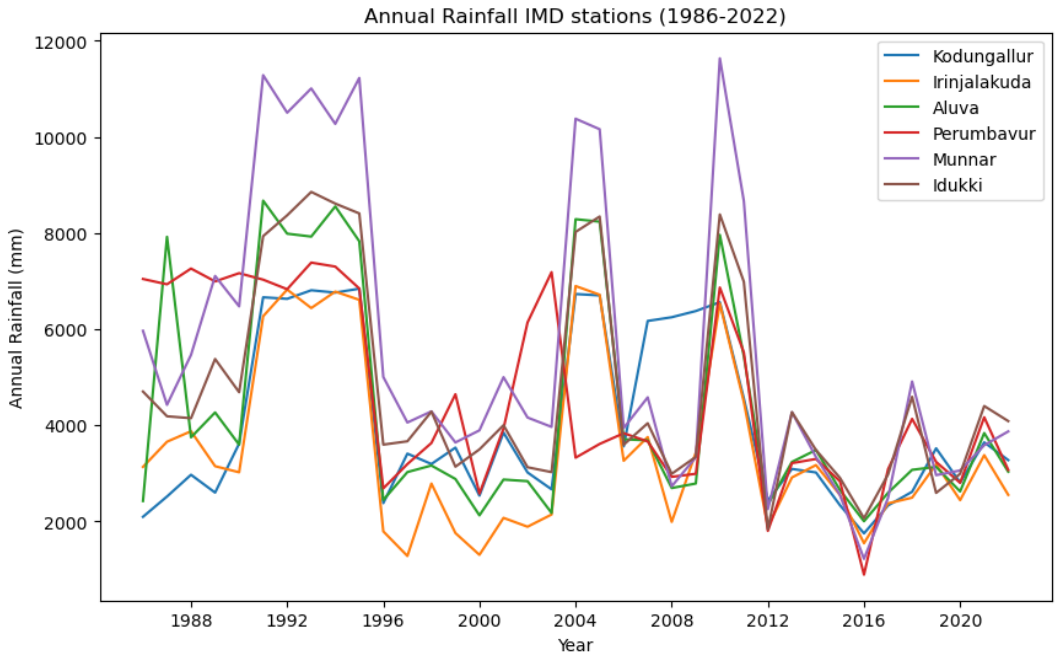

Figure 7: Annual rainfall as per the IMD station data.

Correlation analysis

To check how the IMD station data and IMD gridded data correlated with each other, the Pearson's Correlation Coefficient was used. It is a measure of the degree of linear correlation between two variables and is calculated as follows (Profillidis & Botzoris, 2019).

Pearson's correlation coefficient, $r = \frac{\Sigma(xi-\bar{x})(yi-\bar{y})}{\sqrt{\Sigma(xi-\bar{x})^2(yi-\bar{y})^2}}$

Where x_i and y_i are individual data points.

$\bar{x}$ and $\bar{y}$ are the means of x and y respectively.

Pearson's correlation analysis for the datasets was conducted, using a Python script. Table 19 in annexure 1 shows the values of the correlation coefficient and the corresponding degrees of correlation.

Calculation of Precipitation Extreme Indices

To analyze the precipitation extremes in the historical period (1986-2023), extreme precipitation indices were calculated. These indices were defined by the Expert Team on Climate Change Detection and Indices (ETCCDI) such as, very heavy precipitation days (R20mm), heavy precipitation days (R10mm) and Extremely wet day precipitation (R99p). These indices were calculated for all the five stations for the period 1986 to 2023 using the IMD gridded data. The list of extreme precipitation indices used in this study and the description is given in Table 2. The R20mm captures the days with very high precipitation and is used in multiple studies around the world, but in the context of Kerala it should be noted that there are instances of daily rainfall exceeding 200mm per day, however to stick with the internationally accepted standards this index was used as measure of very heavy precipitation days. The R10mm is comparatively a low threshold and represents days with moderate heavy rainfall however it poses a threat of flooding it continues consecutively for a higher duration. The R99p targets the most extreme events statistically, highlighting the rarest and most severe instances of heavy rainfall. For the calculation of R99p the 99 percentile for daily precipitation in each year is identified and then the precipitation corresponding to these days are summed to obtain the R99p value for each year. The study includes these multiple indices to capture a wider range of extreme precipitation scenarios that might lead to floods. The indices were calculated using Python script.

Indices	Name	Definition	Units
R10mm	Heavy precipitation days	Number of days with at least 10 mm rainfall	Days
R20mm	Very heavy precipitation days	Number of days with at least 20 mm rainfall	Days
R99p	Extremely wet day precipitation	The total annual rainfall on days when daily precipitation exceeds the 99th percentile of the base period.	mm

Table 2: Extreme precipitation indices and their definitions.

4.1.3.Temperature data

The IMD gridded daily temperature data were used as observed temperature data. These datasets incorporate data from 395 quality-controlled temperature measurement stations, which were interpolated using Shepard's (Inverse Distance Weighted) interpolation method to generate gridded temperature fields. (S. Kumar et al., 2020). To match the IMD precipitation datasets, the original IMD maximum temperature gridded data (1° × 1°) were re-gridded to 0.25° × 0.25° by the nearest neighbor interpolation method using Climate Data Operator (CDO). The daily temperature values for the five stations were extracted using the nearest neighbor method in CDO for the period from 1986 to 2023.

Calculation of Temperature Extreme Indices

To analyze the temperature extremes in the historic period, the extreme temperature indices were calculated as defined by the Expert Team on Climate Change Detection and Indices (ETCCDI), such as the maximum value of daily maximum temperature (TXx) and the number of warm days (TX90). For the 90th percentile calculation the base period of 1986 to 2023 was taken. The list of extreme temperature indices used in this study and the description is given in Table 3.

Indices	Name	Definition	Unit
TXx	Maximum value of daily maximum temperature	Maximum of daily maximum temperature in a year	°C
TX90	Warm days	Number of days when the temperature exceeded the 90th percentile of the base period	Days

Table 3: Extreme temperature indices and their definitions

4.1.4.Analyzing Heat waves

For this study we used the definition by IMD definition of a heatwave, which identifies conditions based on temperature thresholds either in absolute temperature or deviations from the normal. A heat wave is officially declared when the following criteria are met continuously for at least two consecutive days:

1) The maximum temperature at a station reaches or exceeds 40 degrees Celsius in plains or 30 degrees Celsius in hilly regions.
2) The average maximum temperatures surpass the climatological average by at least 4.5 degrees Celsius.

The climatological average is calculated based on the period 1980 to 2010. Based on the intensity of the heat wave it is classified to heat wave and severe heat wave. If the departure from the climatological average is between 4.5°C to 6.4°C it is considered a heat wave and if it exceeds 6.4°C it is considered as a severe heat wave.

Heat index or apparent temperature is widely used in studies to express the risk levels to humans from heat waves and is calculated using surface temperature and relative humidity (Hoang et al., 2022)(Hoang et al., 2022). In this study, however the heat index will not be calculated as the relative humidity values for the region were unavailable.

Since temperature data from 1980 to 1985 was not available, the data from 1986 to 2015 was used to calculate the normal temperatures for the region to depict the climatological average. Normal temperatures for each day of the year was calculated by taking the mean of maximum temperatures recorded on that day in the period 1986 to 2015. Normal temperature values were calculated for all the stations. The maximum daily temperature for the five stations were used to derive the number of heatwave days and their intensity.

4.2.Calibrating the Flood model

To model the flood hazard of the region, FastFlood, a browser-based flood simulation model developed by Bout et al. (2023) was used. This online tool is accessible at fastflood.org. The flood model was initially set up and calibrated using the 2018 flood event and was then further used to create 20 and 100 year return period floods for the region. The model set up and calibration procedures are described in the following subsections.

4.2.1.FastFlood model set up

FastFlood browser application required a DEM and event rainfall data to simulate floods. It also requires additional parameters like infiltration, landcover, input discharge that can be

added to the model for a better simulation. For this study the Fast Flood model was initially set up using the 30m Copernicus Global Digital Elevation Model resampled to 90m.The DEM was resampled to 90 m because of the larger size and higher resolution of the 30m DEM, the FastFlood model repeatedly crashed giving out of memory error. The Copernicus 30 m global DEM (GLO30) was downloaded from Open Topography (OpenTopography, n.d) . The Copernicus 30 m global DEM (GLO30) was created from the high resolution commercial radar data acquired through the TanDEM-X mission (2011 to 2015) and was reported to be superior to all other DEMs of similar spatial resolution (30m) (Li et al., 2022). The resampled DEM was then reprojected from the World Geodetic System (WGS) 1984 to Universal Transverse Mercator (UTM) 43 N in ArcMap. For input rainfall, three-day cumulative rainfall was used as it was found to better represent the flood in the region compared to one day, five-day and seven-day cumulative rainfall based on a previous Master's thesis study by Glas (2023) in the neighboring Pamba river basin. Additional parameters like Land cover (World Cover 10m) and Infiltration (based on Soil grids 2.0) for the model domain were downloaded with in the FastFlood Tool itself.

The Manning's surface coefficient is defined by the land cover used. The FastFlood allows automatic downloading of the ESA WorldCover 10 m data. The world cover data is a global land cover dataset which were created using advanced image recognition techniques and data from Sentinel-1 and Sentinel-2, which includes both radar and optical imagery. This map categorizes the Earth's surface into 11 distinct land cover classes at a high resolution of 10 meters. The default values for different land cover types in FastFlood model is shown in Table 18 in Annexure 1.

The infiltration rates were derived within the FastFlood model using the pedotransfer functions based on Saxton et al. (1986) and the global predictions of soil texture and organic matter content from the SoilGrids data. SoilGrids is a comprehensive global soil mapping initiative designed to produce detailed maps of soil properties at a medium spatial resolution (250 m cell size). The development of SoilGrids involves the application of advanced machine-learning techniques to a vast collection of soil observations (240,000) and 400 global environmental covariates(Poggio et al., 2021)

Automatic channels were derived from FastFlood were not able to represent the channels in the region accurately, especially the bifurcation of the river. Figure 8a shows the modelled flood before editing the channel, does not show the bifurcation of the river at Aluva (marked in red) and shows that the majority of the water flows to the southern branch, which is not the case. The channels were further edited using the channel edit tool in Fast Floods, which allows the drawing of channels and culverts. Figure 8b shows the floods modelled after correcting the channels; even though the flood models depicted the bifurcation, the southern branch of the river show reduced flow.

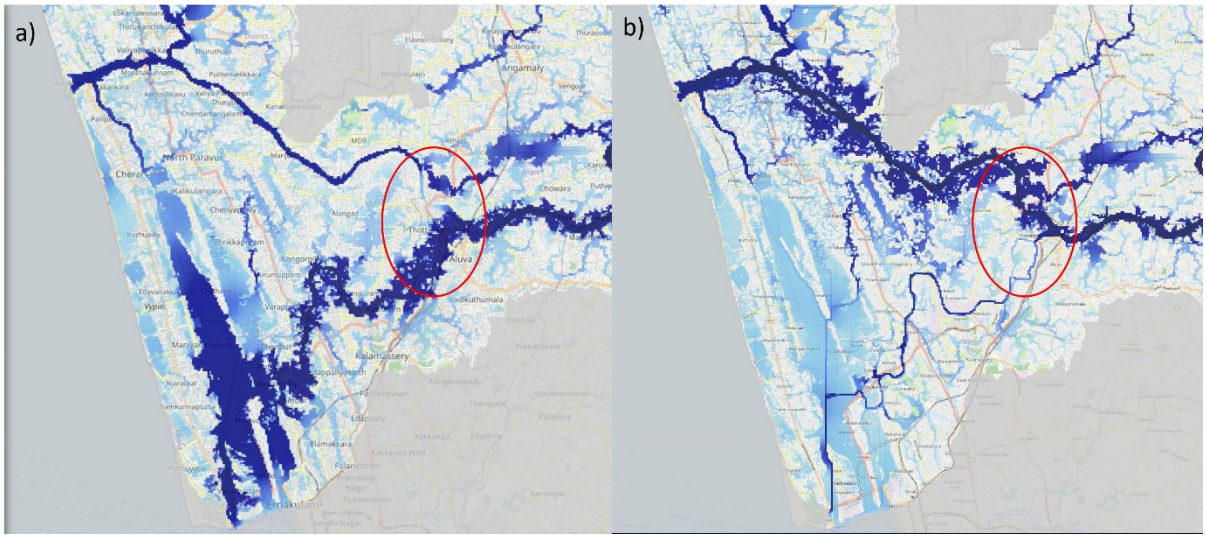

Figure 8: a) The flood modeled before channels edits b) The flood modeled using edited channels.

4.2.2.Calibration of FastFlood

A dataset depicting the 2018 historic flood extent was obtained from KSDMA and used as the observation data for computing the flood modeling error. This historic flood extent was created by the National Remote Sensing Centre (NRSC) from a combination of radar images that was analyzed during the 2018 floods. Since there were no metadata along with this data the exact radar images used to create the flood layer is not known. This was still used as the observed extent as it was officially recognized as the 2018 flood extent by the authorities. This historic flood extent map did not contain the permanent water bodies, and was merged with the map of the permanent water bodies which was also provided by KSDMA to create a comparable observed flood extent in Tiff format with a similar grid size as the simulated flood extent (90m).

To accurately model the peak discharge from the flood simulation it should be compared with the observed peak discharge. The Kalady river gauge was missing the discharge data during the peak event of 2018.Sudheer et al. (2019) used Gridded precipitation datasets of Integrated Multi-satellite Retrievals for GPM (IMERG) to reconstruct 2018 floods in the Periyar River basin and reported that the return period of the rainfall during the 2018 flood in the Periyar River basin was 145 years and the return period of discharge was 142 years. Hence, the 142-year return period discharge of Kalady station calculated using the Gumbel analysis was used as the observed peak discharge.

The FastFlood model was calibrated by modifying parameters such as infiltration, Mannings coefficient, channel dimensions and concentration speed. Considering the large extent of the study area, solver accuracy was kept very high, which will increase iterations of fast sweeping model in the model set-up but also increase the time to run the model (Glas,2023). The model performance was derived using performance indicators such as Cohens Kappa, percentual accuracy and error in peak discharge. To derive the performance indicators the model, classifies pixels of the modeled flood map, based on the observed flood map to true positive (TP), true negative(TN), false positive (FP) and false Negative (FN) and the performance indicators are derived as follows within the model:

$$Percentage\ Accuracy\ =\ (TN\ +\ TP)/(TN + TP + FN + FP)$$

$$Cohens\ Kappa = (((TP + TN)/N) - ((TP + FP)/N + (TN + FN)/N))/(1 - ((TP + FP)/N + (TN + FN)/N))$$

Ranges of Cohens Kappa values and corresponding strength of agreement is given in Table 4 (Landis & Koch, 1977).

Cohen's Kappa	**Strength of agreement**
<0.00	Poor
0.00–0.20	Slight
0.21–0.40	Fair
0.41–0.60	Moderate
0.61–0.80	Substantial
0.81–1.00	Almost perfect

Table 4: Ranges of Cohen's Kappa and their strength of agreement.

Once the flood model was calibrated, flood maps with flood heights for 20 and 100-year return periods were generated for the region.

4.2.3. Population exposure analysis

To calculate the population exposed to 20 and 100-year return periods of floods, population data for the region was downloaded from the WorldPop website (Bondarenko et al., 2020). The primary method for generating WorldPop products involves a weighted dasymetric technique that utilizes a random forest model which creates a predictive weighting layer to dasymetrically redistribute population counts into gridded cells(Leyk et al., 2019). From the Worldpop datsets, the "constrained individual countries 2020 UN adjusted" dataset was used. This was developed by Bondarenko et al. (2020) using a top down method, adjusted to match the United Nations national population 2020 estimates.

This gridded dataset for India was created based on the 2011 census, and the growth rate for the period from 2001 to 2011 was then used to calculate the projection for 2020. This population data with the number of people per pixel for the entire India was first clipped to the study area to calculate the exposure to floods.

The population data had an initial spatial resolution of about 100m; this was further reprojected to UTM zone 43 and re-gridded to the same spatial resolution as the flood map (90m). The re-gridding was done using the nearest neighbour interpolation method in ArcMap. The re-gridded data was aggregated for the lowland, midland and highland to ensure the population remained the same. The flood map with flood heights was reclassified to a binary flood extent map (flood and no flood) and was used to mask the exposed population. The spatial analyst tool in ArcMap was further used to calculate the number of people exposed to floods in the lowlands, midlands and highlands, respectively, for 20 and 100-year return periods.

4.3.Analyzing future hydrometeorological hazards

To derive future climate data, General Circulation Models (GCMs) are essential. However, the coarse resolution of GCM outputs makes them unsuitable for direct use at regional and basin levels (Jaiswal et al., 2020). These GCMs should be downscaled to a higher resolution using either statistical or dynamical methods and bias corrected to address the systematic errors before using them on a regional scale (Kim et al., 2022). Mishra et al. (2020)

developed bias-corrected gridded maximum temperature and precipitation using Empirical Quantile Mapping (EQM) (statistical downscaling method) for different climate scenarios using 13 General Circulation Models (GCM) at a spatial resolution of 0.25° x 0.25° (About 27 Km in Kerala) for 18 river basins in India. Bias correction was performed using the IMD gridded temperature and precipitation datasets.

Using multi-model ensembles of several GCMs have shown to improve the reliability of future projections by averaging out individual model biases and uncertainties (Jose et al., 2022). Multi-model ensembles can be created by either calculating the mean or median of a set of General Circulation Model (GCM) outputs or by assigning weights to different GCMs based on their historical performance. However, this process involves extensive data processing and analysis, which can be time-consuming. Due to the time limitations, a single well-performing climate model was chosen as a representative future scenario for the region.

To model the Future climate, the bias-corrected Earth Consortium 3 (EC 3) climate model was selected from the 13 bias-corrected GCMs created by Mishra et al. (2020); this was based on several studies which reported that EC Earth 3 climate model performs well in modelling the Indian monsoon. The EC Earth 3 climate model was developed by the European EC-Earth consortium with the Swedish Meteorological and Hydrological Institute (SMHI). Mitra, (2021) conducted a comparative study on the skill of the 13 bias-corrected GCMs developed by Mishra et al. (2020) to model the daily spatial pattern of the Indian monsoon using a machine learning based probabilistic graphical model which can identify spatial clusters and found that EC Earth3 performed robustly in modeling the spatial clusters and spatial patterns of monsoon rainfall over India. Reshma & Arunkumar, (2023) used the bias corrected GCM models from Mishra et al. (2020) and ranked them using multi-criteria analysis using correlation coefficients (R), Nash-Sutcliffe efficiency (NSE), normalized root-mean-square error (NRMSE), and absolute normalized mean bias error (ANMBE) as performance metrics to study the change in stream flow in Idamalayar basin (a sub basin of Periyar). The study found that among the 13 bias corrected GCMs EC Earth 3 performed the best.

The SSP2-4.5 and SSP5-8.5 climate scenarios were used to extract different possible pathways for the future. SSPs are Shared Socioeconomic Pathways which consider both the socioeconomic dimensions of climate change adaptations and mitigations along with the emission scenarios. The SSP2-4.5 scenario is often referred to as the middle-of-the-road approach that represents a scenario where global development and technology resemble the historic pattern and the emissions by 2100 is 4.5 W/m^2. The second scenario SSP5-8.5, referred to as "Taking the highway" represents a world that remains heavily dependent on fossil fuels and the emissions would reach 8.5 W/m^2 by 2100 (Riahi et al., 2017). These scenarios are chosen to model intermediate and extreme possible conditions for the future in the study area.

4.3.1.Preprocessing and Extraction of climate data

The EC Earth 3 bias corrected datasets for Indian sub continental river basin from Mishra et al. (2020) were downloaded from Zenodo.org(Mishra et al., 2020a).

This datasets was divided in to 18 sub continental river basin files in text format and contained the maximum temperature and precipitation data for the period 2015 to 2100 for different SSP scenarios. The data for the study area was partly in two sub continental river basin files (the west coast and the south coast).The temperature and precipitation data for both these files were downloaded and combined in to a csv file. Thich was then converted to a NetCDF file using the "table to NetCDF "tool in the ArcMap. The NetCDF file created was then re-gridded using CDO to the same grids as the IMD gridded data. Once

the maximum temperature and precipitation data were extracted for SSP2-4.5 and SSP5-8.5 scenarios, it was then used to extract maximum temperature and rainfall values for the five stations. The data for the stations were extracted using the nearest neighbor interpolation in CDO.

4.3.2.Correlation Analysis

To examine the suitability of the EC Earth 3 climate model data for representing the region a Pearson correlation analysis was done for both precipitation and maximum temperature with the EC Earth 3 and IMD4 datasets for the common time period between 1986 and 2014 , as the historical period of the EC Earth 3 is from 1951 to 2014 and the available historical observation data is from 1986 to 2023. Correlation analysis was done for only four stations (Irinjalakuda, Aluva, Munnar and Idukki) because the EC Earth 3 data was not covering the pixel of the Kodungallur station. The sample extent of the EC Earth 3 dataset is shown in Figure 9.

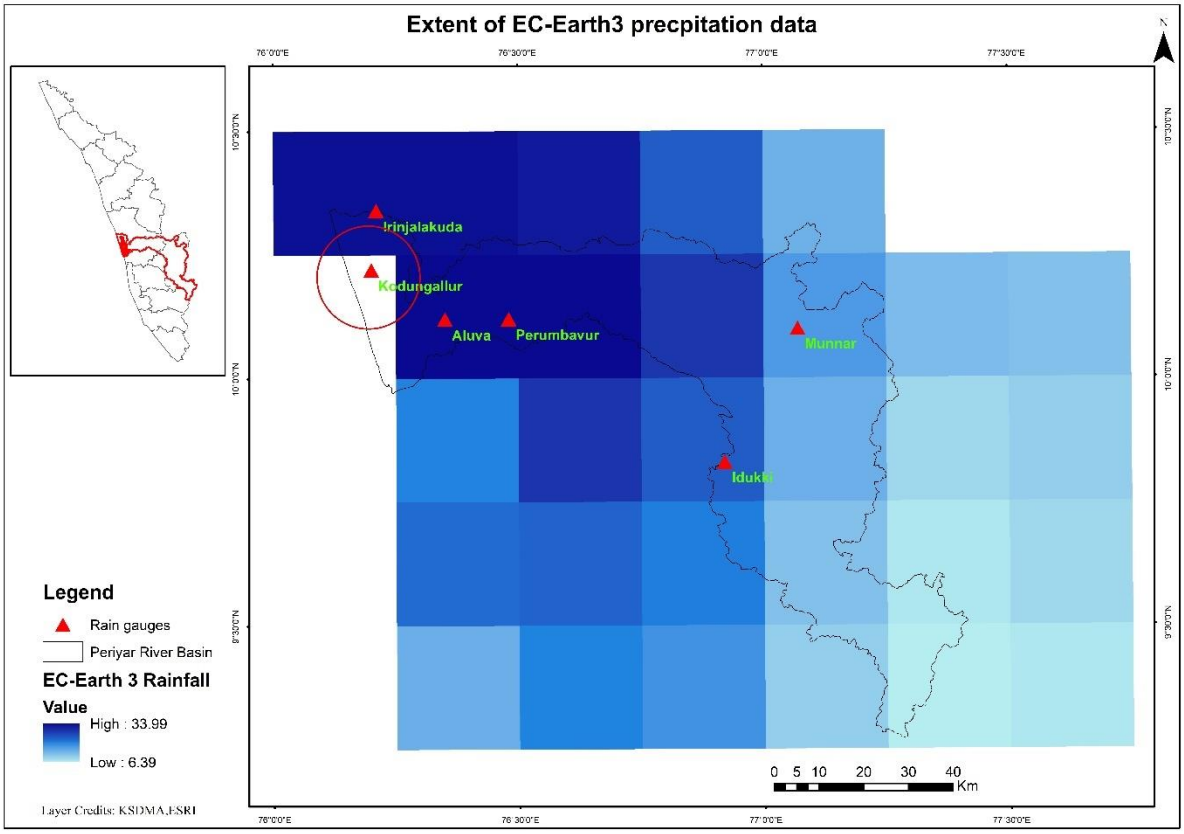

Figure 9: The extent of EC Earth 3 precipitation data. The red circle shows the Kodungallur station, which is not covered by the EC Earth 3 extent.

4.3.3.Calculation of Precipitation Extreme Indices

To analyze the precipitation extremes for the future period (2015-2100), extreme precipitation indices defined in section 4.1.4, such as "*very heavy precipitation days*"(R20mm), "*heavy precipitation days*" (R10mm) and "*extremely wet day precipitation*" (R99p) were used.

The daily precipitation data extracted for each station for the Scenarios SSP2-4.5 and SSP5-8.5 were used to calculate the precipitation extreme indices using a Python script. The calculated indices were further averaged for near term (2015-2045), medium term (2046-2075) and Far term (20176-100) to analyze the relative difference in precipitation extremes. Even though this approach would smoothen the extremes was still used to denote the relative changes in the future terms.

Since there were only one station each in low land (Irinjalakuda) and mid land (Aluva), they were used to represent the low land and mid land respectively. However for the high land there were two stations available (Idukki and Munnar), the mean of these stations were used to represent the high land region. The extreme precipitation indices were calculated station wise as well as region wise for different future periods under SSP2-4.5 and SSP5-8.5 scenarios.

4.3.4.Calculation of Temperature Extreme Indices

To analyze the temperature extremes in the future period, the extreme temperature indices which were defined in section 4.1.6 ,such as the "*maximum value of daily maximum temperature*" (TXx) and the " *number of warm days*"(TX90) were calculated. For the 90th percentile calculation the base period from 1986 to 2023 was kept constant, this was done so that it would be able to compare the change in extreme events directly to the historic conditions. The indices were calculated for both the SSP scenarios (2-4.5 & 5-8.5) for low land, mid land and high land.

4.3.5.Analyzing future heat waves

For identifying the Heat waves in the future climate, the normal temperatures based on the period 1986 to 2015 were used, similar to the historical occurrence analysis. This was done for mainly two reasons, one to compare directly the changes in heatwaves in historic and future periods and secondly, even if higher temperatures becomes the new normal, it is still going to have an impact on the people. The number of heat waves and their intensity was calculated for the SSP2-4.5 and SSP5-8.5 scenarios using the methodology described in section 4.1.7. Also the average change in intensity and frequency of heat waves are calculated for the near, middle and long term.

4.3.6.Flood simulation for future scenarios

To model flood for the future scenarios, the FastFlood model which was calibrated using the 2018 flood was used. The land use parameters of the flood model were not changed and the same land use was assumed for the region through out the future period. Even though this assumption is unrealistic, very low resolution of global future land use and the added complexities in modelling this and high level of uncertainties lead to the decision to continue with the same land use parameters used in the historical period.

The event duration values were maintained at 72 hours and for the rain fall intensity values three-day cumulative rainfall values corresponding with 50 and 100 year return periods were used for the near, medium and far terms. These return periods were calculated by first dividing the future period to three: near term which is the period from 2015 to 2045, medium term corresponds to the period from 2046 to 2075 and the far term is the period from 2076 to 2100. For each of these period the three-day cumulative rainfalls were used to calculate the rainfall corresponding to different return periods using the Gumbel analysis discussed in section 4.1.1.

The flood model was run using the 20 and 100 year return period of the three-day cumulative rainfall for the near term , medium term and far term for the scenarios SSP2-4.5 and SSP5-8.5 to generate corresponding flood maps.

4.3.7.Population exposure analysis for future

To analyze the exposure of population in the future scenarios, global population grids dataset created by X. Wang et al. (2022) was used. These gridded datasets were global population projections from 2020 to 2100 for different SSPs developed from the WorldPop dataset using a Random forest model. The gridded datasets, with a spatial resolution of approximately 1km, are widely used for climate change-related studies (Trancoso et al., 2024;Liu et al., 2024).

Since the population data was at a very low resolution compared to the flood layer (90m), it needed to be re-gridded to a higher resolution for better exposure analysis. The population data was first reprojected from WGS84 to UTM 43N.Then the reprojected data was re-gridded to 90 m using the nearest neighbor interpolation method. The resulting population data was aggregated for the regions (lowland, midland, high land) and were compared with the aggregated sum calculated using the original population data (1Km).It was found that the re-gridded data was exactly 10 times more than the original data due to the nearest neighbor interpolation. The re-gridded data was then corrected using the raster calculator in ArcMap by dividing it by a factor of 10.The re-gridded population data is then used to calculate the exposure to floods and heat waves.

The flood layers simulated for both the SSP scenarios and for various time periods (near , medium and far) where used as the hazard layers and the projected population data for similar periods were used as the element at risk layer. The exposure was calculated by first masking the population layer with the flood layer and then using the zonal statistics tool in ArcMap. The exposure to floods for the low land, mid land and high land were calculated for the combination of both the SSP scenarios and for different future periods.

For the exposure calculation for heat waves, since the analysis was based on only point data, if a station is found to have heat wave in a period then the whole region is assumed to be exposed to heat waves. Essentially this means that the exposure to heat waves will be same as the total population in each region across different time periods and SSP scenarios. This was calculated using the zonal statistics tool in ArcMap. Table 5 shows an overview of the datasets that were used in this study.

S.No	Dataset	Resolution		Source
		Temporal	Spatial	
1	Copernicus DEM	NA	30 m	Open Topography
2	EC Earth 3 Precipitation	Daily	27 Km	Mishra et al.2020
3	EC Earth 3 Temperature	Daily	27 Km	Mishra et al.2020
4	IMD Gridded rainfall	Daily	27 Km	Indian Meteorological Department
5	IMD Gridded Temperature	Daily	100 Km	Indian Meteorological Department
6	River discharge station data	Daily	NA	Kerala State Disaster Management Authority
7	Historical Flood	NA	NA	Kerala State Disaster Management Authority
8	IMD station rainfall	Daily	NA	Indian Meteorological Department
9	World pop population	NA	90 m	Worlpop hub
10	Future population distribution	5 year	900 m	Wang et al. (2022)

Table 5: Overview of the datasets used in the study.

Chapter 5: Results

This chapter presents the results obtained using the methodology discussed in the previous chapter.

5.1.Historical events

The first objective was to analyze the hydrometeorological extreme events in the historical period in the Periyar river basin using the discharge, rainfall and temperature data. The following subsection present the results of this analysis.

5.1.1.River discharge analysis.

The river discharge data from 1980 to 2020 is used to analyze the return period values using the Gumbel analysis, and the results are shown in Figure 10. The return period up to twice the length of the available time series could be derived through Gumbel analysis (El Adlouni & Ouarda, 2010). The discharge data used for Gumbel analysis had a record of 40 years, so it was used to interpolate to derive discharge values up to an 80-year return period.

Figure 10 shows that even though the Kalady gauge is upstream of the other two gauges, it has a higher discharge because the river bifurcates before reaching the other two stations. It is also possible that the missing values in the Marthandavarma and Mangalapuzha river gauges have caused the underestimation of discharge in these two gauges. Return periods of discharge for the three stations are shown in Table 6. The return periods of Marthandavarma and Mangalapuzha are calculated with limited discharge data and is highly likely to be underestimated.

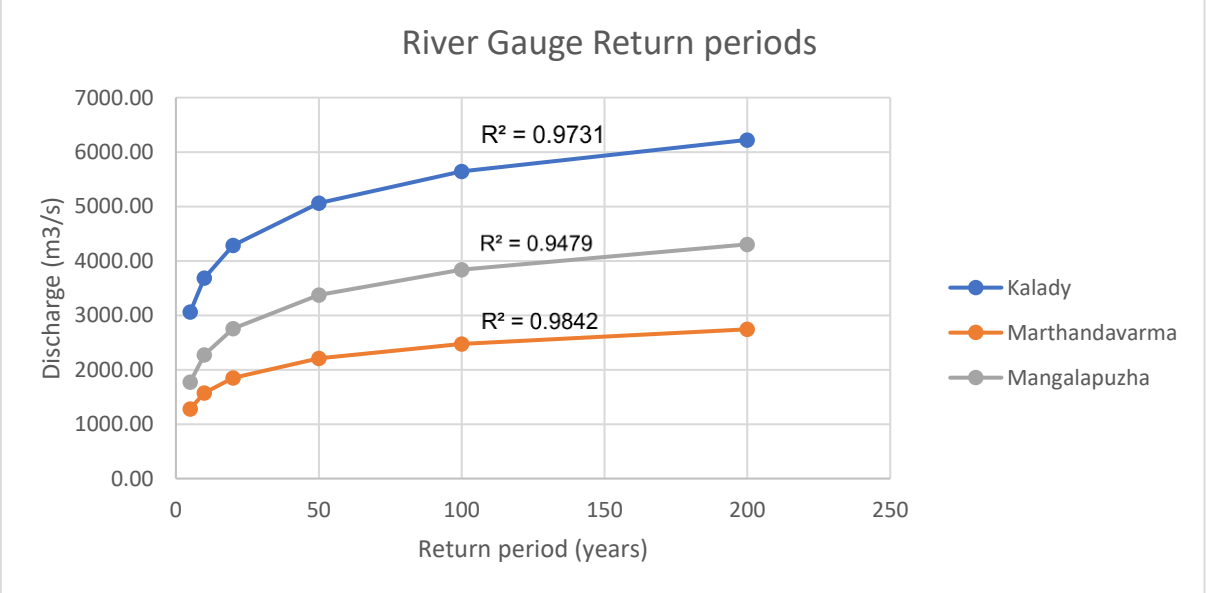

Figure 10:River discharge return periods of River Gauges in the Periyar River Basin

Return period	Discharge (m^3/s)		
	Kalady	Marthandavarma	Mangalapuzha
5	3060	1283	1773
10	3685	1571	2274
20	4285	1848	2754
50	5062	2207	3375
80	5457	2389	3691

Table 6:Discharge corresponding to various return periods for the river gauges in Periyar River basin.

As discussed in section 4.1, the gauges Marthandavarma and Mangalapuzha were missing quite some data and only the Kalady gauge was used to analyze the flood occurrences in the past. Figure 11 shows the maximum daily discharge recorded in the Kalady gauge and the events when it crossed the 5 year return period threshold. In the previous two decades between 1980 and 2000 no recorded discharge exceeded the 5 year return period threshold. On contrary the decade after 2000 show multiple events exceeding the threshold. The events and their corresponding return period are shown in Table 7. This change in trend might indicate an influence of climate change and the return period calculation based on the whole period might have under estimated the river discharge return periods.

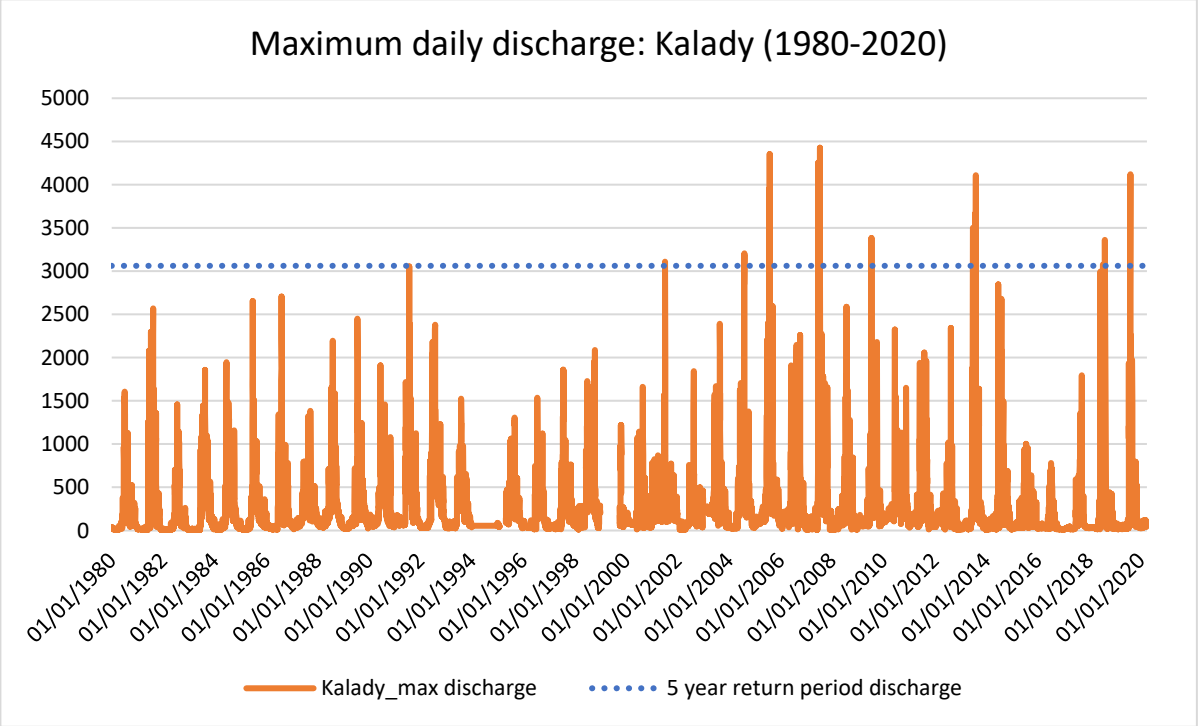

Figure 11: Maximum daily discharges recorded in the Kalady gauge for the period of 1980 to 2020.

Intensity of discharge	Years
5 year RP	2001,2004,2005,2007,2009,2013,2019
10 year RP	2005,2007,2013,2019
20 year RP	2005,2007

Table 7: Years in which various return period events were identified.

It is to be noted that the 2018 flood event is shown as only a 5 year return period event in the graph due to the missing data during the peak of the floods. The discharge corresponding to the event was calculated to be a 142 year return period event as discussed in section 4.2.2.

5.1.2.Correlation analysis

To compare the IMD gridded data and the IMD station data, Pearsons correlation analysis was conducted shows statistical significance for all values with near zero p values. The correlation coefficient values ranged from 0.4 to 0.6 implying a weak positive to moderately positive correlation. Idukki station in the high lands showed the lowest correlation while, Aluva station in the midlands showed the highest correlation. The correlation of Kodungallur station is given in Figure 12a and the corresponding annual precipitation recorded in the rain gauge and IMD gridded data is shown in Figure 12b. Similar plots for the other four stations are shown in Figure 29 of Annexure 1. Figure 12b shows that both the datasets show similar values throughout the time period and only show different values during the years where the station data records very high values. After 2012, no such anomaly in rainfall was observed in the station data.

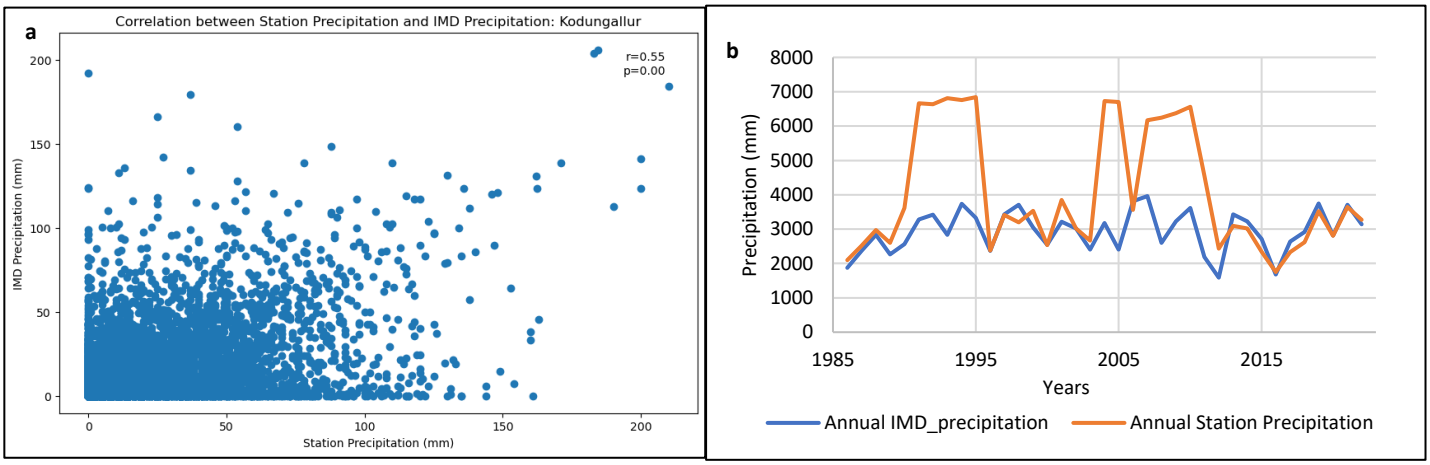

Figure 12: a) Correlation analysis between station rainfall and IMD gridded rainfall for Kodungallur station. b) Annual rainfall comparison between IMD gridded data and the rain gauge station data from 1986 to 2022.

5.1.3.Precipitation extreme indices

The very heavy precipitation days (R20mm) for the stations in the low and mid lands show similar trend with the highest peak recorded in 2007. The highland stations of Idukki and Munnar show comparatively lower 'very heavy precipitation days'. Figure 13a shows the trend in very heavy precipitation days. The midland regions received the highest R20mm rainfall days through out the period. The low and midlands shows a declining trend from 2010 while the highlands shows a steady increase. The average R20mm days for each period are shown in Table 8.

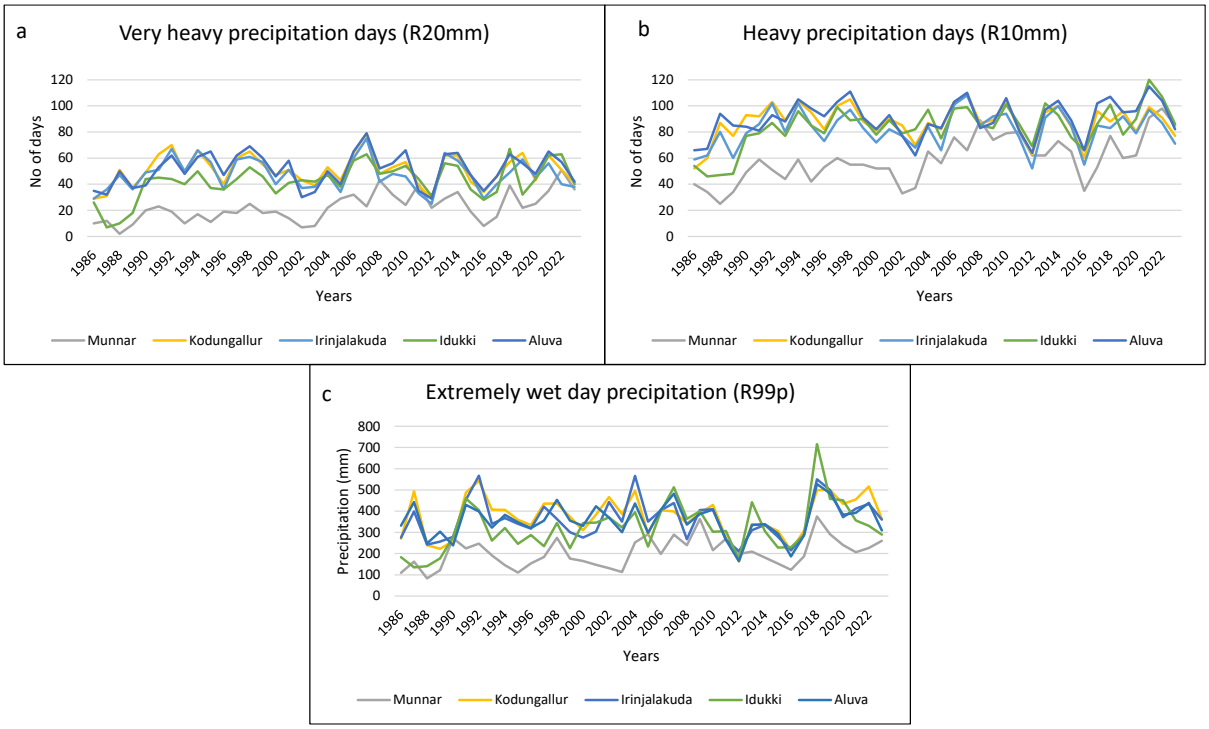

Figure 13: (a) Very heavy precipitation days calculated for the stations in Periyar river basin for the period 1986 to 2023 (b) Heavy precipitation days calculated for all stations in the Periyar River basin. (c) Annual sum of precipitation for days exceeding the 90 percentile rainfall based on the period 1986 to 2023.

Heavy precipitation days (R10mm) shows a similar trend as very heavy precipitation days with mid lands and high lands showing an increasing trend from 1986 to 2023, while the low lands shows an increasing trend from 1986 to 2010 and a decrease from 2010 to 2023. The average number of heavy rainfall days for each period is summarized in Table 8. For most stations, R10mm peaked in 2021, followed by 2007 and 1998. Munnar station shows the lowest heavy precipitation days throughout the period 1986-2023. Figure 13b shows how the number of heavy precipitation days has evolved from 1986 to 2023.

	Average R99p (mm)			**Average R10mm (days)**			**Average R20mm (days)**		
Region	**1986-2000**	**2001-2010**	**2011-2023**	**1986-2000**	**2001-2010**	**2011-2023**	**1986-2000**	**2001-2010**	**2011-2023**
Low lands	359	396	355	84	88	83	50	50	47
Mid lands	350	384	338	89	89	92	51	53	50
High lands	222	294	288	61	76	79	26	36	37

Table 8: Average values for R99p,R10mm and R20mm for the lowlands, midlands and highlands in different time periods.

The extremely wet day precipitation (R99p) for each station for the period 1986 to 2023 is shown in figure 13c. It shows a similar trend to the other precipitation indices , where low lands and midlands stations show a similar trend. The Munnar station shows the lowest R99p values. Unlike the other precipitation indices, R99p clearly shows the 2018 flood event with the highest recorded value for Idukki station. Table 9 shows the average change in R99p for lowlands, midlands and highlands for different time periods. All the

regions show an increasing trend from 1986 to 2010 and a decreasing trend from 2011 to 2023. The decrease is lowest, in high lands which is about a reduction of 2% while Midlands saw a reduction in 11.9% and lowlands a reduction in 10.3% respectively.

5.1.4.Extreme temperature indices

Figure 14a shows the warm days (Tx90) calculated for each station during the period 1986 to 2023. All the stations show similar trends with peaks exceeding 60 days in the years 2019,2016,2010 and 1998. While the number of hot days were lower in the years 2008,2011,2006,2000,1999 and 2015 with all stations having less than 20 warm days. The graph also exhibits a pattern of years with very high and very low Tx90 values repeating consecutively. Table 9, shows the average Tx90 values for lowlands, midlands and highlands for different time periods. All the regions shows a increasing trend from 2010 to 2023. Lowlands and midlands shows a similar trend throughout the period of analysis, however highlands shows a slight reduction in Tx90 values in the period 2001 to 2010.

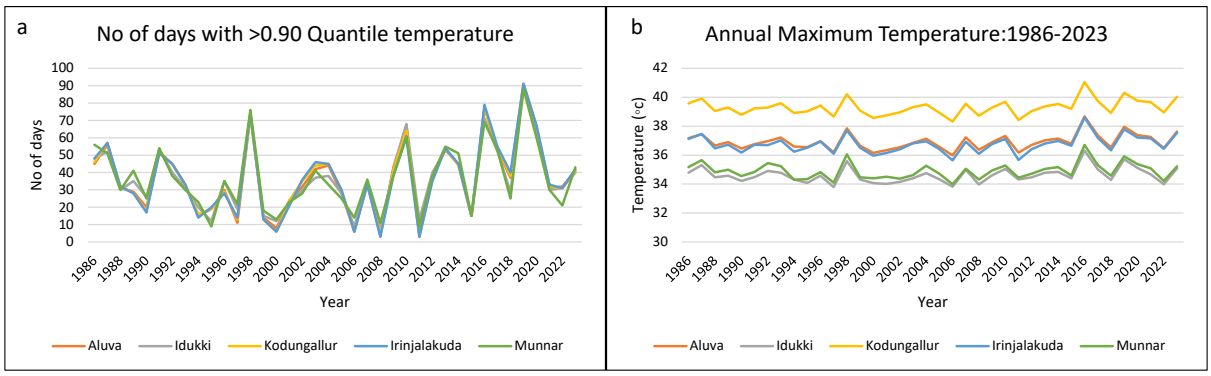

Figure 14: a) Number of Tx90 days for the five stations in the Periyar river basin for the period 1986 to 2023. b) Maximum value of maximum daily temperature (TXx) recorded each year for the five stations in Periyar river basin, from 1986 to 2023.

	Average Tx90 (days)			Average TXx (◦C)		
	1986-2000	**2001-2010**	**2011-2023**	**1986-2000**	**2001-2010**	**2011-2023**
Low land	32	32	45	37.96	37.82	38.26
Mid land	32	32	45	36.84	36.72	37.16
High land	34	31	43	34.72	34.56	34.98

Table 9: Average values of Tx90 days and TXx temperatures calculated for lowland, midland and highland for different time periods.

Annual maxima of maximum daily temperatures (TXx) for all the stations in the Periyar River basin is shown in Figure 14b. The highest temperatures were recorded in the Kodungallur station (lowland) followed by Aluva (midland) and Irinjalakuda (lowland) stations and the lowest were recorded in Munnar and Idukki stations (highlands). Highest maximum daily temperatures were recorded in the year 2016, followed by 1998 and 2019 for all the stations. Table 9 shows the change in average maximum temperature recorded in a year for the lowlands, midlands and highlands for different time periods. It shows that there was a slight decrease in daily maximum temperature for all the regions 1986 to 2010. Over all there is an increase of 0.76%,0.87% and 0.74% in the average maximum daily temperature recorded for lowlands, midlands and highlands respectively throughout the study period (1986-2023).

5.1.5.Heat waves

As per the IMD heat wave definition no heat waves were detected in the period 1986 to 2023 in the stations. Even though as discussed in section 3.1.2 there were instances of extreme high temperatures but only one heat wave warning was issued in 2016 for Palakkad region, which is not in the study region. Also the 2024 heat wave event is not captured as the data analyzed was for the period 1986 to 2023 due to the data availability. Hence the findings agree with the official heat wave records.

5.2.Calibrating the Flood model

The FastFlood model was run with different calibration settings to accurately represent the 2018 flood. Table 10 shows the parameters and the multipliers used for each parameter and the Cohens Kappa percentage accuracy and percentage error in discharge values that were obtained for each test. The test six with multipliers 1.4, 0.3, 1 and 1 for the parameters Mannings N, infiltration, channel dimension and concentration speed respectively showed the highest overall accuracy. It showed a percentage accuracy of 92%, Cohens Kappa of 0.34 and an error in the discharge of 0.47%.

Parameters	**Test1**	**Test2**	**Test3**	**Test4**	**Test5**	**Test6**	**Test7**	**Test8**
Manning's n	1.7	1.7	1.7	1.7	1.5	1.4	1.4	1.4
Infiltration	1	0.5	0.5	0.5	0.2	0.3	0.4	0.4
Channel dimensions	1	1	0.5	0.5	1	1	1	1.2
Concentration speed	1	1	1	0.5	1	1	1.2	1
Cohens Kappa	**0.34**	**0.34**	**0.37**	**0.38**	**0.33**	**0.34**	**0.34**	**0.31**
% Accuracy	**0.92**	**0.91**	**0.92**	**0.92**	**0.92**	**0.92**	**0.92**	**0.92**
% error in discharge	**22.00**	**4.40**	**8.60**	**90.50**	**0.70**	**0.47**	**2.17**	**2.17**

Table 10: Multipliers used for flood model calibration based on the 2018 floods and the accuracy values for each test.

Figure 15 shows the flood extent modeled with FastFlood and the observed historical flood extent for the 2018 flood. The FastFlood modeled floods shows higher flood extent in the highland and traces the smaller channels well in the study area.

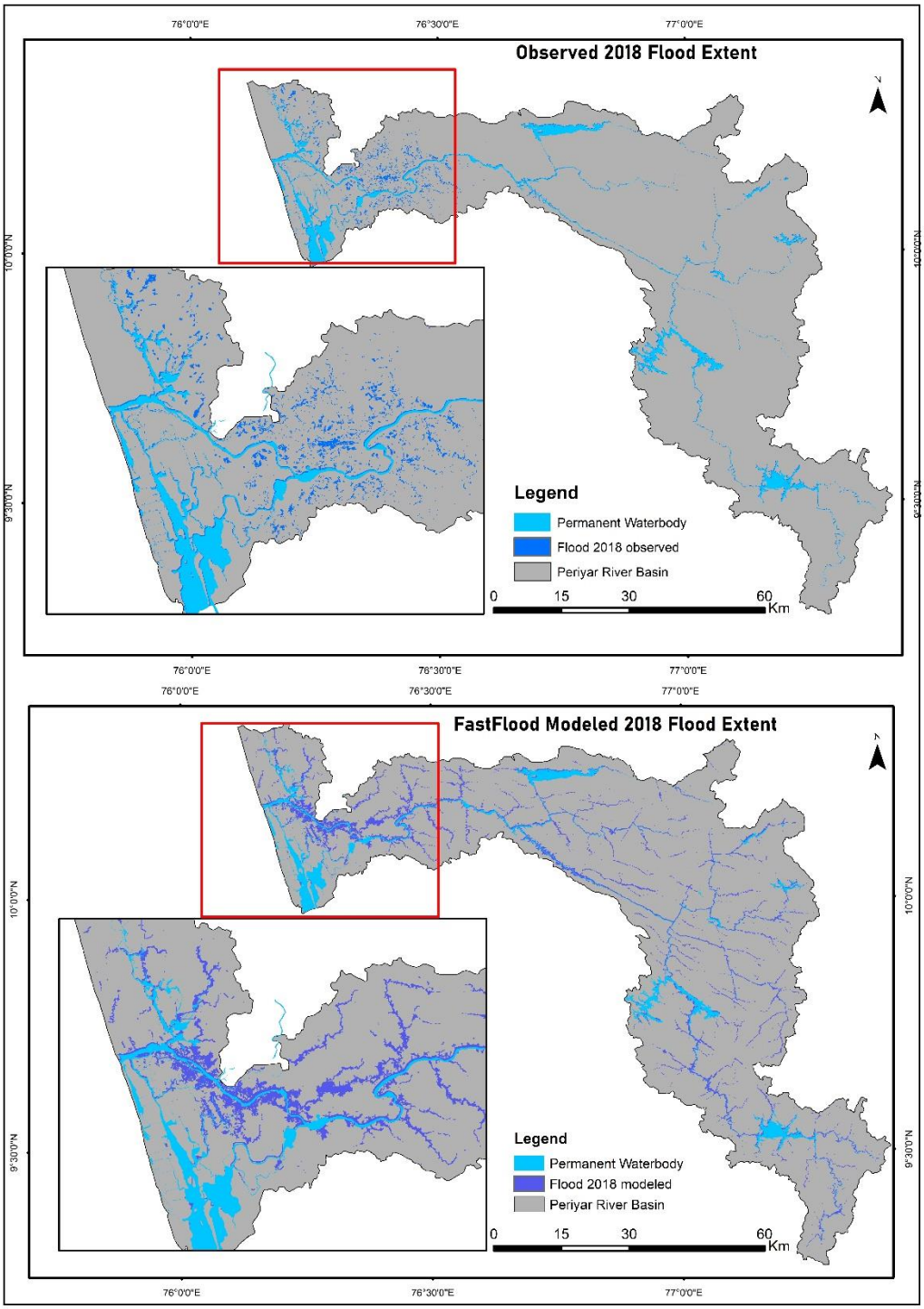

Figure 15: Flood extent comparison Observed flood 2018 extent and flood extent for the same event modelled in FastFloods. The zoomed in sub map is from the portion marked with the red box.

The 20 and 100 year return period of 3 day cumulative rainfall which were 351.3mm and 449.07 respectively were used to simulate corresponding flood extents. The 3 day cumulative rainfall were spread out uniformly in time for the duration of the event (72 hours) representing a uniform rainfall. The flood extent derived for the 20 year and 100 year return period are shown in Figure 16. The total flooded areas corresponding to the

20 and 100 year return periods are shown in Table 11. It shows that even though the increase in 3day cumulative rainfall from 20 to 100 year return period is 27.8%, it resulted in a flooded area change of about 47.1%.

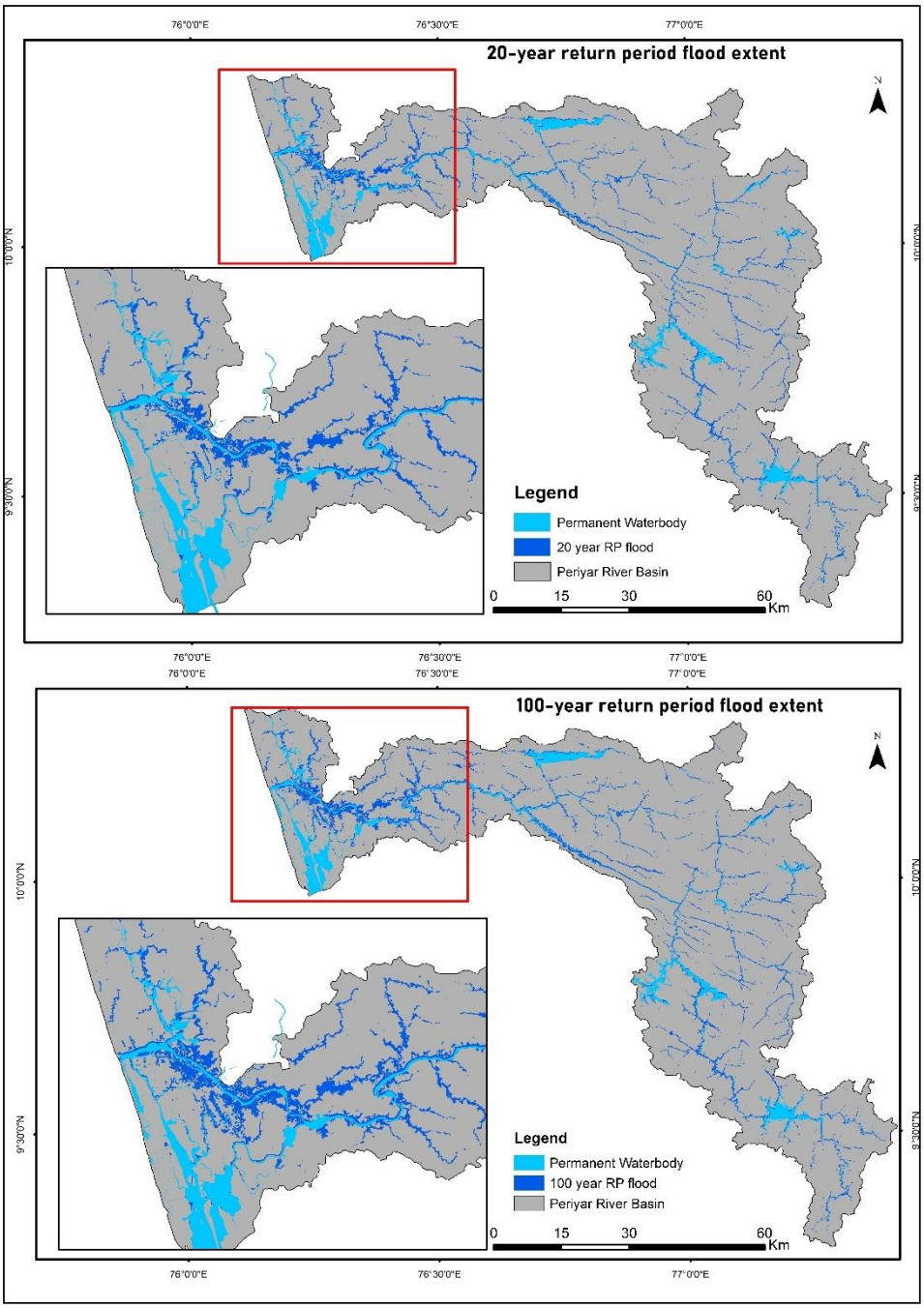

Figure 16: Simulated floods for 20 year return period and 100 year return period in the FastFlood model.

Flood return period	Area Flooded (Km^2)	3 day cumulative rainfall (mm)
20	111.05	351.3
100	163.45	449.07

Table 11: Total flooded area for the 20 and 100 year return period floods.

5.2.1. Population exposure

The population exposed in the Periyar river basin to different return period floods are shown in Figure 17. Midlands had the highest number of people that will be exposed to both 20 and 100 year return periods. For 20 year return period, it was found that 4.9%,11.45% and 8.61% of the population in lowland, midland and highland respectively, were exposed. Whereas, 7.2%,14.3% and 9.7% of the population were exposed in the lowland, midland and highland respectively, for a 100 year return period floods. Table 12 shows the Total population and the population that is exposed to 20 and 100 year return period floods.

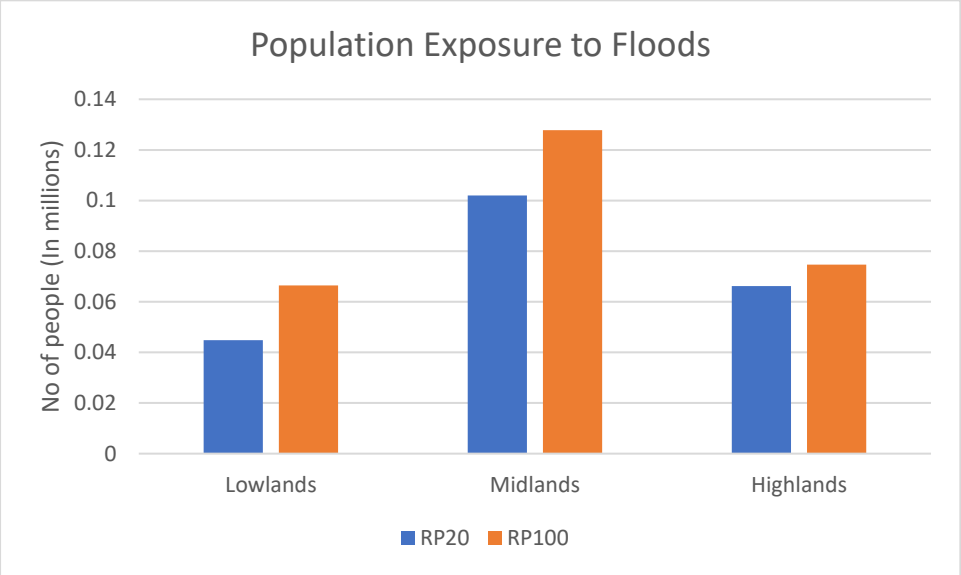

Figure 17: Population exposed to 20 and 100 year return periods in the lowland, midland and highland in the Periyar river basin.

Region	Total population	No of people exposed to floods	
		20 RP	100 RP
Lowlands	912884	44842	66421
Midlands	889450	101928	127804
Highlands	768813	66202	74680

Table 12:Total population and the population exposed to floods.

5.3.Analyzing future hydrometeorological hazards.

5.3.1.Correlation analysis

Precipitation

The Pearsons correlation coefficient calculated for daily rainfall values for all stations when comparing the gridded IMD data with the EC Earth historical data, ranges from 0.14 to 0.22 implying very weak positive correlations between the climate model data and IMD gridded precipitation data. It was not possible to use the original rainfall station data for the correlation analysis due to very high uncertainty and error as discussed in section 4.1.2.

Table 13 shows that the model predictions are found to vary from the actual values of 5.6 to 9.5 mm/ day. In the case of Aluva and Idukki stations, the model tends to overestimate precipitation, whereas, for Irinjalakuda and Munnar stations, the model underestimates the daily precipitation. The precipitation correlation plots for each station can be found in Figure 27 of Annexure 1.

	Irinjalakuda	Aluva	Idukki	Munnar
Correlation Coefficient:	0.21	0.22	0.2	0.14
Mean Absolute Error (mm/day):	9.51	10.54	8.86	5.6
Root Mean Square Error (mm/day):	19.82	20.32	17.06	10.84
Bias (mm/day):	0.27	-1.11	-0.26	0.29

Table 13: Correlation matrices calculated for the stations in Periyar River basin comparing the IMD gridded and EC Earth historical daily rainfall for the period 1986 to 2014.

Temperature

Table 14 shows Pearson's correlation values when comparing the IMD gridded data and the EC Earth 3 daily max temperature data from 1986 to 2014. The correlation coefficient ranges from 0.64 to 0.65 for all stations, implying a moderate positive correlation between the datasets. However, this was expected as the temperature has comparatively less time and spatial variation. The highest variation in correlation is found in Munnar station, where there is a significant difference between the IMD and EC Earth 3 datasets. The temperature correlation plots for each station can be found in Figure 28 of Annexure 1.

	Irinjalakuda	Aluva	Idukki	Munnar
Correlation Coefficient:	0.64	0.65	0.65	0.65
Mean Absolute Error (◦c):	1.99	1.74	1.2	10.44
Root Mean Square Error (◦c):	2.43	2.11	1.56	10.57
Bias (◦c):	1.46	1.42	-0.32	10.44

Table 14: Correlation matrices calculated for the stations in Periyar River basin comparing the IMD gridded and EC Earth maximum daily temperatures for the period 1986 to 2014.

5.3.2.Precipitation Extreme Indices

The precipitation indices calculated for SSP245 and SSP585 scenarios for the four stations in the Periyar River basin are discussed below.

Very Heavy precipitation days

The analysis of "very heavy precipitation days" (R20mm) under SSP2-4.5 and SSP5-8.5 scenarios reveals a general increase over time, particularly towards the far-future period (2076-2100). Figure 18 shows how the R20mm days change throughout each period under both the SSP scenarios.

Under SSP2-4.5, the lowlands and midlands exhibit the highest increase in R20mm days, with the lowlands showing a 23.8% to 28.5% increase, and the midlands a 21.7% to 25.9% increase when compared to the base period (2010-2023). The highlands, however, show a decrease of 6.0% to 9.7%. Under SSP5-8.5, a similar trend is observed with the highest increases in the far term, where lowlands show a 16.3% to 50.3% increase, midlands a 15.1% to 47.1% increase, and highlands show an initial decrease of 8.4% to 17.2% in the near and medium terms, but an increase of 20.2% in the far term. The averaged R20mm days throughout the future periods for both SSP scenarios are shown in Table 15. Aluva in the midlands consistently has the highest values for very heavy precipitation days, while Munnar in the highlands has the lowest. The percentage changes for each period is shown in Table 21 in the Annexure 1.

	Average R99p (mm)			**Average R10mm (days)**			**Average R20mm (days)**		
Scenario:SSP2-4.5									
Region	**Near term**	**Medium term**	**Far term**	**Near term**	**Medium term**	**Far term**	**Near term**	**Medium term**	**Far term**
Low land	437	581	511	93	96	99	58	59	60
Mid land	433	550	490	106	108	112	61	61	63
High land	277	351	313	75	77	77	33	35	34
Scenario:SSP5-8.5									
	Near term	**Medium term**	**Far term**	**Near term**	**Medium term**	**Far term**	**Near term**	**Medium term**	**Far term**
Low land	454	542	789	92	97	109	55	58	71
Mid land	445	506	685	104	108	121	58	60	74
High land	283	322	437	72	76	87	31	34	44

Table 15: Average values of extreme precipitation indices calculated for lowland, midland and highland for different time periods under scenarios SSP2-4.5 and SSP5-8.5.

Heavy precipitation days

From the analysis of heavy precipitation days (R10mm) under SSP2-4.5 and SSP5-8.5 scenarios, it is evident that both climate scenarios predict an overall increase in the number of heavy precipitation days in the future, particularly towards the far future period (2076-2100) .Figure 18 shows how the R10mm days change throughout each period. Regionally, the low land consistently show a higher increasing trend than the mid land and high land regions. The midlands exhibit the highest number of heavy precipitation days. Although the highlands show lower values overall, there is a noticeable decrease in heavy precipitation days in the near and medium terms under SSP5-8.5, followed by an increase in the far term. Munnar station in the highlands shows the lowest values throughout while Aluva in the midlands shows the highest values for heavy precipitation days for both the

scenarios. The averaged R10mm days throughout the future periods for both SSP scenarios are shown in Table 15.

When compared to the base period of 2010 to 2023, lowlands showed a percentage increase of 12.5 to 19, while midlands shows an increase of 14.9% to 21.4% and the highlands shows a decrease of 4.7% to 2 % respectively for the SSP2-4.5 scenario. While for the SSP5-8.5 scenario a percentage increase of 10.4 to 31.6 was observed for the lowlands, while midlands shows an increase of 13.3% to 31.6% and the highlands shows a decrease of 3.4% to 9.0% in the mid and near terms and showed an increase of 9.9% in the far term. The percentage changes for each period is shown in Table 22 in the Annexure 1.

Extremely wet day precipitation

The extremely wet day precipitation (R99p) for each station for the period 2015 to 2100 under the both scenario are shown in Figure 18.Under the SSP2-4.5 scenario, R99p peaks in the middle term (2046-2075) with the highest peak observed in 2074. The lowlands exhibit a significant increase in R99p values with 23.1%, 63.7%, and 43.9% increases for the near, medium, and far terms respectively, compared to the base period (2010-2023). The midlands show similar trends with 28.0%, 62.4%, and 44.79% increases for the same periods. The highlands show a 3.8% decrease in the near term but then increase by 22.0% and 8.7% in the medium and far terms.

Meanwhile, under the SSP5-8.5 scenario, the highest R99p values are found in the far term, with average values ranging from 437.9 mm/year to 789.6 mm/year. The averaged R99p days throughout the future periods for both SSP scenarios are shown in Table 15. Lowlands show the highest R99p values, followed by the midlands and highlands. R99p values show an increasing trend across the near, medium, and far terms for all stations. The lowlands see increases of 27.7%, 52.7%, and 122.1% for the near, medium, and far terms, respectively. The midlands show increases of 31.6%, 49.6%, and 102.5% for the same periods. The highlands initially show a slight decrease of 1.73% in the near term but then increase by 11.7% and 51.9% in the medium and far term. Detailed percentage changes for each period are shown in Table 20 in Annexure 1.

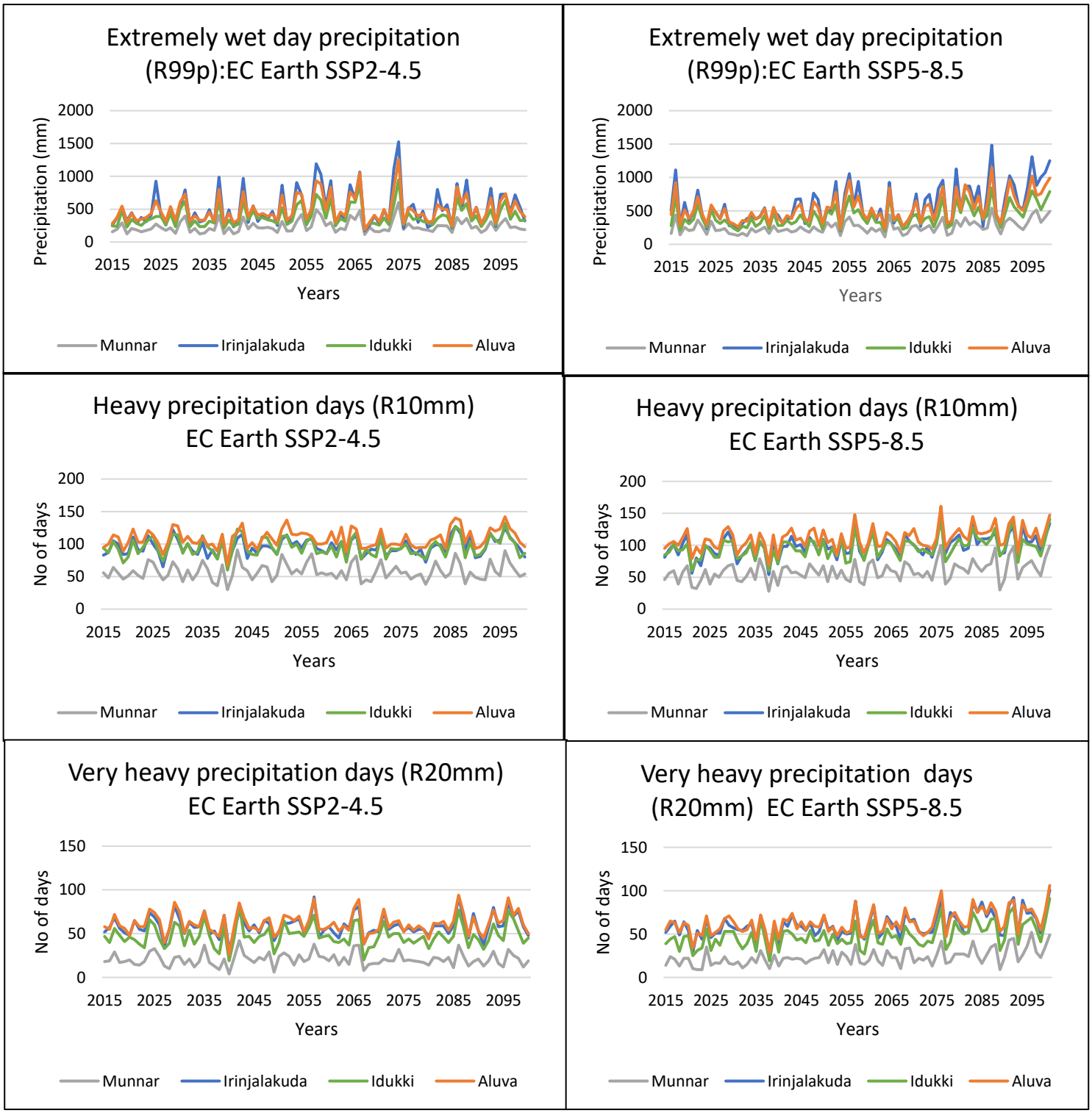

Figure 18: Extreme precipitation indices R99p,R10mm and R20mm calculated for the stations in Periyar river basin under SSP scenarios 2-4.5 and SSP5-8.5.

5.3.3.Extreme temperature indices

The Tx90 days, that is, the days exceeding the 90th percentile temperature for all four stations under scenario SSP2-4.5 and SSP5-8.5, are shown in Figures 19a and 19b, respectively.

Figures 19 a and 19 b show the evolution of Tx90 days under SSP2-4.5 and SSP5-8.5 scenarios, respectively. Under SSP2-4.5, all stations show an increase in Tx90 days throughout the periods, peaking in the far term (2076-2100). Average Tx90 days increase from 16 to 51 in lowlands, 18 to 50 in midlands, and 21 to 47 in highlands from the near to far term. An overall decreasing trend is observed in the near term compared to the base period (2010-2023), but an increasing trend from the medium to far term can be seen. Under SSP5-8.5, all stations exhibit a significant increase in Tx90 days, with the near term having the lowest and the far term the highest. Average Tx90 days rise from 2 to 85 in lowlands, 4 to 79 in midlands, and 8 to 67 in highlands from near to far term, with the far term showing up to an 89% increase compared to the base period (2010-2023). The percentage changes for different periods compared to the base period 2010 to 2023 are shown in Table 23 in Annexure 1. The averaged Tx90 days throughout the future periods for both SSP scenarios are shown in Table 16.

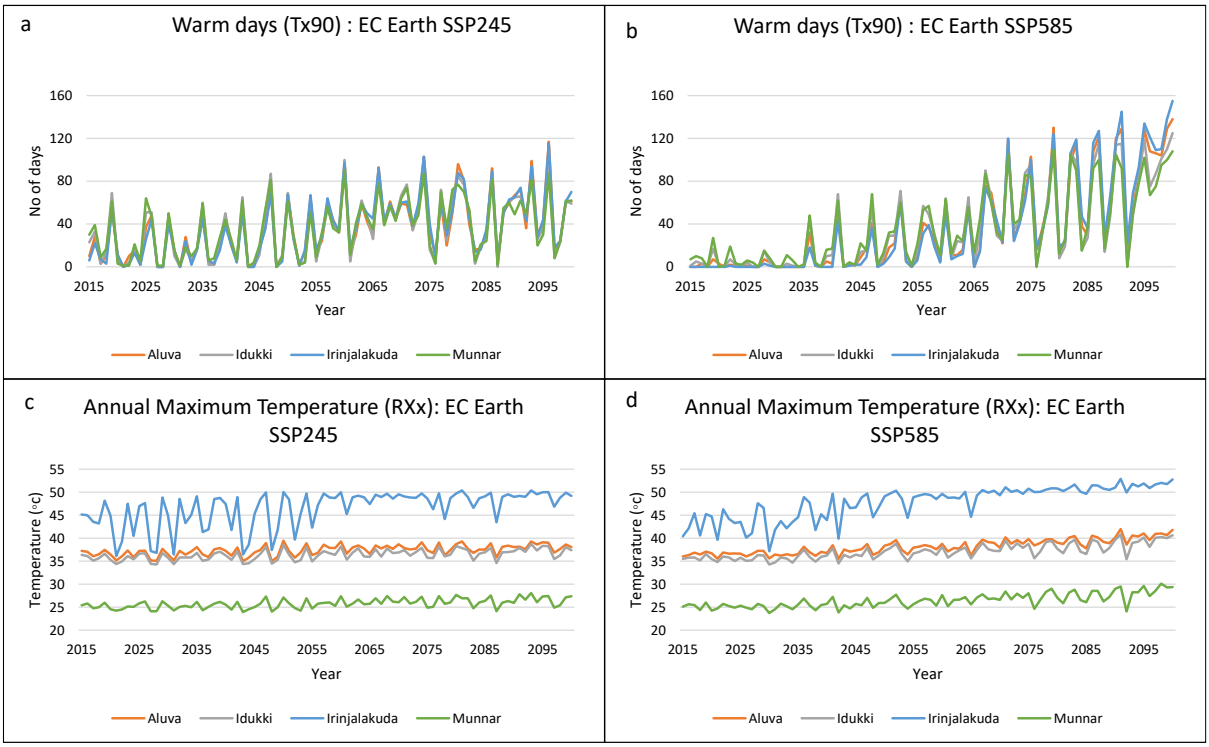

Figure 19: a) Warm days (Tx90) calculated for the scenario SSP2-4.5. b) Warm days (Tx90) calculated for the scenario SSP5-8.5. c) Annual maximum of daily maximum temperature (RXx) calculated for the scenario SSP2-4.5. d) Annual maximum of daily maximum temperature (RXx) calculated for the scenario SSP5-8.5.

The annual Maxima of maximum daily temperatures (TXx) for all the stations in the SSP2-4.5 and SSP5-8.5 scenarios are shown in Figures 19c and 19d, respectively. The Irinjalakuda station shows abnormally high values with a change of about 5 to 10◦c from the base period of 2010 to 2023. Other stations show similar trends, with the lowest maximum daily values recorded in the Idukki station. Both scenarios show an overall increasing trend in maximum daily temperatures from the near term to the far term, indicating a warming climate. Irinjalakuda station consistently shows abnormally high TXx values, with increases ranging from 5 to 10°C compared to the base period (2010-2023).

The lowlands experience significant temperature increases, particularly in the far term. While the midlands show a slight decrease in the near term, they show an increase in the medium and far term. The highlands show the smallest increase compared to other regions but still show a warming trend over time. The changes for the regions in different time periods under both SSP scenarios, compared to the base period (2010-2023), are shown in Table 24 in the Annexure. Under the SSP2-4.5 scenario, the highlands show 3.2°C to 4.5°C lesser temperatures than the base period, while the midlands show a decrease of 0.5°C in the near term and then an increase of 0.5°C to 0.8°C in the medium and far terms, respectively. The lowlands show an increase of 5.5°C, 9.3°C and 10.3°C for near, medium and far terms, respectively, when compared to the base period.

For the SSP5-8.5 scenario, highlands exhibit temperatures that are comparatively 1.78°C to 4.52°C lower than the base period. In the midlands, there is a decrease of 0.4°C in the near term, followed by an increase of 1.1°C to 2.7°C in the medium and far terms, respectively. The lowlands experience significant increases of 5.7°C in the near term, 10.7°C in the medium term, and 12.8°C in the far term compared to the base period. The maximum daily temperatures averaged over each future period (Average TXx) under both scenarios are presented in Table 16.

	Average Tx90 (days)			Average TXx (◦C)		
Scenario: SSP2-4.5						
Region	**Near term**	**Medium term**	**Far term**	**Near term**	**Medium term**	**Far term**
Low land	16	46	51	43.78	47.62	48.65
Mid land	18	44	50	36.61	37.68	37.98
High land	21	44	47	30.41	31.28	31.76
Scenario:SSP5-8.5						
	Near term	**Medium term**	**Far term**	**Near term**	**Medium term**	**Far term**
Low land	2	31	85	43.97	48.99	51.09
Mid land	4	34	79	36.69	38.30	39.89
High land	8	40	67	30.46	31.93	33.20

Table 16: Average values for exterme temperature indices calculated for lowland, midland and highland for different time periods under scenarios SSP2-4.5 and SSP5-8.5.

5.3.4.Heatwaves

The heat wave days calculated for the four stations in the Periyar River basin under scenarios SSP 245 and SSP 585 are shown in Figure 20. As it was observed in section 5.3.3, the maximum temperature values for the Irinjalakuda station were showing very high values; as a result a very high number of heatwave days are predicted in the station. The highest heatwave occurrences are predicted to be in the lowlands, followed by the

midlands and highlands. SSP585 scenarios also show a similar trend with the highest number of heatwave days predicted in the far term for all stations except in the lowlands.

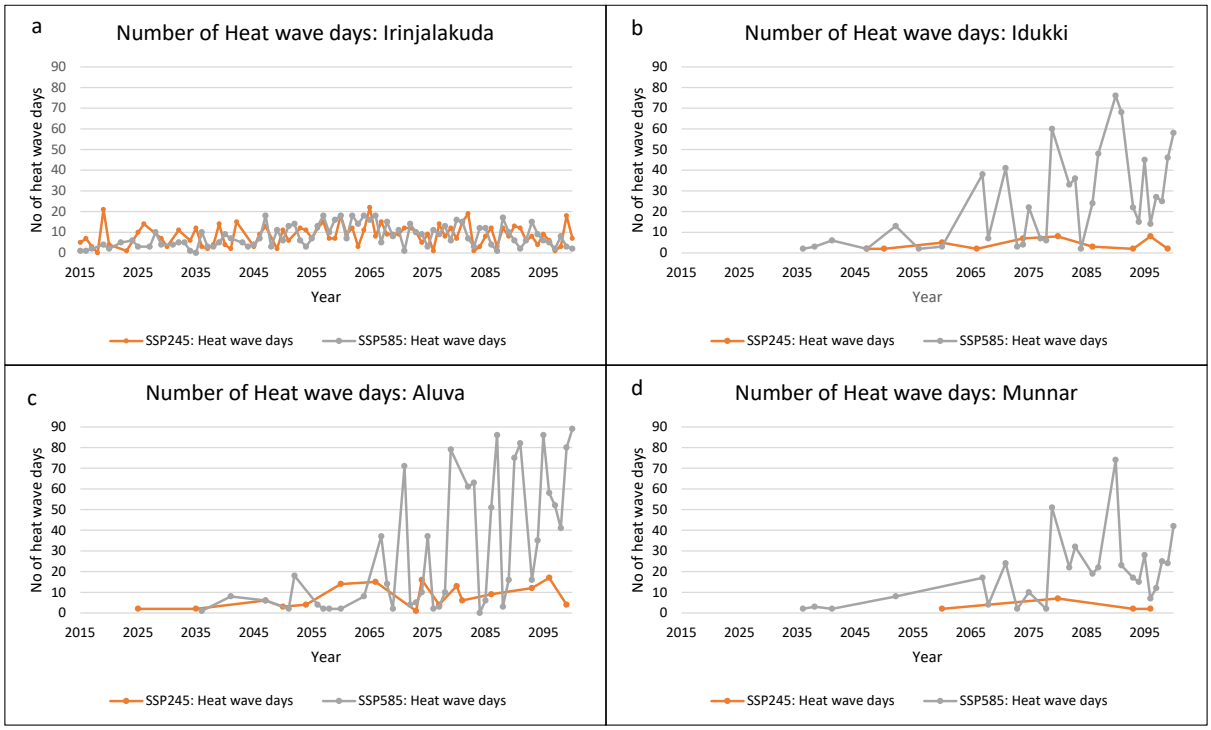

Figure 20: Heat wave days predicted for different stations under SSP scenarios SSP245 and SSP585. The figures a,b,c, and d shows the heat wave days for the stations Irinjalakuda, Idukki, Aluva and Munnar respectively.

The severe heat wave days calculated for the four stations in Periyar River basin under scenarios SSP 245 and SSP 585 are shown in Figure 21. The Irinjalakuda station shows severe heatwave days, even exceeding 150 days in the medium and far term for SSP585. Even the SSP 245 scenario shows a similar pattern with an abnormally high number of days predicted as severe heatwave days. Irinjalakuda station predicts a total of 2636 and 5250 severe heatwave days for SSP245 and SSP585 scenarios, respectively, for the entire period from 2015 to 2100. Aluva, the midland station, shows no severe heatwave for SSP245 and only 114 days for SSP585, of which 109 are predicted to be in the far term. Highland stations, Munnar and Idukki, also do not predict any severe heatwave throughout the period 2015-2100 for SSP245.In the SSP585 scenario, the highland stations only predict severe heatwaves in the far term, with Idukki predicting 24 and Munnar predicting 10 days of severe heatwave days. The number of heatwaves predicted for lowlands, each station in different time periods and SSP scenarios are presented in Table 25 in Annexure 1. The number of heat waves and severe heat waves calculated for each region under both climate scenarios are summarized in Table 17.

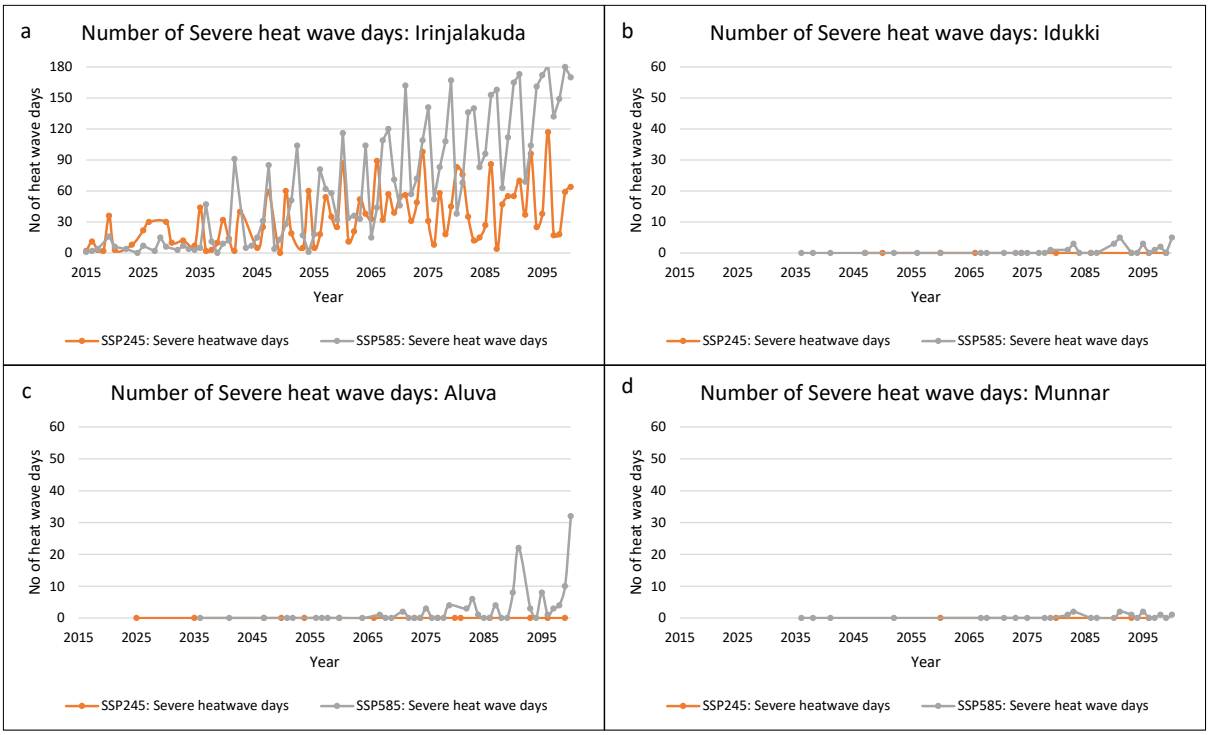

Figure 21: Severe heat wave days predicted for different stations under SSP scenarios SSP245 and SSP585. The figures a,b,c, and d shows the heat wave days for the stations Irinjalakuda, Idukki, Aluva and Munnar respectively.

Region	Period	No of heatwave days recorded		No of Severe heatwave days recorded	
		SSP245	SSP585	SSP245	SSP585
Low land	Near	151	105	328	282
	Medium	285	330	1143	1854
	Far	210	200	1165	3114
Mid land	Near	4	9	0	0
	Medium	59	224	0	6
	Far	65	994	0	109
High land	Near	0	9	0	0
	Medium	10	100	0	0
	Far	17	514	0	17

Table 17: Average number of heat waves and severe heat waves recorded in different regions in near, medium and far term futures under SSP scenarios SSP2-4.5 and SSP5-8.5.

5.3.5.Flood simulation for future scenarios

The flood maps were generated for the 20 and 100-year return period floods in the near term (2015-2045), medium term (2046-2075) and far-term (2076-2100) for scenarios SSP245 and SSP585. Figure 23 shows the flood map created for the 20 and 100-year return period in the near-term future under the SSP245 scenarios. Flood maps for other SSP scenarios and time periods are provided in section A.1 of Annexure 1. The future floods generated showed that the highest flood inundated area (392.1 Km^2) would be for the 100-year return period flood in the medium-term future under the SSP245 scenario. This is followed by the 100-year return period floods in the far term under the SSP585 scenario. Figure 22 shows the total area flooded for different return periods of floods in the SSP245 and SSP585 scenarios.

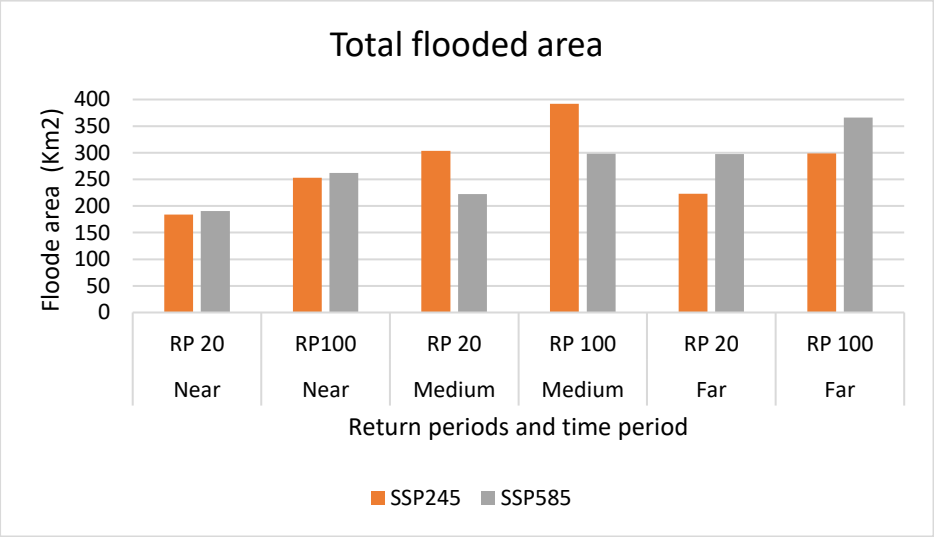

Figure 22: Total flooded area in the Periyar river basin for different time periods and return periods.

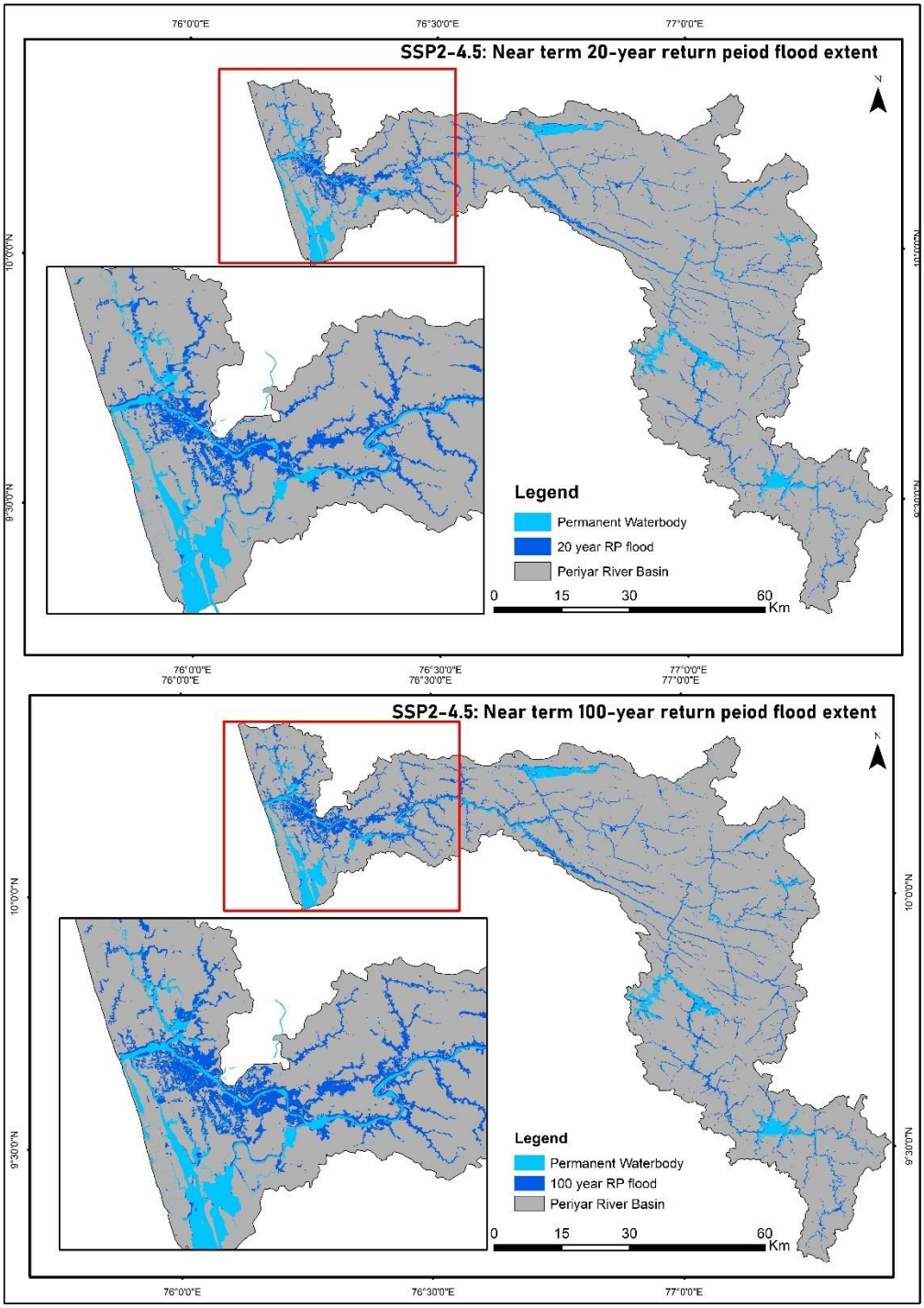

Figure 23: 20 and 100 year return period floods simulated for near term future under SSP2-4.5 scenario

5.3.6.Population exposure in Future scenarios

Exposure to floods

The population exposure to different return periods calculated for different climate scenarios shows that the highest population exposure to floods will be in the midland during the medium term (2046-2075). The SSP245 scenarios show higher population exposure compared to the SSP585 scenario in near, medium and far-term future periods. The lowest exposure was found to be in the highlands during the far-term future period. Throughout the periods, it is observed that the midland had the highest number of exposed people, followed by the lowland and then the highland. Figure 25 shows the population exposed to 20- and 100-year return periods of floods for different future periods under the scenarios SSP245 and SSP585.

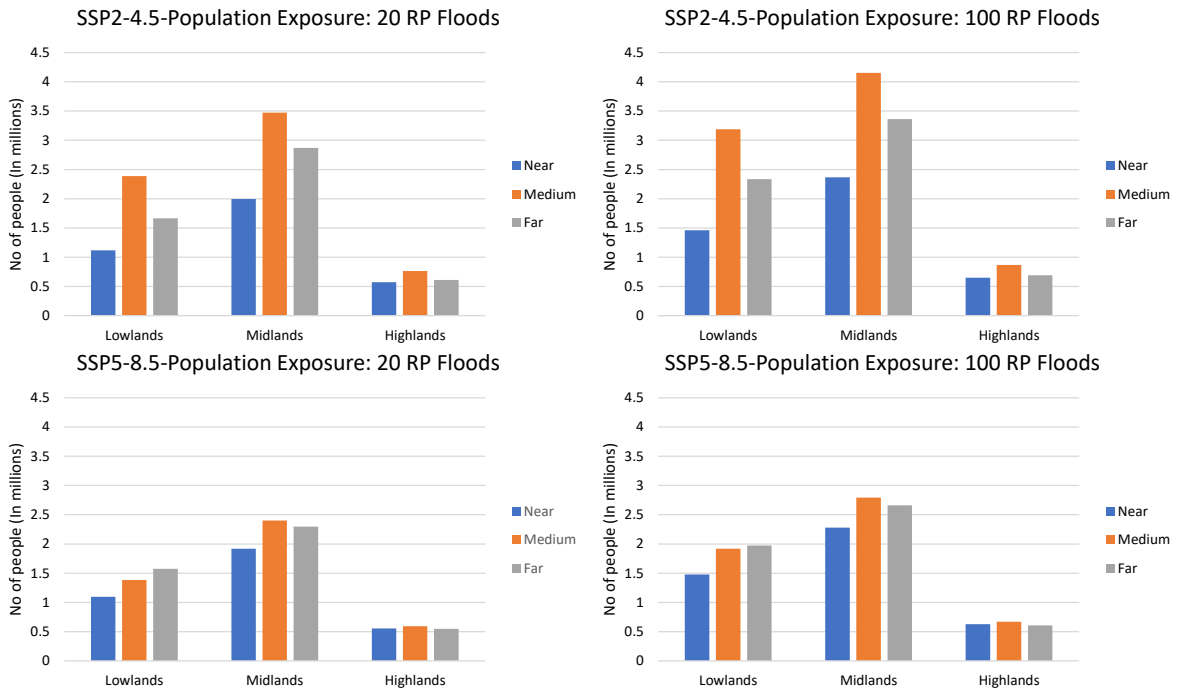

Figure 25:No of people exposed to 20 and 100 year return period floods in lowland, midland and highland for different future periods under the scenarios SSP245 and SSP585.

Exposure to heat waves

Figure 26 shows the number of people exposed to heat waves in the lowland, midland and highland during three different time periods (near, medium and far-term future). Overall there is a general increase in population exposure to heat waves from near to medium term across all the regions. The highest exposure to heatwaves was found in midlands under both SSP scenarios, and both medium and far-term exposures showed that more than 14 million people will be exposed. The lowest population exposure was in the lowlands

during the far-term future under the SSP5-8.5 scenario. In general, the SSP 245 scenario shows higher population exposure values across all the regions.

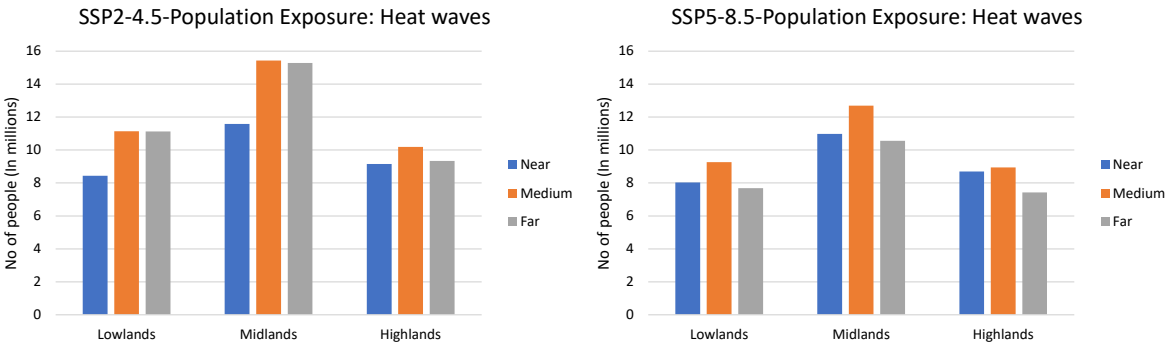

Figure 26: Number of people exposed to heatwaves in the Periyar river basin in different future periods under the scenarios SSP245 and SSP585.

The next chapter will discuss the results that were presented in the results chapter in detail.

Chapter 6: Discussions

6.1.Analysing historical events.

6.1.1.Discharge analysis

Even though the R2 values for the three stations were high, implying a good fit of the Gumbel distribution with the observed data (refer to Figure 10), the large amount of missing data for the Marthandavarma and Mangalapuzha stations makes the predictions of the discharge inaccurate. This justifies only using the Kalady station data for further analysis. The discharge analysis conducted on the Kalady river gauge shows a clear increase in peak discharge events after the year 2001. This sudden shift in trends of having increased peak could be possibly attributed to the missing data in the previous decades spanning from 1980 to 2000. Out of the missing data in the Kalady discharge gauge, 85.4% were missing from the period 1980 to 2000, and 30.5% of this missing data were in the monsoon season (June to September). This missing data in the monsoon season would have reduced the peak observed during these years, resulting in the underestimation of the discharges in different return periods. For instance, the Central Water Commission(CWC) report on the 2018 flood stated that on August 16, a peak discharge of 8800 m3/s was recorded in the Neeleshwaram river gauge. This river gauge is operated by the CWC and is situated about 6 Km upstream of Kalady station, but the highest discharge recorded in the Kalady station record was 4428 m3/s; this underlines the need for a recalculation of the return periods with a more complete record. Despite the missing values and underestimation of the return period, the stream flow in the Periyar River basin does indeed show an increasing trend; this is confirmed by Singh & Chinnasamy (2021), who reported an increase in the annual maximum daily discharge from 1979 to 2018 at a rate of 16 m^3/s per year.

The stream flow in the Periyar river basin is highly influenced by the dams and reservoirs in the region and which are operated mainly for hydroelectric power generation with an aim of maximum power generation (Sudheer et al., 2019)(Sudheer et al., 2019). Since the dam discharge data was not available, it cannot be conclusively said how the discharges recorded were influenced by the dam discharge. Based on the available river discharge data, 2001,2004,2005,2007,2009,2013,2018 and 2019 showed flood events. Out of these years, only 2013,2018, and 2019 were found to be documented in the official records as floods (CWC,2018). Even though the other flood years (2005,2007, and 2009) were found to be mentioned in flood situation reports recorded on the relief web (Relief Web,2005,2007,2009). The scale and extent of the 2018 and 2019 floods might be a primary reason for more focus on these floods in the literature.

6.1.2.Rainfall data analysis

The Pearson correlation analysis between the IMD station data and the gridded IMD datasets for rainfall validates that the rainfall data recorded in the station were indeed very high and highly improbable. The errors in the station data are likely caused by human or machine error. The highest correlation for the precipitation datasets was 0.61, which was found for the Aluva station, which implied a moderate positive correlation. However, this linear correlation only means that the datasets tend to change in a related way. The occasional agreement of the station and the gridded data in the periods 1986 -1988, 1996-2003 and 2012-2022 supports the decision to use the data from gridded IMD4 to represent the respective stations in the Periyar river basin.

The extreme precipitation indices, R20mm, R10mm and R99p calculated, do not show a clear increasing trend of rainfall extreme events from 2000 as the discharge data. This might be because the gridded rainfall data would have smoothened the extremes during the interpolation process. The gridded precipitation datasets, even with high resolutions,

are known to exhibit inherent biases and underestimate rainfall extremes (Bhattacharyya et al., 2022)(Bhattacharyya et al., 2022). All the regions showed higher values for R99p during the period 2001 to 2010, which coincides with the higher number of flood years identified using the discharge data. Also, only the R99p index was able to clearly show the 2018 flood event. Out of the three regions highlands have shown the highest change in precipitation extreme events, but the lowlands and highlands show higher extreme precipitation indices values; this is contrary to the mean annual rainfall for lowland, midland and highland reported by Mathew et al. (2021) based on rain gauges in the river basin which stated the highland received the highest mean annual rainfall, followed by midland and then lowland. However, the paper does not disclose which rainfall stations were used for the study. This underestimation of precipitation in the highland can be possibly attributed to the interpolation technique used to create the dataset and the location of the Munnar station, which lies closer to the rain shadow region of the western ghats which means the value for the Munnar region would be influenced by the rainfall gauge in the rain shadow region underestimating the rainfall in the highland.

Another factor to consider is that that indices like R10mm and R20mm are fixed threshold indices and could be triggered continuously in some regions of the world with higher precipitation trends and should be interpreted with the local climate knowledge (Dunn et al., 2020). This is the case in Kerala, where the daily maximum rainfall can exceed 200mm, considering a low threshold as 20mm will increase the number of times this index is triggered, but this will risk missing out on the extremely high rainfall days in the mix of lower intensity rainfall days.

6.1.3.Temperature data analysis

The extreme temperature indices, which denote the possible temperature extreme events, show a steady increase in such events, implying that temperature extremes are becoming more common. The average Tx90 days in the period 2011-2023 have increased up to 10 days for all three regions when compared to the period 2001 -2010. The years 2016, 2019 and 2024 were the hottest recorded years after 1987 in the state, according to the IMD (Thomas,2024). The TXx values calculated for different regions showed that the lowland and midland recorded a higher increase in temperature than the highlands; this was expected based on the land use and topography of the region. The lowlands and midlands are much more urbanized, with a lot of built-up area, while the lowlands are comparatively less settled and have a lot of forested regions and plantations.

The temperature-gridded data used for the had an initial spatial resolution of about 110 Km, which was re-gridded to the same resolution as the IMD precipitation data (27 Km) using the nearest neighbour interpolation. This lower resolution of the initial data has caused the temperatures in the highland station of Munnar to be overestimated, as the lower resolution means the pixel which contained the Munnar station also included the hotter and drier regions of the nearby district of Palakkad and the neighbouring state of Tamil Nadu. The pixel for the initial IMD temp data and the location of the Munnar station is shown in Figure 35 in Annexure 1. This underlines the need for higher-resolution datasets in the region for accurate analysis.

6.1.4.Heat waves

The heat wave analysis using the IMD definition yielded no results, even though several days in 2016 and 2019 were recorded as the hottest days in the state. The definition of IMD required a difference of 4.5 degrees Celsius from the normal temperature for that day and the presence of similar conditions for at least two consecutive days. Kerala state being a humid state the IMD definition based on maximum temperature alone does not account for the risks of heatwaves in the region. Cvijanovic et al. (2023) examined recent heatwaves in Europe, the United States and Asia and reported that defining and

communicating heat wave alerts based only on maximum temperatures can lead to insufficient warnings for the possible health risks and it should be based on physiological heat stress indices which combines both maximum temperatures and humidity of a region.

The first official record of heatwaves in Kerala was recorded in Palakkad, which is a neighbouring district of the PRB, in April 2024, with 413 heatstroke-related cases reported (Kallungal,2024). Media had reported about 250 cases of sunstroke, out of which 10 died in the summer of 2016 (The New Indian Express, 2016). Similarly, in 2019, the state reported 109 cases of sunstroke, and even though heat warnings were communicated these years, they were not officially considered heatwaves (Onmanorama, 2019).

6.2.Flood modelling and calibration

The flood model set up using Fastfloods to reconstruct the 2018 flood in the region showed relatively higher percentual accuracy (92%) and modelled discharge accuracy (99.5%) compared to the Cohens Kappa (0.34). The higher percentage accuracy is due to the higher number of true negatives (non-flooded regions classified as no floods), which were higher due to the relatively higher surface area of the study region. As per Landis & Koch (1977), Cohen's Kappa values from 0.21 to 0.40 imply a fair agreement. The low value for Cohen's Kappa for the flood model could be explained by the quality of the observed radar flood extent and the coarse resolution of the DEM used. The uncertainty in the observed flood extent arises because the methodology followed for the flood extent delineation from the radar image was not known. The flood extent delineation using the radar imageries is mostly done using thresholding methods and is known to be affected by speckle noise, double noise (double bounce reflection) and vegetation effects (dense vegetation cover)Foroughnia et al., 2022). Since the Periyar River basin is densely vegetated in most of the region (85%), there is a possibility of underestimating the floods using SAR imagery.

The other possible reason for a low Cohen's Kappa value is the coarse resolution of the DEM (90m). A coarser DEM could not capture the small topographic features resulting in inaccurate channel generation and flow routing. This effect could be seen when comparing the observed and the modelled floods, where the modelled flood shows lesser flood extent in the lower river channel after bifurcation. Coarser DEM was selected for computational efficiency due to the large size of the river basin. This has resulted in a problematic trade-off sacrificing the accuracy of the flood model. For future analysis, higher resolution DEMs should be used to model the sub-basins of the Periyar River basin to get a more accurate flood model.

The 20 and 100-year return period floods were generated by inputting corresponding 3-day cumulative rainfalls to the FastFlood model. The model was run in such a way that the rainfall is spread uniformly in the study for the entire duration (72 hours). No peak events were simulated. This is a deviation from reality as often the rainfall is non-uniform with peak intensities at different times and places. This consideration would have flattened the peak discharge generated, but since we are only considering the flood extent for this study, it may not present a considerable difference.

The analysis also reveals the nonlinear relationship between the three-day cumulative rainfall and the flooded area. Although the increase in 3-day cumulative rainfall from the 20-year return period to the 100-year return period is 27.8%, this incremental rise leads to a disproportionately larger increase in the flooded area, amounting to approximately 47.1%. This suggests that even a slight increase in rainfall might mean a significantly larger flood. This amplification in flooded areas might be because higher cumulative rainfall may saturate the soil more quickly, reducing infiltration rates and increasing the runoff. This additional runoff might create bottlenecks in channels, causing the water to spread out over larger areas. This could also be the result of the topography of the region,

especially the lowland region, which is mostly flat; this means that a small rise in water level can spread horizontally over a larger area. However, this nonlinear relationship between three-day cumulative rainfall and flooded area cannot be conclusively said as this is only based on two return periods.

6.2.1.Population exposure

Exposure analysis to 20-year and 100-year return period floods in the current time period showed that the highest number of exposed people are in the midland, followed by the highland and lowland, respectively. This may be attributed to the large flood susceptible regions and higher population density in the midlands. Ramesh et al. (2022) observed that the increased urbanization in the midlands and lowlands has disrupted the natural flow of water both over the surface and into the ground, creating artificial barriers resulting in flood scenarios across these regions.

Exposure occurs when a hazard and element at risk overlap and does not mean that the highly exposed region has the highest risk. So, based on the exposure calculation, we cannot conclude that the midlands have the highest risk towards floods. For that, the vulnerability of the population and their coping capacity should also be assessed.

The population dataset used in the WorldPop gridded population data is highly based on the 2011 census data and the population changes from 2001 to 2011 (which was 1.37%). However, the population growth rate has decreased to 0.68% from 2011 to 2020, which means that the population estimates shown in the Worldpop data might be overestimated (Ranjan, 2023)(Ranjan, 2023). Even though there is this possibility of underestimation since there was no census conducted in India after 2011, this gridded population remains the best estimate we have of the population distribution in the region.

6.3.Analyzing future hydrometeorological hazards

6.3.1.Correlation analysis

The correlation analysis between the IMD gridded precipitation data and the bias-corrected EC -Earth precipitation data for the period (1986 to 2014) shows very weak positive correlations across all the stations in the Periyar River basin. The Pearson correlation coefficients range from 0.14 to 0.22, indicating that the climate model data does not closely follow the observed IMD data for the observed period. Additionally, the bias values, which measure the average tendency of the model to overestimate or underestimate, show that the EC earth data does not uniformly overestimate or underestimate the rainfall across all regions in the Periyar river basin; it underestimates the daily rainfall for two stations (Irinjalakuda and Munnar) and overestimates the daily rainfall for two stations (Aluva and Idukki). This shows that the modelled precipitation is inconsistent across different locations within the basin.

Accurately simulating precipitation remains a significant challenge for climate models, particularly at high resolutions or on a daily timescale; this complexity often leads to typical biases such as the underestimation or overestimation of precipitation (Kesavavarthini et al., 2023)(Kesavavarthini et al., 2023). EC Earth 3 dataset used for the study was statistically bias corrected using Empirical Quantile Mapping (EQM) still shows biases in the study region. The low correlation between the precipitation datasets might also be because, in this study, we have only taken the pixel values for the stations as opposed to a weighted average over the entire region.

In contrast to the precipitation analysis, the correlation coefficients for maximum daily temperatures show moderate positive correlations between the IMD gridded data and the EC Earth data, ranging from 0.64 to 0.65 across all stations. This suggests that the model's predictions for temperature align more closely with the observed data compared to

precipitation. The mean absolute error (MAE) for temperature varies from 1.2°C to 10.44°C, with Munnar station showing the highest MAE, indicating significant deviations from the observed values. Similarly, the RMSE ranges from 1.56°C to 10.57°C, with the highest values again observed in Munnar, highlighting the errors in Munnar station discussed in subsection 6.1. The EC Earth value for maximum temperature ranges from 23°C to 28°C, which is more representative of the region than the gridded IMD maximum temperature dataset.

For the other stations, however, the biases vary; with the Irinjalakuda and Aluva stations, the EC Earth 3 data underestimates the maximum temperature, while for the Idukki station, it overestimates the maximum temperatures. For the Idukki station, EC Earth overestimates both the precipitation and the maximum temperature. While for the Aluva station it overestimates the precipitation and underestimates the maximum temperature. Meanwhile, the Irinjalakuda and Munnar stations consistently underestimate both precipitation and maximum temperature.

The majority of studies prefer multi-model ensembles (MMEs) to a single GCM as they perform better in projecting future climate (Jose et al., 2022). Since this was a methodological trial, we had only used the EC Earth model 3. The correlation analysis shows that for future work, MMEs should be considered over a single climate model.

6.3.2.Extreme precipitation indices

The precipitation extreme indices calculated for the SSP245 and SSP585 scenarios across different regions of the Periyar river basin(lowland, midland, and highland) for the near, medium and far-term future portray a detailed projection of future precipitation patterns, including the very heavy precipitation days (R20mm), heavy precipitation days (R10mm) and extremely wet day precipitation (R99p).

Under the SSP 245 scenario, all the stations show a similar pattern for all three extreme indices with varying intensity. For all the extreme precipitation indices, highland stations showed the lowest values. Even though the extreme precipitation indices of the Munnar station for the initial period (1986 to 2023) had shown such similar values the Idukki station has shown a reduction in extreme precipitation indices. Under SSP2-4.5, the medium-term (2046-2075) is predicted to have higher R99p values, implying that even though the number of days with R10mm and R20mm will be comparatively lower than the far-term, it would bring a higher amount of rainfall. This signifies a period of higher-intensity rainfall with fewer rainfall days, which might lead to flash floods and landslides(Montrasio et al., 2011; Tamm et al., 2023). Conversely, for the far term, the values of R10mm and R20m are slightly higher compared to the R99p values, implying a period with more rainfall days but with slightly lower intensities. Compared to the base period (1986-2023), the precipitation indices in the lowland and midland show an increasing trend, but noticeably, in the highland region, the extreme precipitation indices show a sudden decrease (3.8% for R99p,4.74% for R10mm and 9.76% for R20mm) in the near term. Even though there is an increase in medium and far term the R10mm and R20m days does not reach the baseline period levels. However, the R99p value does increase to 22.09% in the medium term before it drops again to 8.72 %; this signifies that during the medium term, in the highland, very high-intensity rainfall could be expected for shorter periods.

Under the SSP585 scenario, the extreme precipitation indices are predicted to peak in the far term. All the stations in the region show similar trend with the Munnar station having the lowest values for the extreme precipitation indices. Meanwhile, the highest precipitation indices are predicted to be in the lowland and midland regions. The SSP585 scenario predicts very high values for R99p values in the far term, which shows an increase of 122.9%,102.56% and 51.95% for lowland, highland and midland, respectively.

However, the R10mm and R20mm values do not show such extreme increase, which again signifies a shift towards lower duration high-intensity rainfall. The higher changes in R20mm compared to the R10mm rainfall also support this.

The spatial distribution of these extreme precipitation events reveals significant variability across different regions within the basin. The highland shows a comparatively lower number of extreme events compared to the lowland and midland. This pattern highlights the influence of elevation and local climatic conditions on precipitation extremes. Also, depending on the scenario, the peak of extreme events changes from medium term for SSP245 to far term for SSP585.

6.3.3.Extreme temperature indices.

Extreme temperature indices calculated Tx90 and TXx shows a general increasing trend from 2015 to 2100 for all the stations. This supports the study by (C & Ramesh, 2023), which projected the changes in temperatures over the entire region and found that the west coast of India (a larger region which include Periyar river basin) is projected to have an increasing trend in maximum temperatures and the warm days (Tx90) will intensify about 5.6 times in the region under SSP585 scenario.

Tx90 values calculated shows that for the SSP245 and SSP585 scenarios the near term will have comparatively lower hot days even compared with the base period. Also the far term is predicted to have the highest number of Tx90 days for both scenarios. Highland shows a higher number of Tx90 days for the near and medium term for both scenarios, while the lowland and midland show a higher peaks in the Tx90 days for the far term. This suggests that the lowlands are at comparatively higher risk to extreme heat events in the near and medium term than the lowland and highland regions. The main difference in the occurrence of Tx90 days in the SSP scenarios are that , under the SSP585 near term all stations predicts values lower than 30 days per year until 2035 and this exponentially increases in the far term with above 100 days per year recorded as warm days. Where as for the SSP245 scenario the increase in Tx90 days is more gradual and in the far term it predicts about 80 days per year as warm days.

Tx90 days for the future periods is defined as the days exceeding the 0.90 quantile temperatures based on the temperatures of the period 2015-2100, the 0.90 quantile temperature in this time period is higher than the 0.90 quantile temperature for 1986-2023 this means that the Tx90 alone should not be alone considered to tell if a period is hotter than the base period. Adding TXx values to the analysis paints a better understanding of this changes from the base period.

The TXx value analysis shows that under both scenarios the highlands predicts lower maximum annual temperatures throughout the near, medium and far term periods compared to the base period. This can be traced back to the fact that the Munnar station was overestimating the daily maximum temperature as discussed in section 6.1. However the midlands too does show a slight decrease in maximum temperature for both scenarios in the near term. Another anomaly that is observed is the temperature predictions for the Irinjalakuda station which during the base period showed maximum temperatures between 35°C and 40°C, predicts temperatures between 40°C and 50°C and occasionally exceeding 50°C. Given that the EC Earth 3 was underestimating the maximum temperatures in the historical period (1986-2014) when compared to the IMD dataset makes this increasing trend remarkably high. As per the extreme temperature indices the lowlands are predicted to have more extreme temperatures followed by midlands and then lowlands.

6.3.4.Heatwaves

Under the SSP245 scenarios scenario the number of heatwaves remains relatively low for midland (Aluva) and highland stations (Idukki and Munnar) with mostly below 10 heat wave days recorded per year. However the lowland station (Irinjalakuda) records above 10 days and shows heatwaves more frequently. The heatwave occurrence can be seen affected by the elevation as the lowlands predicted the highest number of heatwaves, followed by midland and highland. The Munnar station only predicts heatwaves in four years throughout the period from 2015-2100, this could be attributed to the fact that the heatwave calculation is based on the normal temperatures which were calculated for each day based on the maximum temperatures for that day for the period (1986 to 2015) and the historical maximum temperature data from IMD were overestimated.

Under the SSP585 scenario, which is a higher emission scenario shows a increased heatwave trend with peaks in the Far term for all but the Irinjalakuda station. All stations except Irinjalakuda , still shows an increasing trend in heatwaves with elevation. However when sever heatwave days are taken into account Irinjalakuda station also follows this trend.

The severe heat wave days that is the days exceeding 6.5 °C are mainly predicted for the Irinjalakuda station which predicts up to 180 days of severe heat days per year. This is alarmingly high and need to be further verified with additional analysis by considering other climate models. Severe heatwave days for other stations are zero for the SSP245 scenario and under 10 days for the highland stations and under 30 for the midland station. This anomaly in the Irinjalakuda station might be because the pixel of Irinjalakuda station was located under the west coast river basin while all the other station pixels are located in the southern coast basin as per the bias corrected climate dataset by Mishra et al. (2020) which was used for this study. It is possible that the observed data used for bias correcting different sub basins were weighted average of that region which would mean the climate dataset of these sub basins might show different trends. However Mishra et al. (2020) have not explicitly stated how the bias correction was done on separate river basins.

Overall an increasing trend in heatwaves and severe heatwaves with peaks in the far term could be seen for both SSP scenarios, implying more prevalence of heatwaves by the end of the century with a significant increase from medium term. This finding is supported by C & Ramesh (2023) which states that the Heatwaves are not only increasing but also accelerating under various climate change scenarios in the western coast of India.

6.3.5.Future flood simulations

The flood maps generated for 20-year and 100-year return periods across near term (2015-2045), medium term (2046-2075), and far term (2076-2100) under scenarios SSP245 and SSP585 provide shows how the flood inundation would change. The highest inundated area was predicted to be in the medium term under SSP245 scenario which is followed by inundation caused in the Far term under the SSP585 scenario. This inundation area is mainly dependent on the 3day cumulative rainfall for the period as expected and follow the same order. Additionally the extreme precipitation indices too shows a similar trend with higher peaks in these periods. The lowest inundation occurs in the near term for both scenarios for 20 year return period floods.

The evolution of the inundated area for the 20 and 100 year return period floods under SSP245 and SSP585 scenarios shows that the 20 year return period are having more % increase than the 100 year return period floods. For instance the 20 year return period flooded area for the near, medium and far period are 66%, 173% and 100% more under SSP245 scenario and 72%,100% and 168% respectively under SSP585 scenario when

compared to the base period of 1986-2023. While for the 100 year return period flooded regions the changes are 55%,140% and 82% for the SSP245 and 60%,82% and 124% respectively for SSP585 scenario. This suggests that depending on the SSP scenario, the flood hazard varies and peaks through different periods.

When comparing the floods generated for the future period it should be noted that the future flood were generated by assuming that the landuse of the region remain same, which in reality is not the case. Future works in the region should make use of modeled landuse changes to incorporate the possible changes in the landcover to model floods more accurately depicting future conditions. Moreover flood models are susceptible to a high levels of uncertainty due to the complexity of underlying physical processes and limitations in the availability and quality of data(V. Kumar et al., 2023). The uncertainties discussed in the section 6.2. regarding the coarse resolution of the DEM used, lower Cohens Kappa of the model, using uniform rainfall rate throughout the region and low agreement between climate model data and observations, will be propagated to the future flood predictions too adding to the uncertainties of the floods generated.

6.3.6. Population exposure in future scenarios.

Population exposure to floods calculated in the Periyar river basin shows how exposure to flood would change under different SSP scenarios and time periods for different return period floods. Similar to the hazard extent, the highest population exposure is found to be in the medium term under the SSP245 scenario. However, unlike the flood extent, the population exposure is found to be comparatively higher for the SSP245 scenario than the SSP585 scenario.

The projected gridded population data for the future developed by Wang et al. (2022) is developed based on the Worldpop dataset by sampling 8 regions across the globe, excluding the uninhabitable regions; India is part of the South and East Asia (SEA) region, which had about 24000 sample points. Even though it is expected that the SSP585 scenario, which is a fossil-fueled development, would show a higher population than the SSP245 scenario, in the case of the Periyar basin, it shows the opposite trend. A similar trend was observed by Wang et al. (2022) in Delhi (the capital of India), which showed during SSP5 a decrease in the spread of population around the city and more concentration within the city. This means that the population under the SSP5 scenario will be more concentrated in the cities, and since there were no major cities in the inundated regions, it shows a decrease in exposure.

In terms of the regions, it is found that the midland showed the highest exposure, followed by the lowland and highland. This exposure trend can be attributed to the population distribution in the regions and the topography of the region making the regions differently susceptible to floods. Another shortcoming of the exposure calculated is that the flood generated does not take into account the possible flood mitigation measures that might be implemented in the regions, but this exposure calculation gives an overview of the possible future with no mitigation measures in place.

The heatwave exposure is calculated by considering all the people present in the region as exposed to heatwaves, this was done because the heatwave analysis was conducted based on stations and if a station recorded heatwave, the whole region is considered to be under heatwave. A more detailed exposure analysis based on the heatwave index is eminent to accurately calculate the people exposed and eventually the population at risk of heatwaves.

As per the calculated exposure SSP245 medium term in the midland showed the highest exposure, followed by the SSP585 medium term in midland. However, as discussed above, these exposure values are driven by the population in the region. Considering the higher

probability of heatwave occurrence in the lowlands and midlands, the population in those regions might be more exposed than in the highlands. Also, if the vulnerability of people in the regions is not the same, due to the highly urbanized nature of lowlands and midlands, there is a possibility of additional effects like "urban heat islands" in the region, making people in this region more vulnerable than in the highlands.

Chapter 7: Conclusions

The main objective of this study was to model the evolution of hot, dry extremes, like heat waves, and wet extremes, like extreme precipitation and floods in the Periyar river basin under different climate scenarios. To achieve this, the study was further broken down into three sub-objectives. The first sub-objective was to analyze the past (1986-2023) hydrometeorological events in the region; this was studied using river discharge records, precipitation and maximum temperature data. It was found that the extreme precipitation indices and peak discharges show an increasing trend from 1986 to 2023, with higher peaks concentrated in the period 2001 to 2010. Similarly, the extreme temperature indices also showed an increasing trend from 1986 to 2023, but the peaks were concentrated to the end of the period (2011-2023). Heatwave analysis found that there were no heatwave events as per the IMD definition, even though there were years which recorded significant changes in temperatures and impacted people. In terms of the regions affected, the lowlands and midlands showed higher precipitation extreme events followed by the highlands, whereas midlands showed the highest increase in extreme temperature events followed by the lowlands and highlands. In the historical term, there were no official cases of compounding heat wave–flood events; however, 2019 was an extremely hot year and had floods.

The sub-objective two was to set up a flood model for the PRB with the FastFlood app predominantly using global datasets and calibrate it with historical flood datasets. The flood model simulated for the 2018 floods showed a percentage accuracy of 92% with a Cohen's Kappa coefficient of 0.34, implying a fair agreement with the observed flood extent. This suggests that the flood model primarily based on freely available datasets performs fairly in modelling floods in the Periyar river basin. However, the lower Cohen's Kappa underlines the need for calibrating the model with higher-quality observation data and higher-resolution DEM.

The sub-objective three was to evaluate the changes in the hydrometeorological hazards and their occurrences change under SSP2-4.5 and SSP5-8.5 climate scenarios using best-fit GCMs from CMIP6. The EC Earth 3 dataset used to predict the future climate showed very weak positive correlations for precipitation and a moderate positive correlation for the temperature data when compared to the observed IMD data for the period. The extreme precipitation indices calculated showed a general increasing trend of extreme precipitation events under both SSP scenarios. However, the peaks differed; for the SSP245 scenario, it was found that the highest number of extreme precipitation is found to be in the medium term, which is characterized by a lower number of rainfall days with high-intensity rainfalls and for the SSP585 scenario, peak extreme precipitation events are found to be in the far term. The lowland region shows the highest values for precipitation extremes, while the highlands predict the lowest values.

The extreme temperature indices calculated for the future period also show an increase from the near-term to the far-term future under both SSP245 and 585 scenarios. The extreme indices peak in the far term for both SSP scenarios, which implies a higher number of extreme heat events to be concentrated in this period. The exposure calculated for the floods for different periods showed that under-population exposure will be higher for the SSP245 scenario than the SSP585 scenario, and the midland region has higher exposure to floods than the lowland and highland regions under both scenarios. The heatwave exposure also shows the highest population exposure under the SSP245 scenario, with the Midlands having the higher number of exposed people under both scenarios.

The study shows that compounding heatwaves and floods were not common in the historic period, other than the year 2019, when there were really hot temperatures in the summer period (March to May) followed by floods in the monsoon season (June to September).

However, looking at future extreme heat and precipitation events under SSP scenarios 245 and 585 using bias-corrected EC Earth 3 datasets shows that both heatwaves and floods will become more frequent and intense, especially in the medium term under SSP245 and in the Far term under SSP585, making the occurrence of compounding heatwaves and floods highly probable. It should be noted that the correlation values between observed IMD data and EC- Earth3 were very low, implying a large uncertainty in the modelled future scenarios.

It is crucial to take mitigation measures to reduce the impacts of such compounding heat-flood events, especially in the Periyar River basin, where the majority of people are dependent on outdoor activities for livelihood. The mitigation measures should consider the impacts of both dry and wet extremes to make the region more resilient. For instance, the dams and reservoirs in the region should start operating considering this impending increase in compounding heat wave–flood hazard instead of only focusing on maximizing energy generation. This study emphasizes the need for better observation data in the region, as only with accurate observation data can future hazards be modelled and mitigated. Another concern for the region is the increased unplanned urbanisation, the authorities should promote green infrastructure in the region and conserve the wetlands in the region.

7.1.Future considerations.

There were many uncertainties and limitations to the study conducted; these are discussed here, along with what should be considered to improve a future study.

One of the main challenges for the study was the irregularity and missing values in the observation datasets. Hazard modelled for a region is only as good as the observational data that is based on. The study underlines the importance of having accurate and complete observation data for precipitation temperature and river discharge. The Gumbel analysis for the river discharges should be recalculated with a more complete dataset. Using higher-resolution gridded datasets like CHIRPS (for precipitation) and CHIRTS (for maximum temperature) can capture the precipitation and temperature values with more detail. The unavailability of dam discharge remains a concern because without these values, the flood model considers the basin as a free catchment, and the influence of dam operations is not considered.

Another limitation of the study was that it was based on a point approach, considering only the available five stations in the Periyar River basin. A future analysis using the gridded datasets to calculate a weighted average of the whole region might give a clearer picture of the regional changes and reflect changes in the basin as a whole. Including the heat index values to also include the impact of heatwaves on the human body would paint a better picture of the spatial distribution of heatwaves and also account for additional processes such as the urban heat islands.

The future climate was projected using only one climate model, increasing the uncertainty of the projected climate; the future climate analysis should be repeated with a multi-model ensemble of several climate models. The flood model can be improved by running the model with a higher resolution for a smaller subbasin, especially for the lowland and midland regions, as they were found to be more susceptible to floods. Also, for future flood modelling, the future land use changes modelled for the respective SSP scenarios should be used to create more accurate flood maps.

References

Abhilash, S., Krishnakumar, E. K., Vijaykumar, P., Sahai, A. K., Chakrapani, B., & Gopinath, G. (2019). Changing Characteristics of Droughts over Kerala, India: Inter-Annual Variability and Trend. *Asia-Pacific Journal of Atmospheric Sciences*, *55*(1), 1–17. https://doi.org/10.1007/s13143-018-0060-9

Alves, P. B. R., Loc, H. H., De Silva, Y., Penny, J., Babel, M., & Djordjévic, S. (2023). The dual-risks context: A systematic literature review for the integrated management of flood and drought risks. In *International Journal of Disaster Risk Reduction* (Vol. 96). Elsevier Ltd. https://doi.org/10.1016/j.ijdrr.2023.103905

Arsad, F., Hod, R., Ahmad, N., Ismail, R., Mohamed, N., Baharom, M., Osman, Y., Radi, M., & Tangang, F. (2022). The Impact of Heatwaves on Mortality and Morbidity and the Associated Vulnerability Factors: A Systematic Review. *International Journal of Environmental Research and Public Health*, *19*, 16356. https://doi.org/10.3390/ijerph192316356

Awasthi, A., Vishwakarma, K., & Pattnayak, K. C. (2022). Retrospection of heatwave and heat index. *Theoretical and Applied Climatology*, *147*(1–2), 589–604. https://doi.org/10.1007/s00704-021-03854-z

Barriopedro, D., García-Herrera, R., Ordóñez, C., Miralles, D. G., & Salcedo-Sanz, S. (2023). Heat Waves: Physical Understanding and Scientific Challenges. *Reviews of Geophysics*, *61*(2), e2022RG000780. https://doi.org/https://doi.org/10.1029/2022RG000780

Benjamin, H. (2024, May). Why Kerala swelters in an unprecedented heatwave. *Onmanorama.*

https://www.onmanorama.com/content/mm/en/kerala/top-news/2024/05/04/heatwave-alert-kerala-reasons-el-nino-global-warming-summer-kallakadal.html

Bhattacharyya, S., Sreekesh, S., & King, A. (2022). Characteristics of extreme rainfall in different gridded datasets over India during 1983–2015. *Atmospheric Research*, *267*, 105930. https://doi.org/https://doi.org/10.1016/j.atmosres.2021.105930

Boithias, L., Sauvage, S., Lenica, A., Roux, H., Abbaspour, K. C., Larnier, K., Dartus, D., & Sánchez-Pérez, J. M. (2017). Simulating Flash Floods at Hourly Time-Step Using the SWAT Model. *Water*, *9*(12). https://doi.org/10.3390/w9120929

Bondarenko, M., Nieves, J., Sorichetta, A., Stevens, F., Gaughan, A., & Tatem, A. (2020). *wpgpRFPMS: Random Forest population modelling R scripts v0.1.0*.

Brutsaert, W. (2017). Global land surface evaporation trend during the past half century: Corroboration by Clausius-Clapeyron scaling. *Advances in Water Resources*, *106*, 3–5. https://doi.org/https://doi.org/10.1016/j.advwatres.2016.08.014

Central Water Commission. (2018). *Study report Kerala floods of August 2018*. https://sdma.kerala.gov.in/wp-content/uploads/2020/08/CWC-Report-on-Kerala-Floods.pdf

C, N., & Ramesh, K. V. (2023). Projected changes in heat wave characteristics over India. *Climatic Change*, *176*(10). https://doi.org/10.1007/s10584-023-03618-w

Chen, C. A., Hsu, H. H., & Liang, H. C. (2021). Evaluation and comparison of CMIP6 and CMIP5 model performance in simulating the seasonal extreme precipitation in the Western North Pacific and East Asia. *Weather and Climate Extremes*, *31*. https://doi.org/10.1016/j.wace.2021.100303

Chen, Y., Liu, A., & Cheng, X. (2020). Quantifying economic impacts of climate change under nine future emission scenarios within CMIP6. *Science of The Total Environment*, *703*, 134950. https://doi.org/https://doi.org/10.1016/j.scitotenv.2019.134950

Cvijanovic, I., Mistry, M. N., Begg, J. D., Gasparrini, A., & Rodó, X. (2023). Importance of humidity for characterization and communication of dangerous heatwave conditions. *Npj Climate and Atmospheric Science*, *6*(1), 33. https://doi.org/10.1038/s41612-023-00346-x

de Brito, M. M. (2021). Compound and cascading drought impacts do not happen by chance: A proposal to quantify their relationships. *Science of the Total Environment*, *778*. https://doi.org/10.1016/j.scitotenv.2021.146236

de Macedo, M., Mangukiya, N. K., Fava, M. C., Sharma, A., da Silva, R., Agarwal, A., Razzolini, M. T., Mendiondo, E. M., Goel, N. K., Kurian, M., & Nardocci, A. C. (2024). Performance analysis of physically-based (HEC-RAS, CADDIES) and AI-based (LSTM) flood models for two case studies. *Proceedings of IAHS*, *386*, 41–46. https://doi.org/10.5194/piahs-386-41-2024

Dunn, R. J. H., Alexander, L. V, Donat, M. G., Zhang, X., Bador, M., Herold, N., Lippmann, T., Allan, R., Aguilar, E., Barry, A. A., Brunet, M., Caesar, J., Chagnaud, G., Cheng, V., Cinco, T., Durre, I., de Guzman, R., Htay, T. M., Wan Ibadullah, W. M., … Bin Hj Yussof, M. N. (2020). Development of an Updated Global Land In Situ-Based Data Set of Temperature and Precipitation Extremes: HadEX3. *Journal of Geophysical Research: Atmospheres*, *125*(16), e2019JD032263. https://doi.org/https://doi.org/10.1029/2019JD032263

Economic times. (2024, June). From water crisis to flooding: How Delhi went from extreme heat to rivers on roads in just 24 hours. *Economic Times.*https://economictimes.indiatimes.com/news/india/how-indias-capital-went-from-extreme-heat-to-heavy-floods/articleshow/111336100.cms?from=mdr

El Adlouni, S., & Ouarda, T. B. M. J. (2010). Frequency Analysis of Extreme Rainfall Events. In *Rainfall: State of the Science* (pp. 171–188). American Geophysical Union (AGU). https://doi.org/https://doi.org/10.1029/2010GM000976

ENVIS.(n.d.). Kerala state of environment and related issues. Kerenvis.

http://kerenvis.nic.in/Database/CLIMATE_829.aspx

Foroughnia, F., Alfieri, S. M., Menenti, M., & Lindenbergh, R. (2022). Evaluation of SAR and Optical Data for Flood Delineation Using Supervised and Unsupervised Classification. *Remote Sensing*, *14*(15). https://doi.org/10.3390/rs14153718

Gidden, M. J., Riahi, K., Smith, S. J., Fujimori, S., Luderer, G., Kriegler, E., van Vuuren, D. P., van den Berg, M., Feng, L., Klein, D., Calvin, K., Doelman, J. C., Frank, S., Fricko, O., Harmsen, M., Hasegawa, T., Havlik, P., Hilaire, J., Hoesly, R., … Takahashi, K. (2019). Global emissions pathways under different socioeconomic scenarios for use in CMIP6: a dataset of harmonized emissions

trajectories through the end of the century. *Geoscientific Model Development*, *12*(4), 1443–1475. https://doi.org/10.5194/gmd-12-1443-2019

Gopinath, G., Surendran, U., Abhilash, S., NagaKumar, K. C. V., & Anusha, C. K. (2020). Assessment of drought with a real-time web-based application for drought management in humid tropical Kerala, India. *Environmental Monitoring and Assessment*, *192*(11). https://doi.org/10.1007/s10661-020-08665-9

Gu, L., Chen, J., Yin, J., Slater, L. J., Wang, H. M., Guo, Q., Feng, M., Qin, H., & Zhao, T. (2022). Global Increases in Compound Flood-Hot Extreme Hazards Under Climate Warming. *Geophysical Research Letters*, *49*(8). https://doi.org/10.1029/2022GL097726

Hakim, D. K., Gernowo, R., & Nirwansyah, A. W. (2024). Flood prediction with time series data mining: Systematic review. *Natural Hazards Research*, *4*(2), 194–220. https://doi.org/https://doi.org/10.1016/j.nhres.2023.10.001

Herrera, P. A., Marazuela, M. A., & Hofmann, T. (2022). Parameter estimation and uncertainty analysis in hydrological modeling. *WIREs Water*, *9*(1), e1569. https://doi.org/https://doi.org/10.1002/wat2.1569

Hoang, T. L. T., Dao, H. N., Cu, P. T., Tran, V. T. T., Tong, T. P., Hoang, S. T., Vuong, V. V, & Nguyen, T. N. (2022). Assessing heat index changes in the context of climate change: A case study of Hanoi (Vietnam). *Frontiers in Earth Science*, *10*. https://doi.org/10.3389/feart.2022.897601

Hunt, K. M. R., & Menon, A. (2020). The 2018 Kerala floods: a climate change perspective. *Climate Dynamics*, *54*(3–4), 2433–2446. https://doi.org/10.1007/s00382-020-05123-7

Iqbal, M., Rabbani, A., Haq, F., & Bhimani, S. (2022). The floods of 2022: Economic and health crisis hits Pakistan. *Annals of Medicine and Surgery*, *84*. https://doi.org/10.1016/j.amsu.2022.104800

Jaiswal, R. K., Lohani, A. K., & Tiwari, H. L. (2020). Development of framework for assessment of impact of climate change in a command of water resource project. *Journal of Earth System Science*, *129*(1), 58. https://doi.org/10.1007/s12040-019-1328-x

Ji, J. S., Xia, Y., Liu, L., Zhou, W., Chen, R., Dong, G., Hu, Q., Jiang, J., Kan, H., Li, T., Li, Y., Liu, Q., Liu, Y., Long, Y., Lv, Y., Ma, J., Ma, Y., Pelin, K., Shi, X., … Huang, C. (2023). China's public health initiatives for climate change adaptation. *The Lancet Regional Health - Western Pacific*, *40*, 100965. https://doi.org/https://doi.org/10.1016/j.lanwpc.2023.100965

Jose, D. M., Vincent, A. M., & Dwarakish, G. S. (2022). Improving multiple model ensemble predictions of daily precipitation and temperature through machine learning techniques. *Scientific Reports*, *12*(1), 4678. https://doi.org/10.1038/s41598-022-08786-w

Jyoteeshkumar reddy, P., Perkins-Kirkpatrick, S. E., & Sharples, J. J. (2021). Intensifying Australian Heatwave Trends and Their Sensitivity to Observational Data. *Earth's Future*, *9*(4), e2020EF001924. https://doi.org/https://doi.org/10.1029/2020EF001924

Kallungal, D.(2024, April). Sizzling heat wave keeps Kerala on its toes; mercury soars to second highest since 1901. *The Hindu.* https://www.thehindu.com/news/national/kerala/sizzling-heat-wave-keeps-kerala-on-its-toes-mercury-soars-to-second-highest-since-1901/article68114827.ece

Kappes, M. S., Gruber, K., Frigerio, S., Bell, R., Keiler, M., & Glade, T. (2012). The MultiRISK platform: The technical concept and application of a regional-scale multihazard exposure analysis tool. *Geomorphology*, *151–152*, 139–155. https://doi.org/10.1016/j.geomorph.2012.01.024

Karim, F., Armin, M. A., Ahmedt-Aristizabal, D., Tychsen-Smith, L., & Petersson, L. (2023). A Review of Hydrodynamic and Machine Learning Approaches for Flood Inundation Modeling. *Water*, *15*(3). https://doi.org/10.3390/w15030566

Kerala state disaster management authority. (2019). Flood and Landslide 2019.

https://sdma.kerala.gov.in/wp-content/uploads/2020/03/Memorandum-pages-deleted-Copy-compressed.pdf

Kesavavarthini, T., Rajesh, A. N., Venkata Srinivas, C., & Kumar, T. V. L. (2023). Bias correction of CMIP6 simulations of precipitation over Indian monsoon core region using deep learning algorithms. *International Journal of Climatology*, *43*(8), 3749–3767. https://doi.org/https://doi.org/10.1002/joc.8056

Kim, K. B., Kwon, H.-H., & Han, D. (2022). Intercomparison of joint bias correction methods for precipitation and flow from a hydrological perspective. *Journal of Hydrology*, *604*, 127261. https://doi.org/https://doi.org/10.1016/j.jhydrol.2021.127261

Kumar, A. (2023, July).GOI reports 120 heatwave deaths in Kerala: Gaffe or mala fid?. *The Times of India* https://timesofindia.indiatimes.com/city/thiruvananthapuram/goi-reports-120-heatwave-deaths-in-kerala-gaffe-or-mala-fide/articleshow/102066208.cms

Kumar, R., & Mishra, V. (2020). Increase in Population Exposure Due to Dry and Wet Extremes in India Under a Warming Climate. *Earth's Future*, *8*(12). https://doi.org/10.1029/2020EF001731

Kumar, S., Chanda, K., & Pasupuleti, S. (2020). Spatiotemporal analysis of extreme indices derived from daily precipitation and temperature for climate change detection over India. *Theoretical and Applied Climatology*, *140*(1), 343–357. https://doi.org/10.1007/s00704-020-03088-5

Kumar, V., Sharma, K. V., Caloiero, T., Mehta, D. J., & Singh, K. (2023). Comprehensive Overview of Flood Modeling Approaches: A Review of Recent Advances. *Hydrology*, *10*(7). https://doi.org/10.3390/hydrology10070141

Landis, J. R., & Koch, G. G. (1977). The Measurement of Observer Agreement for Categorical Data. *Biometrics*, *33*(1), 159–174. https://doi.org/10.2307/2529310

Lazin, R., Shen, X., Moges, S., & Anagnostou, E. (2023). The role of Renaissance dam in reducing hydrological extremes in the Upper Blue Nile Basin: Current and future climate scenarios. *Journal of Hydrology*, *616*, 128753. https://doi.org/https://doi.org/10.1016/j.jhydrol.2022.128753

Leyk, S., Gaughan, A. E., Adamo, S. B., de Sherbinin, A., Balk, D., Freire, S., Rose, A., Stevens, F. R., Blankespoor, B., Frye, C., Comenetz, J., Sorichetta, A., MacManus, K., Pistolesi, L., Levy, M., Tatem, A. J., & Pesaresi, M. (2019). The spatial allocation of population: a review of large-scale gridded population data products and their fitness for use. *Earth System Science Data*, *11*(3), 1385–1409. https://doi.org/10.5194/essd-11-1385-2019

Li, H., Zhao, J., Yan, B., Yue, L., & Wang, L. (2022). Global DEMs vary from one to another: an evaluation of newly released Copernicus, NASA and AW3D30 DEM on selected terrains of China

using ICESat-2 altimetry data. *International Journal of Digital Earth*, *15*(1), 1149–1168. https://doi.org/10.1080/17538947.2022.2094002

Liu, Z., Ying, J., He, C., Guan, D., Pan, X., Dai, Y., Gong, B., He, K., Lv, C., Wang, X., Lin, J., Liu, Y., & Bryan, B. (2024). Scarcity and quality risks for future global urban water supply. *Landscape Ecology*, *39*. https://doi.org/10.1007/s10980-024-01832-0

Lyon, B. (2009). Southern Africa Summer Drought and Heat Waves: Observations and Coupled Model Behavior. *Journal of Climate*, *22*(22), 6033–6046. https://doi.org/10.1175/2009JCLI3101.1

Mathew, M., K, S., Mathew, M., Palanisamy, A., & Padmalal, D. (2021). Spatiotemporal variability of rainfall and its effect on hydrological regime in a tropical monsoon-dominated domain of Western Ghats, India. *Journal of Hydrology: Regional Studies*, *36*, 100861. https://doi.org/10.1016/j.ejrh.2021.100861

Meng, Y., Hao, Z., Feng, S., Zhang, X., & Hao, F. (2022a). Increase in compound dry-warm and wet-warm events under global warming in CMIP6 models. *Global and Planetary Change*, *210*. https://doi.org/10.1016/j.gloplacha.2022.103773

Meng, Y., Hao, Z., Feng, S., Zhang, X., & Hao, F. (2022b). Increase in compound dry-warm and wet-warm events under global warming in CMIP6 models. *Global and Planetary Change*, *210*. https://doi.org/10.1016/j.gloplacha.2022.103773

Mishra, A. K. (2021). Observing a severe flooding over southern part of India in monsoon season of 2019. *Journal of Earth System Science*, *130*(1), 2. https://doi.org/10.1007/s12040-020-01509-7

Mishra, V., Aaadhar, S., Shah, H., Kumar, R., Pattanaik, D. R., & Tiwari, A. D. (2018). The Kerala flood of 2018: combined impact of extreme rainfall and reservoir storage. *Hydrology and Earth System Sciences Discussions*, *2018*, 1–13. https://doi.org/10.5194/hess-2018-480

Mishra, V., Bhatia, U., & Tiwari, A. D. (2020a). *Bias corrected climate projections from CMIP6 models for Indian sub-continental river basins*. Zenodo. https://doi.org/10.5281/zenodo.3874046

Mishra, V., Bhatia, U., & Tiwari, A. D. (2020b). Bias-corrected climate projections for South Asia from Coupled Model Intercomparison Project-6. *Scientific Data*, *7*(1). https://doi.org/10.1038/s41597-020-00681-1

Mitra, A. (2021). A Comparative Study on the Skill of CMIP6 Models to Preserve Daily Spatial Patterns of Monsoon Rainfall Over India. *Frontiers in Climate*, *3*. https://doi.org/10.3389/fclim.2021.654763

Montrasio, L., Valentino, R., & Losi, G. L. (2011). Towards a real-time susceptibility assessment of rainfall-induced shallow landslides on a regional scale. *Natural Hazards and Earth System Sciences*, *11*(7), 1927–1947. https://doi.org/10.5194/nhess-11-1927-2011

Munir, B. A., Ahmad, S. R., & Hafeez, S. (2020). Integrated Hazard Modeling for Simulating Torrential Stream Response to Flash Flood Events. *ISPRS International Journal of Geo-Information*, *9*(1). https://doi.org/10.3390/ijgi9010001

Nambudiri, S. (2021, November). At 3,522mm, Kerala records highest rainfall since 1961.*Times of India*. https://timesofindia.indiatimes.com/city/kochi/at-3522mm-state-records-highest-rainfall-since-1961/articleshow/87918277.cms

Onmanorama. (2019, March). Summer heat: 109 sunburn incidents in Kerala. *Manorama.*https://www.onmanorama.com/news/kerala/2019/03/30/summer-heat-kerala-hot-weather-sunburn.html

OpenTopography - *Copernicus Global Digital Elevation Models*. (n.d.). https://portal.opentopography.org/datasetMetadata?otCollectionID=OT.032021.4326.1

Pai, D. S., Sridhar, L., Rajeevan, M., Sreejith, O. P., Satbhai, N. S., & Mukhopadyay, B. (2014). *Development of a new high spatial resolution (0.25° × 0.25°) Long Period (1901-2010) daily gridded rainfall data set over India and its comparison with existing data sets over the region* (Vol. 65, Issue 1).

Panda, D. K., Mishra, A., Kumar, A., Mandal, K. G., Thakur, A. K., & Srivastava, R. C. (2014). Spatiotemporal patterns in the mean and extreme temperature indices of India, 1971-2005. *International Journal of Climatology*, *34*(13), 3585–3603. https://doi.org/10.1002/joc.3931

Pecelj, M. M., Lukić, M. Z., Filipović, D. J., Protić, B. M., & Bogdanović, U. M. (2020). Analysis of the Universal Thermal Climate Index during heat waves in Serbia. *Natural Hazards and Earth System Sciences*, *20*(7), 2021–2036. https://doi.org/10.5194/nhess-20-2021-2020

Poggio, L., de Sousa, L. M., Batjes, N. H., Heuvelink, G. B. M., Kempen, B., Ribeiro, E., & Rossiter, D. (2021). SoilGrids 2.0: producing soil information for the globe with quantified spatial uncertainty. *SOIL*, *7*(1), 217–240. https://doi.org/10.5194/soil-7-217-2021

Preet Lal Aniket Prakash, A. K. P. K. S. P. S. A. C. P. P. S., & Khan, M. L. (2020). Evaluating the 2018 extreme flood hazard events in Kerala, India. *Remote Sensing Letters*, *11*(5), 436–445. https://doi.org/10.1080/2150704X.2020.1730468

Profillidis, V. A., & Botzoris, G. N. (2019). Statistical Methods for Transport Demand Modeling. *Modeling of Transport Demand*, 163–224. https://doi.org/10.1016/B978-0-12-811513-8.00005-4

Qian, C., Ye, Y., Bevacqua, E., & Zscheischler, J. (2023). Human influences on spatially compounding flooding and heatwave events in China and future increasing risks. *Weather and Climate Extremes*, *42*, 100616. https://doi.org/https://doi.org/10.1016/j.wace.2023.100616

Ramesh, M. V., Sudarshan, V. C., Harilal, G. T., Singh, B., Sudheer, A., & Ekkirala, H. C. (2022). Kerala Floods 2018: Causative Factors that Transformed Single Event to Multi-hazard Disaster. In S. Kolathayar, I. Pal, S. C. Chian, & A. Mondal (Eds.), *Civil Engineering for Disaster Risk Reduction* (pp. 61–82). Springer Nature Singapore. https://doi.org/10.1007/978-981-16-5312-4_5

Ranjan, P. (2023). *Sustainable Development in India: Is Population Stagnation Enough to Achieve It* (pp. 149–158).

Ravindra, K., Bhardwaj, S., Ram, C., Goyal, A., Singh, V., Venkataraman, C., Bhan, S. C., Sokhi, R. S., & Mor, S. (2024). Temperature projections and heatwave attribution scenarios over India: A systematic review. *Heliyon*, *10*(4), e26431. https://doi.org/https://doi.org/10.1016/j.heliyon.2024.e26431

Reddy, N. M., & Saravanan, S. (2023). Extreme precipitation indices over India using CMIP6: a special emphasis on the SSP585 scenario. *Environmental Science and Pollution Research*, *30*(16), 47119–47143. https://doi.org/10.1007/s11356-023-25649-7

Ren, J., Wang, W., Wei, J., Li, H., Li, X., Liu, G., Chen, Y., & Ye, S. (2023). Evolution and prediction of drought-flood abrupt alternation events in Huang-Huai-Hai River Basin, China. *Science of the Total Environment*, *869*. https://doi.org/10.1016/j.scitotenv.2023.161707

Reshma, C., & Arunkumar, R. (2023). Assessment of impact of climate change on the streamflow of Idamalayar River Basin, Kerala. *Journal of Water and Climate Change*, *14*(7), 2133–2149. https://doi.org/10.2166/wcc.2023.456

Riahi, K., van Vuuren, D. P., Kriegler, E., Edmonds, J., O'Neill, B. C., Fujimori, S., Bauer, N., Calvin, K., Dellink, R., Fricko, O., Lutz, W., Popp, A., Cuaresma, J. C., KC, S., Leimbach, M., Jiang, L., Kram, T., Rao, S., Emmerling, J., … Tavoni, M. (2017). The Shared Socioeconomic Pathways and their energy, land use, and greenhouse gas emissions implications: An overview. *Global Environmental Change*, *42*, 153–168. https://doi.org/https://doi.org/10.1016/j.gloenvcha.2016.05.009

Sadhwani, K., & Eldho, T. I. (2023). Assessing the Vulnerability of Water Balance to Climate Change at River Basin Scale in Humid Tropics: Implications for a Sustainable Water Future. *Sustainability (Switzerland)*, *15*(11). https://doi.org/10.3390/su15119135

Sadhwani, K., Eldho, T. I., & Karmakar, S. (2023). Investigating the influence of future landuse and climate change on hydrological regime of a humid tropical river basin. *Environmental Earth Sciences*, *82*(9). https://doi.org/10.1007/s12665-023-10891-6

Sauter, C., Catto, J. L., Fowler, H. J., Westra, S., & White, C. J. (2023). Compounding Heatwave-Extreme Rainfall Events Driven by Fronts, High Moisture, and Atmospheric Instability. *Journal of Geophysical Research: Atmospheres*, *128*(21), e2023JD038761. https://doi.org/https://doi.org/10.1029/2023JD038761

Sauter, C., Fowler, H. J., Westra, S., Ali, H., Peleg, N., & White, C. J. (2023). Compound extreme hourly rainfall preconditioned by heatwaves most likely in the mid-latitudes. *Weather and Climate Extremes*, *40*, 100563. https://doi.org/https://doi.org/10.1016/j.wace.2023.100563

Sauter, C., White, C. J., Fowler, H. J., & Westra, S. (2023). Temporally compounding heatwave–heavy rainfall events in Australia. *International Journal of Climatology*, *43*(2), 1050–1061. https://doi.org/10.1002/joc.7872

Saxton, K. E., Rawls, W. J., Romberger, J. S., & Papendick, R. I. (1986). Estimating Generalized Soil-water Characteristics from Texture. *Soil Science Society of America Journal*, *50*(4), 1031–1036. https://doi.org/https://doi.org/10.2136/sssaj1986.03615995005000040039x

Shafii, N. Z., Saudi, A. S. M., Pang, J. C., Abu, I. F., Sapawe, N., Kamarudin, M. K. A., & Mohamad, M. H. N. (2023). Association of Flood Risk Patterns with Waterborne Bacterial Diseases in Malaysia. *Water*, *15*(11). https://doi.org/10.3390/w15112121

Shah, M. A. R., Renaud, F. G., Anderson, C. C., Wild, A., Domeneghetti, A., Polderman, A., Votsis, A., Pulvirenti, B., Basu, B., Thomson, C., Panga, D., Pouta, E., Toth, E., Pilla, F., Sahani, J., Ommer, J., El Zohbi, J., Munro, K., Stefanopoulou, M., … Zixuan, W. (2020). A review of hydro-meteorological hazard, vulnerability, and risk assessment frameworks and indicators in the context of nature-based solutions. *International Journal of Disaster Risk Reduction*, *50*, 101728. https://doi.org/https://doi.org/10.1016/j.ijdrr.2020.101728

Singh, V., Lohani, A. K., & Jain, S. K. (2022). Reconstruction of extreme flood events by performing integrated real-time and probabilistic flood modeling in the Periyar river basin, Southern India. *Natural Hazards*, *112*(3), 2433–2463. https://doi.org/10.1007/s11069-022-05272-4

Sreelash, K., Sharma, R. K., Gayathri, J. A., Upendra, B., Maya, K., & Padmalal, D. (2018). Impact of Rainfall Variability on River Hydrology: A Case Study of Southern Western Ghats, India. *Journal of the Geological Society of India*, *92*(5), 548–554. https://doi.org/10.1007/s12594-018-1065-9

Sudheer, K. P., Murty Bhallamudi, S., Narasimhan, B., Thomas, J., Bindhu, V. M., Vema, V., & Kurian, C. (2019). Role of dams on the floods of August 2018 in Periyar River Basin, Kerala. *Current Science*, *116*(5), 780–794. https://doi.org/10.18520/cs/v116/i5/780-794

Sun, J., Chen, W., Hu, B., Xu, Y. J., Zhang, G., Wu, Y., Hu, B., & Song, Z. (2023). Roles of reservoirs in regulating basin flood and droughts risks under climate change: Historical assessment and future projection. *Journal of Hydrology: Regional Studies*, *48*. https://doi.org/10.1016/j.ejrh.2023.101453

Sunstroke in state. (2016, May). *The New Indian Express.* https://www.newindianexpress.com/states/kerala/2016/May/03/11-more-struck-by-sunstroke-in-state-932081.html

Tamm, O., Saaremäe, E., Rahkema, K., Jaagus, J., & Tamm, T. (2023). The intensification of short-duration rainfall extremes due to climate change – Need for a frequent update of intensity–duration–frequency curves. *Climate Services*, *30*, 100349. https://doi.org/https://doi.org/10.1016/j.cliser.2023.100349

Tebaldi, C., Debeire, K., Eyring, V., Fischer, E., Fyfe, J., Friedlingstein, P., Knutti, R., Lowe, J., O'Neill, B., Sanderson, B., van Vuuren, D., Riahi, K., Meinshausen, M., Nicholls, Z., Tokarska, K. B., Hurtt, G., Kriegler, E., Lamarque, J.-F., Meehl, G., … Ziehn, T. (2021). Climate model projections from the Scenario Model Intercomparison Project (ScenarioMIP) of CMIP6. *Earth System Dynamics*, *12*(1), 253–293. https://doi.org/10.5194/esd-12-253-2021

The Centre for Research on the Epidemiology of Disasters. (2020). Human cost of disasters: an overview of the last 20 years. https://www.undrr.org/publication/human-cost-disasters-overview-last-20-years-2000-2019

Thomas, V. (2024, April). What is the heatwave that makes Kerala stiflingly hot. *Manorama.* https://www.onmanorama.com/news/kerala/2024/04/30/heatwave-kerala-summer-high-temperature-climate-change.html

Thompson, V., Mitchell, D., Hegerl, G. C., Collins, M., Leach, N. J., & Slingo, J. M. (2023). The most at-risk regions in the world for high-impact heatwaves. *Nature Communications*, *14*(1), 2152. https://doi.org/10.1038/s41467-023-37554-1

Trancoso, R., Syktus, J., Toombs, N., Ahrens, D., Wong, K. K.-H., & Pozza, R. D. (2020). Heatwaves intensification in Australia: A consistent trajectory across past, present and future. *Science of The Total Environment*, *742*, 140521. https://doi.org/https://doi.org/10.1016/j.scitotenv.2020.140521

Tripathi Neha Goel and Davis, N. (2020). Natural Hazards and Climate Change: Lessons and Experiences from Kerala Flood Disaster. In G. J. and B. M. and C. M. P. D. and M. A. Leal Filho Walter and Nagy (Ed.), *Climate Change, Hazards and Adaptation Options: Handling the Impacts*

of a Changing Climate (pp. 563–583). Springer International Publishing. https://doi.org/10.1007/978-3-030-37425-9_29

Try, S., Tanaka, S., Tanaka, K., Sayama, T., Khujanazarov, T., & Oeurng, C. (2022). Comparison of CMIP5 and CMIP6 GCM performance for flood projections in the Mekong River Basin. *Journal of Hydrology: Regional Studies*, *40*. https://doi.org/10.1016/j.ejrh.2022.101035

United Nations International Strategy for Disaster Reduction. (2009). *United Nations International Strategy for Disaster Reduction, terminology on disaster risk reduction*. www.preventionweb.net

van den Bout, B., Jetten, V. G., van Westen, C. J., & Lombardo, L. (2023). A breakthrough in fast flood simulation. *Environmental Modelling & Software*, *168*, 105787. https://doi.org/https://doi.org/10.1016/j.envsoft.2023.105787

van Vliet, M. T. H., Thorslund, J., Strokal, M., Hofstra, N., Flörke, M., Ehalt Macedo, H., Nkwasa, A., Tang, T., Kaushal, S. S., Kumar, R., van Griensven, A., Bouwman, L., & Mosley, L. M. (2023). Global river water quality under climate change and hydroclimatic extremes. *Nature Reviews Earth & Environment*, *4*(10), 687–702. https://doi.org/10.1038/s43017-023-00472-3

Vera Glas. (2023). *The applicability of fast flood simulation for risk informed decision-making concerning flood risk reduction under a changing climate -a case study of pamba-basin kerala, india* [Unpublished master's thesis]. University of Twente.

Vijaykumar, P., Abhilash, S., Sreenath, A. V., Athira, U. N., Mohanakumar, K., Mapes, B. E., Chakrapani, B., Sahai, A. K., Niyas, T. N., & Sreejith, O. P. (2021). Kerala floods in consecutive years - Its association with mesoscale cloudburst and structural changes in monsoon clouds over the west coast of India. *Weather and Climate Extremes*, *33*. https://doi.org/10.1016/j.wace.2021.100339

Wang, T., Tu, X., Singh, V. P., Chen, X., & Lin, K. (2021). Global data assessment and analysis of drought characteristics based on CMIP6. *Journal of Hydrology*, *596*. https://doi.org/10.1016/j.jhydrol.2021.126091

Wang, X., Meng, X., & Long, Y. (2022). Projecting 1 km-grid population distributions from 2020 to 2100 globally under shared socioeconomic pathways. *Scientific Data*, *9*(1). https://doi.org/10.1038/s41597-022-01675-x

Ward, P. J., Daniell, J., Duncan, M., Dunne, A., Hananel, C., Hochrainer-Stigler, S., Tijssen, A., Torresan, S., Ciurean, R., Gill, J. C., Sillmann, J., Couasnon, A., Koks, E., Padrón-Fumero, N., Tatman, S., Tronstad Lund, M., Adesiyun, A., Aerts, J. C. J. H., Alabaster, A., … De Ruiter, M. C. (2022). Invited perspectives: A research agenda towards disaster risk management pathways in multi-(hazard-)risk assessment. *Natural Hazards and Earth System Sciences*, *22*(4), 1487–1497. https://doi.org/10.5194/nhess-22-1487-2022

Yapo, A. L. M., Kouassi, B. K., Diawara, A., Yoroba, F., Famien, A. M. L., Touré, P. R., Kouadio, K., Tiemoko, D. T., Sylla, M. B., & Diedhiou, A. (2023). Changes in the Seasonal Cycle of Heatwaves, Dry and Wet Spells over West Africa Using CORDEX Simulations. *Atmosphere*, *14*(10). https://doi.org/10.3390/atmos14101582

YIN, H., & SUN, Y. (2018). Characteristics of extreme temperature and precipitation in China in 2017 based on ETCCDI indices. *Advances in Climate Change Research*, *9*(4), 218–226. https://doi.org/https://doi.org/10.1016/j.accre.2019.01.001

Yu, D., Xie, P., Dong, X., Hu, X., Liu, J., Li, Y., Peng, T., Ma, H., Wang, K., & Xu, S. (n.d.). *Improvement of the SWAT model for event-based flood forecasting on a sub-daily time scale*. https://doi.org/10.5194/hess-2017-180

Zhang, W., & Villarini, G. (2020). Deadly Compound Heat Stress-Flooding Hazard Across the Central United States. *Geophysical Research Letters*, *47*(15), e2020GL089185. https://doi.org/https://doi.org/10.1029/2020GL089185

Zhang, Y., You, Q., Ullah, S., Chen, C., Shen, L., & Liu, Z. (2023). Substantial increase in abrupt shifts between drought and flood events in China based on observations and model simulations. *Science of the Total Environment*, *876*. https://doi.org/10.1016/j.scitotenv.2023.162822

Zhao, T., & Dai, A. (n.d.). *CMIP6 Model-Projected Hydroclimatic and Drought Changes and Their Causes in the Twenty-First Century*. https://doi.org/10.1175/JCLI-D-21

Zheng, K., Xian, Z., Liao, W., & Chen, Y. (2024). Urbanization impacts on sequential flood-heatwave events in the Guangdong-Hong Kong-Macao Greater Bay Area, China. *Urban Climate*, *55*, 101878. https://doi.org/https://doi.org/10.1016/j.uclim.2024.101878

Annexure 1

Class	Manning's Coefficient
Forest	0.12
Shrubs	0.1
Grass	0.03
Crops	0.05
Building	0.02
Bare	0.01
Snow	0.01
Water	0.01
Wetland	0.09
Mangroves	0.14
Moss	0.07

Table 18: Default values for Mannings Coefficient for various land covers.

Pearson 's correlation coefficient	Degree of Correlation
1	Perfect positive correlation
0.8 to 1	Very strong positive correlation
0.6 to 0.8	Strong positive correlation
0.4 to 0.6	Moderate positive correlation
0.2 to 0.4	Weak positive correlation
0 to 0.2	Very weak positive correlation
0	No correlation
-0.2 to 0	Very weak negative correlation
-0.4 to -0.2	Weak negative correlation
-0.6 to -0.4	Moderate negative correlation
-0.8 to -0.6	Strong negative correlation
-1 to -0.8	Very strong negative correlation
-1	Perfect negative correlation

Table 19: Pearson's correlation coefficient and their degree of correlation strength

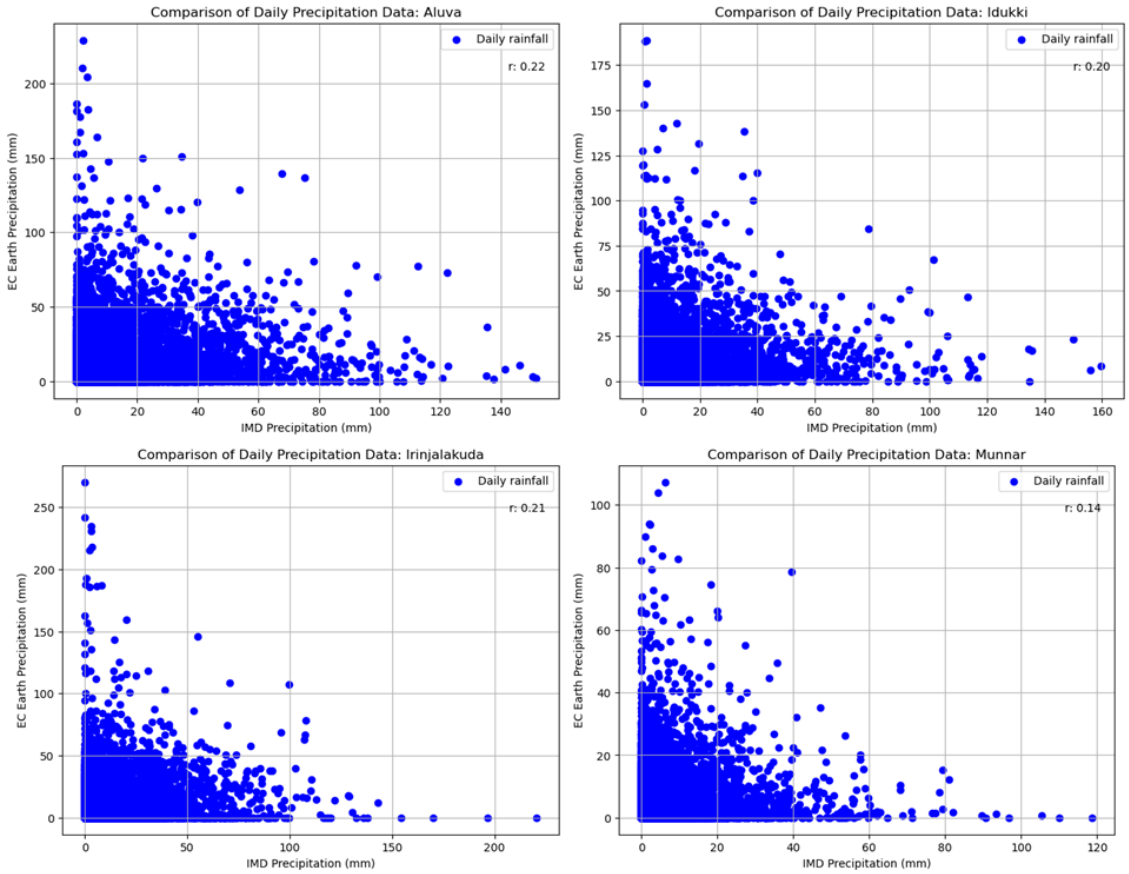

Figure 27: Daily rainfall comparison between IMD gridded data and EC Earth 3 data for different stations for the period (1986-2014).

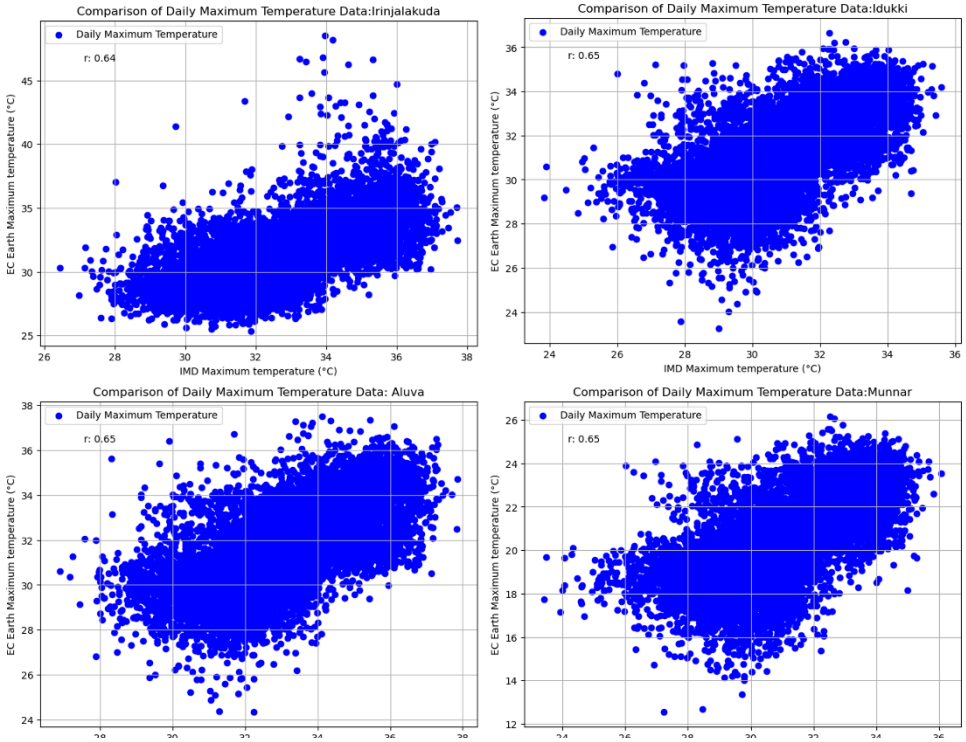

Figure 28: Daily temperature data comparison between IMD gridded data and EC Earth 3 data for different stations for the period (1986-2014).

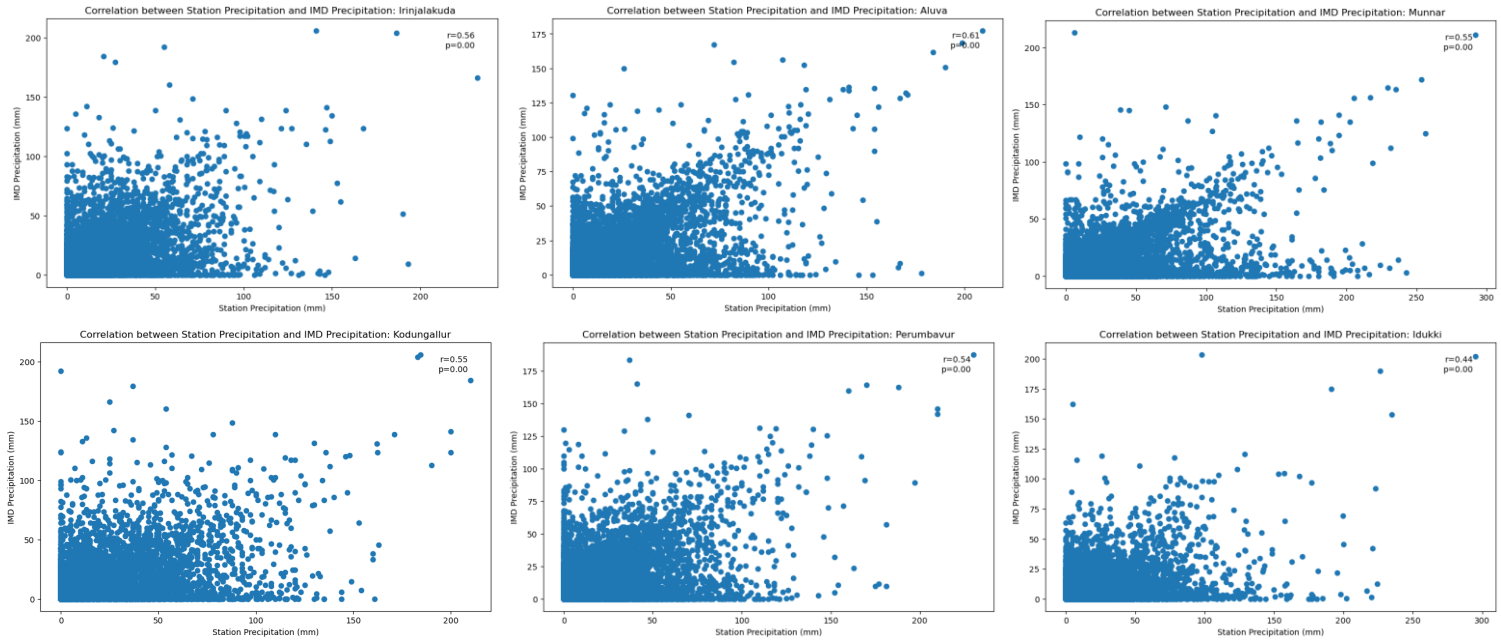

Figure 29:IMD station precipitation plotted against IMD gridded data for daily rainfall.

	% change in Average R99p precipitation:SSP245		
Period	**Lowland**	**Midland**	**Highland**
2015-2045	23.17	28.03	-3.86
2046-2075	63.75	62.44	22.09
2076-2100	43.98	44.79	8.72
	% change in Average R99p precipitation:SSP585		
Period	**Lowland**	**Midland**	**Highland**
2015-2045	27.76	31.62	-1.73
2046-2075	52.7	49.65	11.74
2076-2100	122.19	102.56	51.95

Table 20: Percentage change in average R99p compared to the base period 2010-2023.

	% change in R20mm days:SSP245		
Period	**Lowland**	**Midland**	**Highland**
2015-2045	23.82	21.74	-9.76
2046-2075	24.47	22.67	-6.08
2076-2100	28.51	25.92	-8.22
	% change in R20mm days:SSP585		
Period	**Lowland**	**Midland**	**Highland**
2015-2045	16.68	15.16	-17.22
2046-2075	23.48	20.33	-8.42
2076-2100	50.38	47.12	20.22

Table 21: Percentage change in average number of R20mm days compared to the base period 2010-2023.

	% change in R10mm days:SSP245		
Period	**Lowland**	**Midland**	**Highland**
2015-2045	12.51	14.9	-4.74
2046-2075	15.06	17.46	-2.76
2076-2100	19.37	21.43	-2
	% change in R10mm days:SSP585		
Period	**Lowland**	**Midland**	**Highland**
2015-2045	10.49	13.36	-9.09
2046-2075	17.35	17.86	-3.42
2076-2100	31.66	31.65	9.95

Table 22: Percentage change in average number of R20mm days compared to the base period 2010-2023.

	% Change in Tx90 days:SSP245		
Period	**Lowland**	**Midland**	**Highland**
2015-2045	-65.23	-59.64	-52.03
2046-2075	1.85	-2.37	1.16
2076-2100	13.78	11.2	10.28
	% Change in Tx90 days:SSP585		
Period	**Lowland**	**Midland**	**Highland**
2015-2045	-94.84	-90.11	-80.31
2046-2075	-31.04	-24.67	-7.36
2076-2100	89.42	76.27	56.14

Table 23: Percentage change in average Tx90 days compared to the base period 2010-2023.

	Change in maximum daily temperature: SSP245		
Period	**Lowland**	**Midland**	**Highland**
2015-2045	5.52	-0.55	-4.57
2046-2075	9.36	0.52	-3.7
2076-2100	10.39	0.82	-3.22
	Change in maximum daily temperature: SSP5-8.5		
Period	**Lowland**	**Midland**	**Highland**
2015-2045	5.71	-0.47	-4.52
2046-2075	10.73	1.14	-3.05
2076-2100	12.83	2.73	-1.78

Table 24: Percentage change in maxima of maximum daily temperature TXx compared to the base period 2010-2023.

A.1.Flood maps simulated for various future periods

Station		**No of heatwave days recorded**		**No of Severe heatwave days recorded**	
	Period	**SSP245**	**SSP585**	**SSP245**	**SSP585**
Irinjalakuda	2015-2045	151	105	328	282
	2046-2075	285	330	1143	1854
	2076-2100	210	200	1165	3114
Aluva	2015-2045	4	9	0	0
	2046-2075	59	224	0	6
	2076-2100	65	994	0	109
Idukki	2015-2045	0	11	0	0
	2046-2075	18	135	0	0
	2076-2100	23	612	0	24
Munnar	2015-2045	0	7	0	0
	2046-2075	2	65	0	0
	2076-2100	11	415	0	10

Table 25: The number of heatwaves predicted for lowlands midlands and highlands in different time periods and SSP scenarios

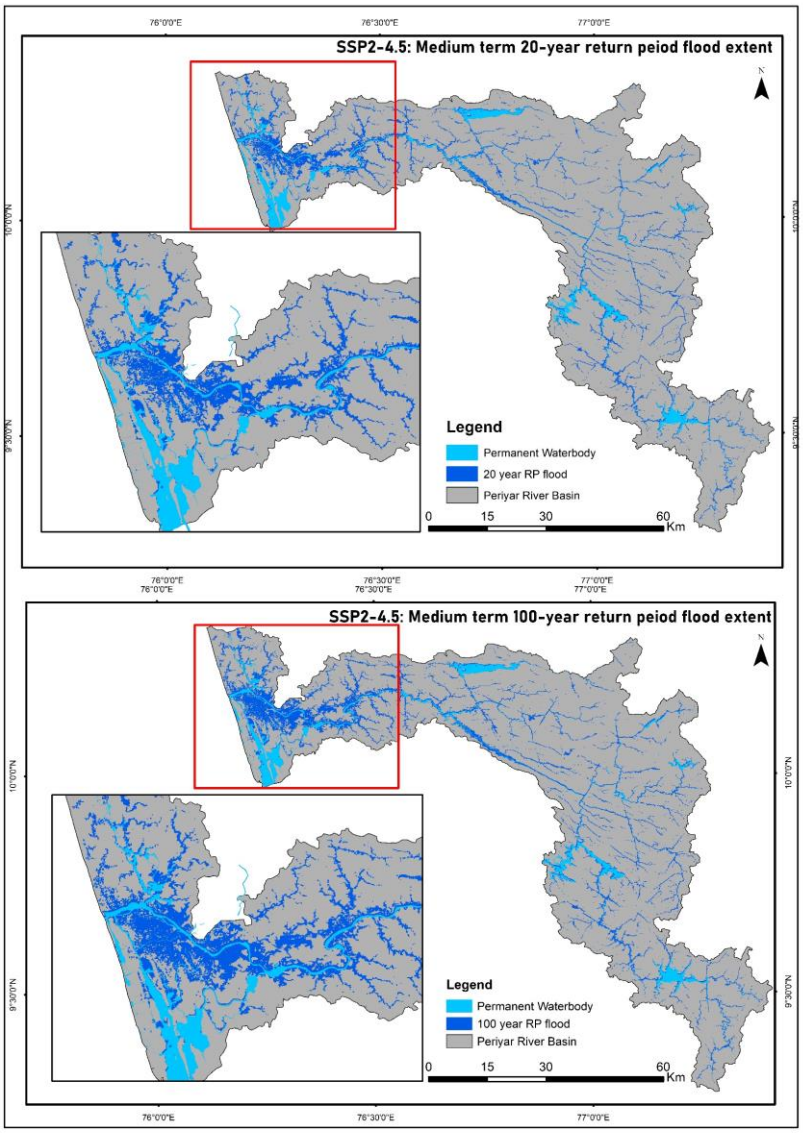

Figure 30: Flood simulated for 20 and 100 year return periods in Medium term under SSP2-4.5 scenario.

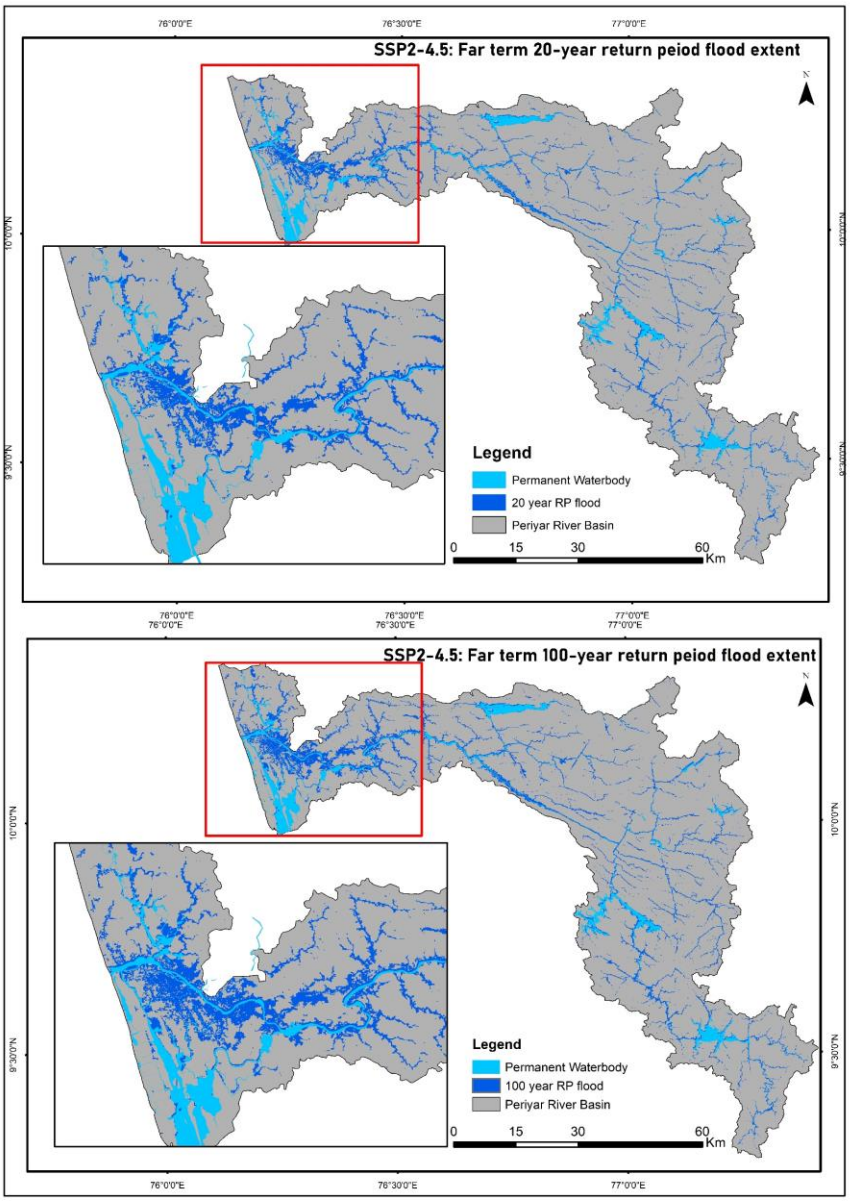

Figure 31: Flood simulated for 20 and 100 year return periods in Far term under SSP2-4.5 scenario.

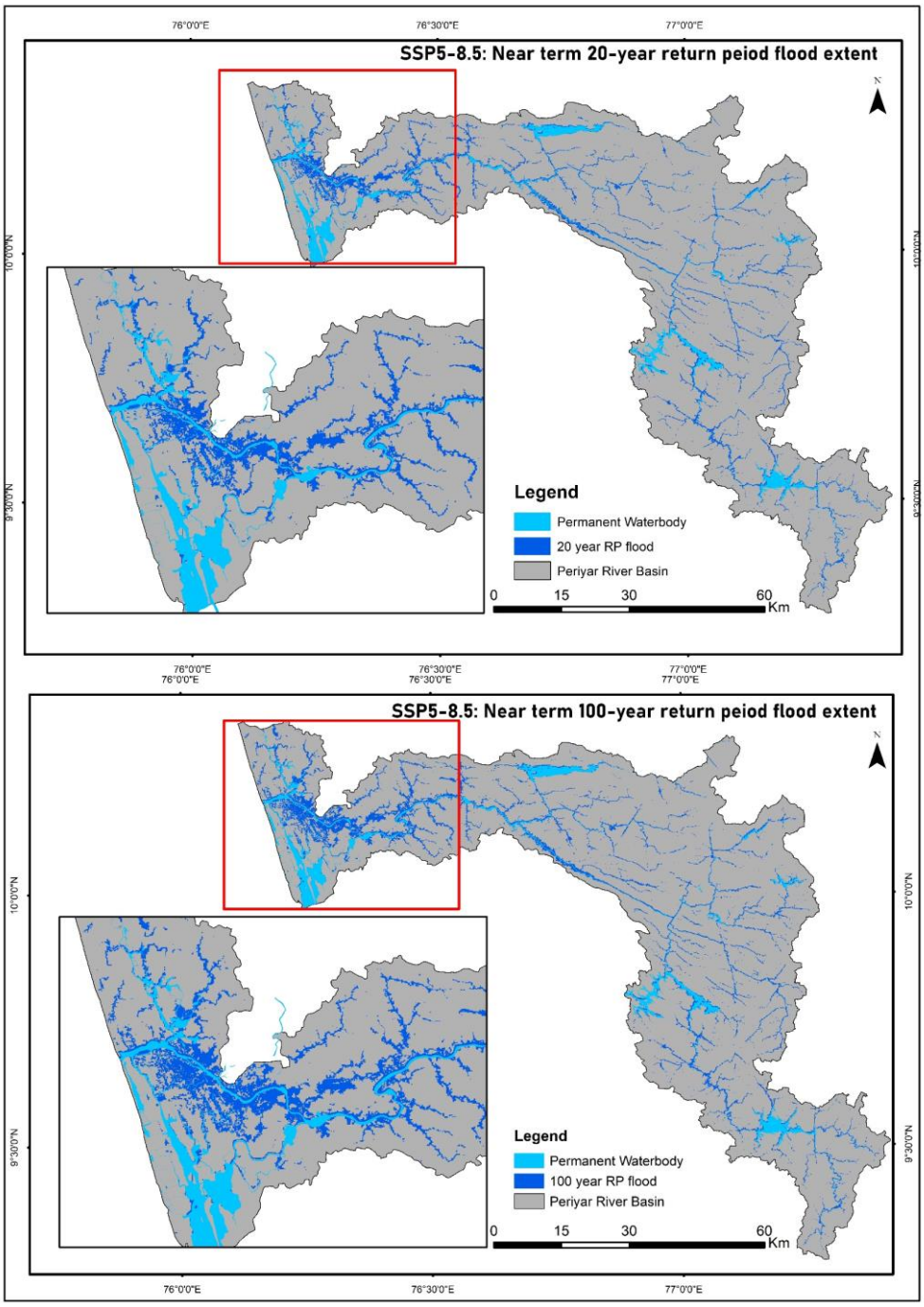

Figure 32: Flood simulated for 20 and 100 year return periods in Near term under SSP5-8.5 scenario.

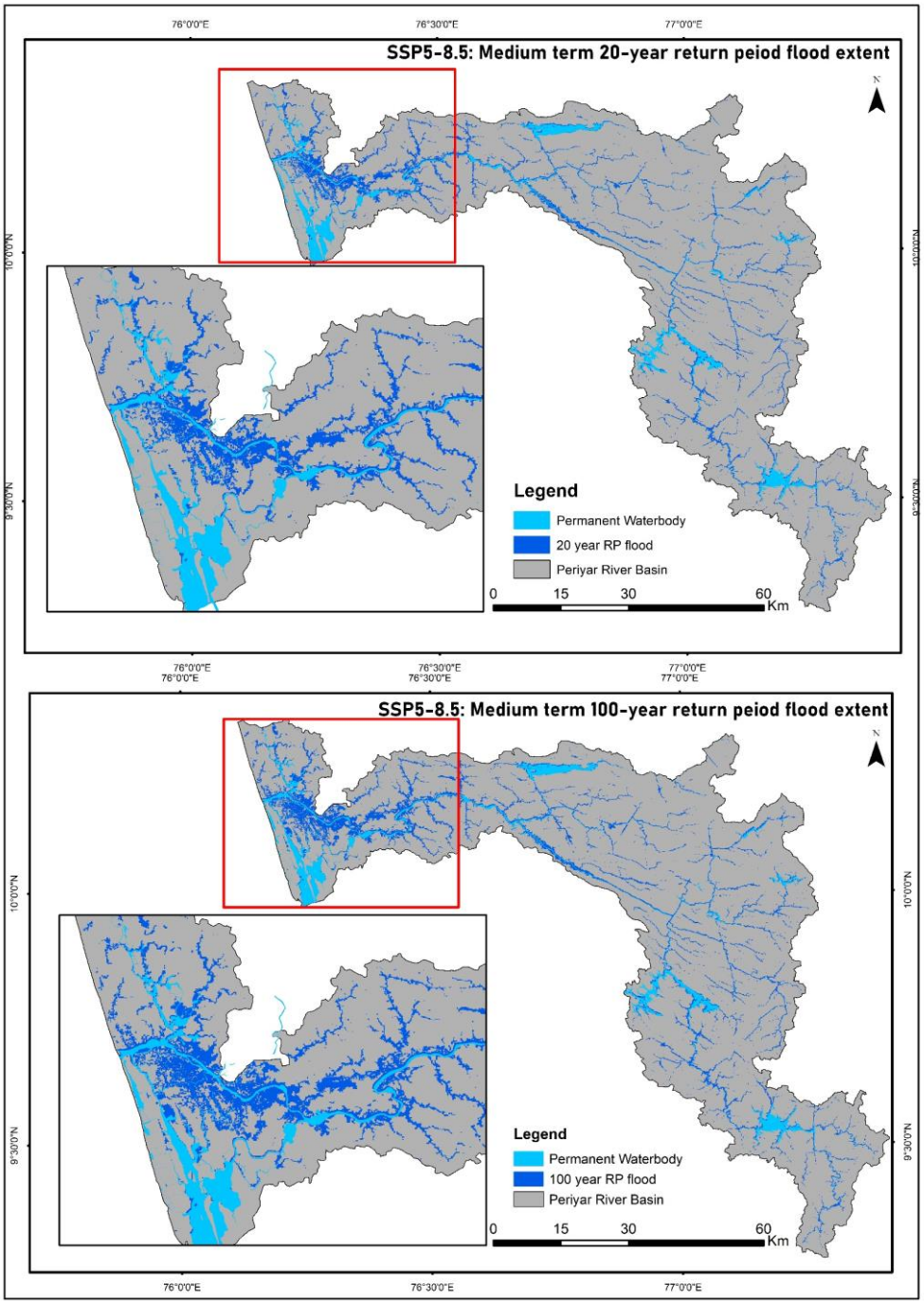

Figure 33: Flood simulated for 20 and 100 year return periods in Medium term under SSP5-8.5 scenario.

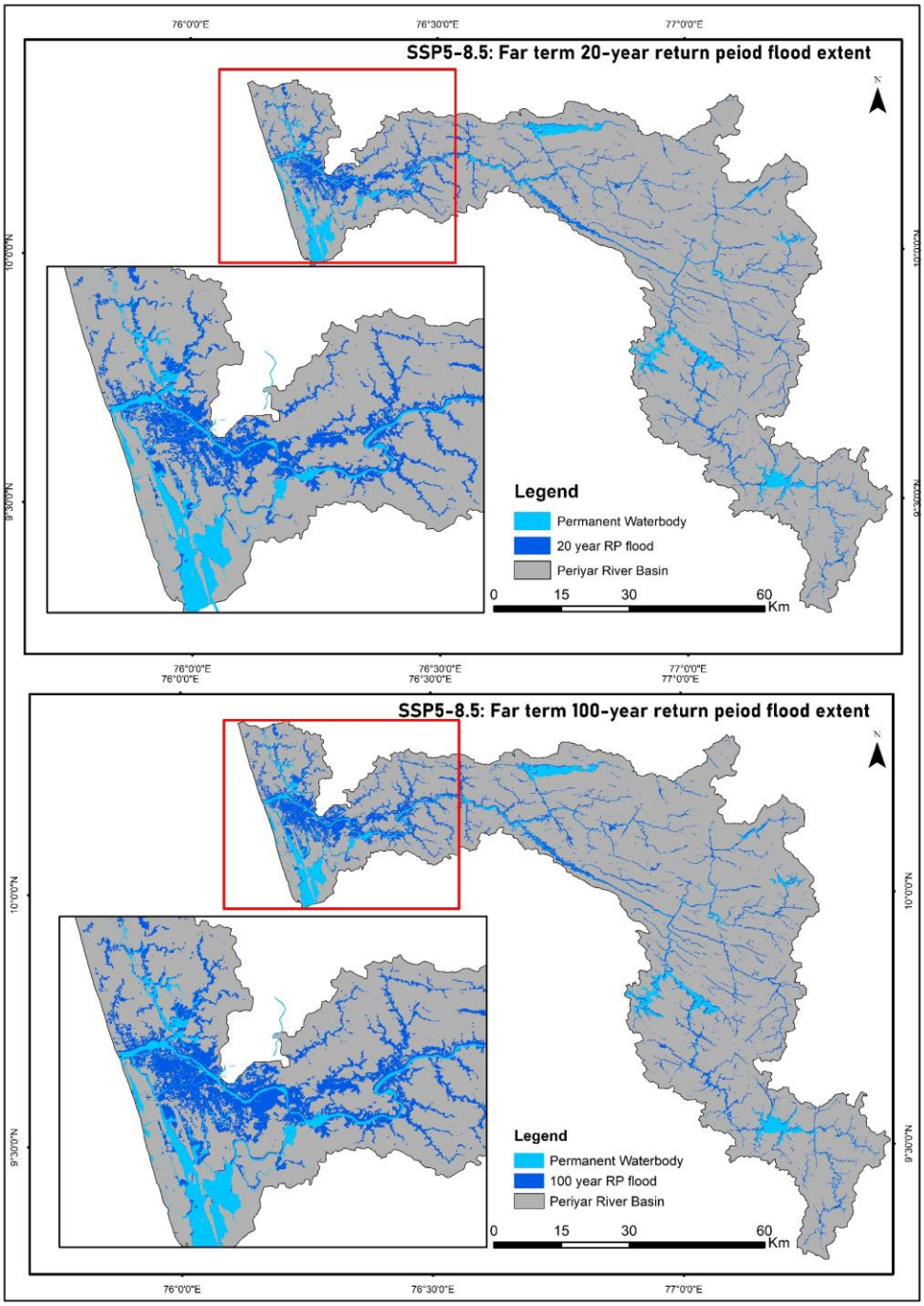

Figure 34: Flood simulated for 20 and 100 year return periods in Medium term under SSP5-8.5 scenario.

Figure 35: The representation of the original gridded temperature data for Munnar.